CONFIDENTIAL

Copy
RM L53J01

NACA RM L53J01

RESEARCH MEMORANDUM

CLASSIFICATION CHANGED

UNCLASSIFIED

To ____

By authority of NACA Res abs YRN-115 Date 5-8-57 effective at 6-13-57

CALCULATED LATERAL FREQUENCY RESPONSE AND LATERAL OSCILLATORY CHARACTERISTICS FOR SEVERAL HIGH-SPEED AIRPLANES IN VARIOUS FLIGHT CONDITIONS

By Byron M. Jaquet

Langley Aeronautical Laboratory
Langley Field, Va.

CLASSIFIED DOCUMENT

This material contains information affecting the National Defense of the United States within the meaning of the espionage laws, Title 18, U.S.C., Secs. 793 and 794, the transmission or revelation of which in any manner to an unauthorized person is prohibited by law.

NATIONAL ADVISORY COMMITTEE FOR AERONAUTICS

WASHINGTON

December 10, 1953

[redacted]

NATIONAL ADVISORY COMMITTEE FOR AERONAUTICS

RESEARCH MEMORANDUM

CALCULATED LATERAL FREQUENCY RESPONSE AND LATERAL OSCILLATORY CHARACTERISTICS FOR SEVERAL HIGH-SPEED AIRPLANES IN VARIOUS FLIGHT CONDITIONS

By Byron M. Jaquet

SUMMARY

Calculations have been made to determine the effects of Mach number and altitude on the lateral frequency response, the lateral response to a lateral sinusoidal gust distribution, and the period and damping of the lateral oscillation for the North American F-86A, Grumman F9F-2, Republic F-84, Douglas D-558-II, and Bell X-1 airplanes without autopilots. Aeroelastic and unsteady lift effects have not been included in the calculations and may have a large effect on the results for certain flight conditions. The results of the investigation are presented, without analysis, for reference purposes.

INTRODUCTION

In order to improve the poor damping of the Dutch roll oscillation of many current high-speed airplanes resort has frequently been made to the use of autopilots. Autopilot characteristics are generally available in the form of frequency-response characteristics rather than in equation form. Hence, the lateral-frequency-response characteristics of airplanes have become an increasingly more important factor in the analysis of the stability of an airplane-autopilot system.

Numerous studies have been made of the dynamic stability of airplanes from the standpoint of period and damping of the lateral oscillation (see, for example, refs. 1 to 5, although only a relatively few studies of the frequency-response characteristics of high-speed airplanes have been made (see, for example, refs. 6 to 11). A thorough study of the lateral-frequency-response characteristics, using transient-flight results, was made for a 35° swept-wing fighter airplane in the investigation reported in reference 11. A survey of various techniques for the stability analysis of automatically controlled aircraft is presented in reference 12.

The present paper presents the results of calculations made to determine the effects of Mach number and altitude on the period and damping of the lateral oscillation and on the transfer functions resulting from aileron or rudder deflection for the North American F-86A, Grumman F9F-2, Republic F-84, Douglas D-558-II, and Bell X-1 airplanes without autopilots. In addition, because of the importance of the response of airplanes to atmospheric turbulence (ref. 13) the yaw response of the aforementioned airplanes to a sinusoidal lateral gust distribution was calculated for several Mach numbers and altitudes.

The results of the investigation are presented without analysis for reference purposes.

COEFFICIENTS AND SYMBOLS

The data presented herein are in the form of standard NACA coefficients of forces and moments and symbols and are referred to the stability axes shown in figure 1. The symbols and coefficients used herein are defined as follows:

L lift, lb

W weight, lb

Y lateral force, lb

L' rolling moment, ft-lb

N yawing moment, ft-lb

q dynamic pressure, lb/sq ft

S area, sq ft

b span, ft

A aspect ratio, b^2/S

ρ mass density of air, slugs/cu ft

V airspeed, ft/sec

$pb/2V$	wing-tip helix angle, radians
$rb/2V$	yawing-angular-velocity parameter, radians
p	rolling-angular velocity about X-axis, radian/sec
r	yawing-angular velocity about Z-axis, radian/sec
δ_a	total aileron deflection, deg
δ_r	rudder deflection, deg
ϕ	angle of bank, radians

$\dot{\phi} = \frac{d\phi}{dt}$, radian/sec

ψ	angle of yaw, radians unless otherwise noted

$\dot{\psi} = \frac{d\psi}{dt}$, radian/sec

β	angle of sideslip, radians
σ	angle of airstream with respect to initial flight-path direction of airplane, radians unless otherwise noted.
α	angle of attack of fuselage reference line, deg (see fig. 1)
Λ	angle of sweepback of wing, deg (subscript denotes chord line)
η	inclination of principal longitudinal axis of airplane with respect to flight path, positive when principal axis is above flight path at nose, deg (see fig. 1)
ϵ	angle between reference axis and principal axis, positive when reference axis is above principal axis, deg (see fig. 1)
γ	angle of flight path to horizontal axis, positive in a climb, deg (see fig. 1)
μ_b	relative density factor, $W/g\rho S_w b_w$
g	acceleration of gravity, ft/sec/sec
ω	frequency, radians/sec
ω_n	natural frequency, radians/sec

ω_b nondimensional frequency, $\omega \frac{b_w}{V}$

k_{X_0} radius of gyration in roll about principal longitudinal axis, ft

k_{Z_0} radius of gyration in yaw about principal vertical axis, ft

K_{X_0} nondimensional radius of gyration in yaw about principal longitudinal axis, K_{X_0}/b_w

K_{Z_0} nondimensional radius of gyration in yaw about principal vertical axis, K_{Z_0}/b_w

K_X nondimensional radius of gyration in roll about longitudinal stability axis, $\sqrt{{K_{X_0}}^2 \cos^2\eta + {K_{Z_0}}^2 \sin^2\eta}$

K_Z nondimensional radius of gyration in yaw about vertical stability axis, $\sqrt{{K_{Z_0}}^2 \cos^2\eta + {K_{X_0}}^2 \sin^2\eta}$

K_{XZ} nondimensional product of inertia parameter, $\left({K_{Z_0}}^2 - {K_{X_0}}^2\right)\sin \eta \cos \eta$

t time, sec

s_b nondimensional time parameter, tV/b

D_b differential operator, d/ds_b

$T_{1/2}$ time for oscillation to damp to one-half amplitude, sec

P period of oscillation, sec

ξ ratio of actual to critical damping, $\frac{0.693}{T_{1/2}\omega_n}$

H altitude, ft

M Mach number

R Reynolds number

Subscripts:

H horizontal tail

v vertical tail

w wing

F fuselage

M at any Mach number

M = 0 at Mach number 0

C_L lift coefficient, L/qS_w

C_Y lateral-force coefficient, Y/qS_w

C_l rolling-moment coefficient, L'/qS_wb_w

C_n yawing-moment coefficient, N/qS_wb_w

$C_{L_\alpha} = \frac{\partial C_L}{\partial \alpha}$, per radian

$C_{n_\beta} = \frac{\partial C_n}{\partial \beta}$, per radian

$C_{l_\beta} = \frac{\partial C_l}{\partial \beta}$, per radian

$C_{Y_\beta} = \frac{\partial C_Y}{\partial \beta}$, per radian

$C_{n_p} = \frac{\partial C_n}{\partial \frac{pb}{2V}}$, per radian

$$C_{l_p} = \frac{\partial C_l}{\partial \frac{pb}{2V}}, \text{ per radian}$$

$$C_{Y_p} = \frac{\partial C_Y}{\partial \frac{pb}{2V}}, \text{ per radian}$$

$$C_{n_r} = \frac{\partial C_n}{\partial \frac{rb}{2V}}, \text{ per radian}$$

$$C_{l_r} = \frac{\partial C_l}{\partial \frac{rb}{2V}}, \text{ per radian}$$

$$C_{Y_r} = \frac{\partial C_Y}{\partial \frac{rb}{2V}}, \text{ per radian}$$

$$C_{l_{\delta_a}} = \frac{\partial C_l}{\partial \delta_a}, \text{ per deg}$$

$$C_{n_{\delta_a}} = \frac{\partial C_n}{\partial \delta_a}, \text{ per deg}$$

$$C_{Y_{\delta_a}} = \frac{\partial C_Y}{\partial \delta_a}, \text{ per deg}$$

$$C_{l_{\delta_r}} = \frac{\partial C_l}{\partial \delta_r}, \text{ per deg}$$

$$C_{n_{\delta_r}} = \frac{\partial C_n}{\partial \delta_r}, \text{ per deg}$$

$$C_{Y_{\delta_r}} = \frac{\partial C_Y}{\partial \delta_r}, \text{ per deg}$$

CALCULATION METHODS

Equations of Lateral Motion

The linear nondimensional equations of lateral motion, referred to the stability system of axes of figure 1, are:

Roll:

$$\left(2\mu_b K_X^2 D_b^2 - \frac{1}{2} C_{l_p} D_b\right)\varphi + \left(2\mu_b K_{XZ} D_b^2 - \frac{1}{2} C_{l_r} D_b\right)\psi - C_{l_\beta}\beta = C_{l_{\delta_a}}\delta_a + C_{l_{\delta_r}}\delta_r$$

Yaw:

$$\left(2\mu_b K_{XZ} D_b^2 - \frac{1}{2} C_{n_p} D_b\right)\varphi + \left(2\mu_b K_Z^2 D_b^2 - \frac{1}{2} C_{n_r} D_b\right)\psi - C_{n_\beta}\beta = C_{n_{\delta_r}}\delta_r + C_{n_{\delta_a}}\delta_a \qquad (1)$$

Sideslipping:

$$\left(-\frac{1}{2} C_{Y_p} D_b - C_L\right)\varphi + \left[\left(2\mu_b - \frac{1}{2} C_{Y_r}\right) D_b - C_L \tan\gamma\right]\psi + \left(2\mu_b D_b - C_{Y_\beta}\right)\beta = C_{Y_{\delta_r}}\delta_r + C_{Y_{\delta_a}}\delta_a$$

For the present investigation, $\tan\gamma$, $C_{n_{\delta_a}}$, $C_{Y_{\delta_a}}$, $C_{l_{\delta_r}}$, and $C_{Y_{\delta_r}}$ were assumed to be negligible and were considered to be equal to zero.

Transfer Functions

In order to find the amplitude and phase relationship of β, ϕ, and ψ resulting from unit sinusoidal variations in δ_a and δ_r, equations (1) are solved by the method of determinants, a substitution is made for the sinusoidal variations of control deflection, and the resulting expressions are separated into real and imaginary parts. The first step in the operation gives equations (2) which are similar to those presented in references 14 (with the initial conditions of zero) and 15. These equations are:

$$\left.\begin{aligned}
\frac{\beta}{\delta_a} &= \frac{a_1 D_b^{\,3} + a_2 D_b^{\,2} + a_3 D_b}{\Delta} C_{l_{\delta_a}} \\
\frac{\beta}{\delta_r} &= \frac{b_1 D_b^{\,3} + b_2 D_b^{\,2} + b_3 D_b}{\Delta} C_{n_{\delta_r}} \\
\frac{\varphi}{\delta_a} &= \frac{c_o D_b^{\,3} + c_1 D_b^{\,2} + c_2 D_b + c_3}{\Delta} C_{l_{\delta_a}} \\
\frac{\varphi}{\delta_r} &= \frac{d_o D_b^{\,3} + d_1 D_b^{\,2} + d_2 D_b + d_3}{\Delta} C_{n_{\delta_r}} \\
\frac{\psi}{\delta_a} &= \frac{e_o D_b^{\,3} + e_1 D_b^{\,2} + e_2 D_b + e_3}{\Delta} C_{l_{\delta_a}} \\
\frac{\psi}{\delta_r} &= \frac{f_o D_b^{\,3} + f_1 D_b^{\,2} + f_2 D_b + f_3}{\Delta} C_{n_{\delta_r}}
\end{aligned}\right\} \qquad (2)$$

where

$$\Delta = AD_b^{\,5} + BD_b^{\,4} + CD_b^{\,3} + DD_b^{\,2} + ED_b$$

and A, B, C, D, and E are given on page 35 of reference 14 and

$$a_1 = 4\mu_b{}^2K_{XZ} + \mu_bK_Z{}^2C_{Y_p} - \mu_bK_{XZ}C_{Y_r}$$

$$a_2 = -\mu_bC_{n_p} + 2\mu_bC_LK_Z{}^2 + \frac{1}{4}\,C_{n_p}C_{Y_r} - \frac{1}{4}\,C_{n_r}C_{Y_p}$$

$$a_3 = -\frac{1}{2}\,C_LC_{n_r}$$

$$b_1 = -4\mu_b{}^2K_X{}^2 + \mu_bK_X{}^2C_{Y_r} - \mu_bK_{XZ}C_{Y_p}$$

$$b_2 = \mu_bC_{l_p} - 2\mu_bC_LK_{XZ} + \frac{1}{4}\,C_{l_r}C_{Y_p} - \frac{1}{4}\,C_{l_p}C_{Y_r}$$

$$b_3 = \frac{1}{2}\,C_LC_{l_r}$$

$$c_0 = 4\mu_b{}^2K_Z{}^2$$

$$c_1 = -2\mu_bK_Z{}^2C_{Y_\beta} - \mu_bC_{n_r}$$

$$c_2 = 2\mu_bC_{n_\beta} + \frac{1}{2}\,C_{n_r}C_{Y_\beta} - \frac{1}{2}\,C_{n_\beta}C_{Y_r}$$

$$c_3 = 0 \text{(since } \tan\gamma = 0\text{)}$$

$$d_0 = -4\mu_b{}^2K_{XZ}$$

$$d_1 = 2\mu_bK_{XZ}C_{Y_\beta} + \mu_bC_{l_r}$$

$$d_2 = -2\mu \; C_{l_\beta} + \frac{1}{2} C_{l_\beta} C_{Y_r} - \frac{1}{2} C_{l_r} C_{Y_\beta}$$

$$d_3 = 0(\text{since } \tan \gamma = 0)$$

$$e_0 = -4{\mu_b}^2 K_{XZ}$$

$$e_1 = \mu_b C_{n_p} + 2\mu_b C_{Y_\beta} K_{XZ}$$

$$e_2 = \frac{1}{2} C_{n_\beta} C_{Y_p} - \frac{1}{2} C_{n_p} C_{Y_\beta}$$

$$e_3 = C_L C_{n_\beta}$$

$$f_0 = 4{\mu_b}^2 {K_X}^2$$

$$f_1 = -\mu_b C_{l_p} - 2\mu_b {K_X}^2 C_{Y_\beta}$$

$$f_2 = \frac{1}{2} C_{l_p} C_{Y_\beta} - \frac{1}{2} C_{l_\beta} C_{Y_p}$$

$$f_3 = -C_L C_{l_\beta}$$

Substituting $i\omega_b$ for the operator D_b in equations (2) results in a complex number of the form $C_{n_{\delta_r}}$ or $C_{l_{\delta_a}}(a + bi)$ which is changed to the form $C_{n_{\delta_r}}$ or $C_{l_{\delta_a}}\left(Re^{i\theta}\right)$ where $R = \sqrt{a^2 + b^2}$ and $\theta = \tan^{-1} \frac{b}{a}$. The transfer functions were then computed over a range of nondimensional frequencies ω_b which are related to ω radian/sec by $\omega = \omega_b \frac{V}{b_W}$.

In order to obtain the transfer functions $\frac{\dot{\varphi}}{\delta_a, \delta_r}$ and the corresponding phase angles, the magnitude of $\frac{\varphi}{\delta_a, \delta_r}$ was multiplied by ω and $\frac{\pi}{2}$ was added to the phase angle to obtain the phase angle $\theta \frac{\dot{\varphi}}{\delta_a, \delta_r}$. A similar procedure was used for $\frac{\dot{\psi}}{\delta_a, \delta_r}$ and the corresponding phase angles.

In addition to the transfer functions the period and damping of the lateral oscillation were calculated from the roots of the characteristic equation Δ. The damping ratio ξ (ref. 12) was calculated from $\xi = \frac{0.693}{T_{1/2}\omega_n}$ where ω_n is the natural frequency in radians per second and the damping ratio is the ratio of actual to critical damping.

Sinusoidal Lateral Gust Response

Only the response in yaw to a sinusoidal lateral-gust disturbance was calculated for the subject airplanes and penetration effects along the fuselage were not considered. The gust disturbance σ was considered to be an effective sinusoidally varying sideslip angle which produces an additional $C_{l_\beta}\beta$ and $C_{n_\beta}\beta$ on the right side of the roll and yaw equations of motion (equations (1) in Calculation Methods). This effective sideslip angle was considered to be equal numerically to β.

From the transfer functions we have

$$\frac{\psi_1}{\sigma} = \frac{e_o D_b^{\,3} + e_1 D_b^{\,2} + e_2 D_b + e_3}{\Delta} C_{l_\beta}$$

and

$$\frac{\psi_2}{\sigma} = \frac{f_o D_b^{\,3} + f_1 D_b^{\,2} + f_2 D_b + f_3}{\Delta} C_{n_\beta}$$

The amplitude of ψ with respect to C_{l_β} and C_{n_β} is

$$\frac{\psi}{\sigma} = \frac{\psi_1}{\sigma} + \frac{\psi_2}{\sigma}$$

which upon substitution of $D_b = i\omega_b$ gives

$$\frac{\psi}{\sigma} = R_1 e^{i(\theta_1+\pi)} + R_2 e^{i\theta_2}$$

$$\frac{\psi}{\sigma} = R_1 \cos(\theta_1 + \pi) + iR_1 \sin(\theta_1 + \pi) + R_2 \cos \theta_2 + iR_2 \sin \theta_2$$

or

$$\frac{\psi}{\sigma} = R_3 e^{i\theta_3}$$

where the amplitude ratio R_3 is equal to

$$\sqrt{\left[R_1 \cos(\theta_1 + \pi) + R_2 \cos \theta_2\right]^2 + \left[R_1 \sin(\theta_1 + \pi) + R_2 \sin \theta_2\right]^2}$$

and the phase angle θ_3 is equal to

$$\tan^{-1}\left[\frac{R_1 \sin\left(\theta_1 + \pi\right) + R_2 \sin \theta_2}{R_1 \cos\left(\theta_1 + \pi\right) + R_2 \cos \theta_2}\right]$$

and

$$\sin^{-1}\left\{\frac{R_1 \sin\left(\theta_1 + \pi\right) + R_2 \sin \theta_2}{\sqrt{\left[R_1 \cos(\theta_1 + \pi) + R_2 \cos \theta_2\right]^2 + \left[R_1 \sin(\theta_1 + \pi) + R_2 \sin \theta_2\right]^2}}\right\}$$

The factor π was added to θ_1 to account for a change in sign of C_{l_β} since C_{l_β} is usually negative. The expression $\frac{\psi}{\sigma}$ was multiplied by 1000 feet per second for the gust velocity and divided by V in feet per second to obtain the relative amplification factor $\frac{\psi}{\sigma} \frac{1000}{V}$ as was used in reference 13.

PERTINENT AIRPLANE DATA

Geometry

The airplanes selected for the present investigation were the North American F-86A, Grumman F9F-2, Republic F-84, Douglas D-558-II, and Bell X-1. Pertinent geometric and mass data are given in tables I and II and a drawing of each airplane is presented in figure 2. The airplane mass data were obtained from unpublished results, the Flight Research Division of the Langley Aeronautical Laboratory, from reference 1 for the Bell X-1 airplane. and from references 2 and 3 for the Douglas D-558-II airplane.

Stability Derivatives

Low-speed data.- Scale models of the North American F-86A and Grumman F9F-2 airplanes were obtained from the Langley Hydrodynamics Division and were tested in the Langley stability tunnel to determine the necessary static and rotary derivatives. These data are presented in figure 3 since they have not been presented before. Scale models of the Douglas D-558-II and the Bell X-1 were previously investigated in the Langley stability tunnel, (refs. 2 and 16, respectively). The static derivatives of the Republic F-84 at a low Mach number were obtained from unpublished results. The rotary-stability derivatives for the Republic F-84 airplane wing-fuselage combination were determined by the methods described in reference 17. The vertical-tail increments of the rolling and yawing derivatives were calculated by the use of the equations presented in references 18 and 19 and the experimental values of C_{Y_β} of the vertical tail.

Mach number effects.- For all airplanes considered, the derivatives of the wing-fuselage combination, with certain exceptions, were corrected for the effects of Mach number by the methods of reference 20. In making these corrections the experimental variation of C_{L_α} with Mach number was used when available (refs. 21 and 22). The derivatives C_{n_β}, C_{Y_β}, C_{n_r}, and C_{Y_r} were those not corrected for the effects of Mach number. The fuselage generally is the major contributor to these derivatives at low angles of attack and the effects of Mach number on these fuselage derivatives are usually small in this angle-of-attack range.

The vertical-tail derivatives for all airplanes considered were corrected for Mach number effects by determining the effective aspect ratio of the tail at a low Mach number ($M \approx 0$) from the experimental $C_{Y_{\beta_V}}$ and reference 23. The methods of reference 20 were used to determine Mach number corrections to the vertical-tail lift-curve slope for the effective aspect ratio. All vertical-tail derivatives were then corrected for Mach number effects by using the ratio $\frac{\left(C_{L_\alpha}\right)_M}{\left(C_{L_\alpha}\right)_{M=0}}$.

The total airplane derivative at a given angle of attack and Mach number was then determined by the sum of the vertical-tail contribution and the wing-fuselage-combination contribution.

The variation of C_L with Mach number for several angles of attack for each airplane is presented in figure 4 and the variation of the static and rotary derivatives with Mach number for each airplane is presented in figure 5.

Aileron and rudder effectiveness.- The aileron effectiveness $C_{l_{\delta_a}}$ and rudder effectiveness $C_{n_{\delta_r}}$ and the sources for each airplane are given in the following table:

Airplane	$C_{l_{\delta_a}}$, per deg	Reference	$C_{n_{\delta_r}}$, per deg	Reference
North American F-86A	-0.0015	24	-0.0010	24
Grumman F9F-2	-.0015	25	-.0007	26
Republic F-84	-.0021	Unpublished tests	-.0017	Unpublished tests
Douglas D-558-II	-.00115	27	-.0012	28
Bell X-1	-.00152	Unpublished tests	-.00246	Unpublished tests

These values were assumed to be constant for all flight conditions.

RESULTS

Presentation of Results

The flight conditions investigated are indicated in table II. Because there are a large number of figures in the present paper they are indexed in the following table:

The results of the present investigation are presented in the form of plots of P (period) and $T_{1/2}$ (time to damp to one-half amplitude) of the lateral oscillation of each airplane against Mach number for various altitudes (fig. 6), plots of the lateral frequency response against frequency for various flight conditions (figs. 9 to 16), and plots of the yaw response to a sinusoidal lateral-gust distribution against frequency ratio for various flight conditions (figs. 17 to 21).

General Comments

Aeroelastic and unsteady lift effects have not been included in the calculations and may have a large effect on some of the derivatives, especially at the low altitude investigated (1000 feet). The investigation of reference 11 on the F-86A airplane has indicated a large aeroelastic effect on the derivatives C_{l_p}, C_{n_r}, and $C_{n_{\delta_r}}$ at high speeds at an altitude of 10,000 feet. The results for the F-84 airplane are believed to be applicable for models through D only, since, for later models, the fuselage was lengthened by adding a section between the wing and the tail and this change would alter the derivatives.

The period and damping of the lateral oscillation are compared with the Bureau of Aeronautics criterion (ref. 29) and with flight data when available (fig. 6). Except for the D-558-II airplane, calculations were not made for specific flight-test conditions and hence, in some cases, an exact comparison between calculated and flight results is not possible. The agreement between the calculated and flight values (ref. 30) of $T_{1/2}$ for the D-558-II airplane is poor (fig. 6(e)). The flight frequency-response characteristics (fig. 11) and the period and damping characteristics (fig. 6(b)) of the F9F-2 airplane were obtained from the Langley Flight Research Division and are actually for the F9F-3 airplane with tip tanks empty. Since the F9F-3 airplane differs from the F9F-2 airplane only in that a larger, slightly heavier engine is used in model -3 it is believed that the results presented herein are applicable to both models. The value of ${K_{X_0}}^2$ (table II) used in the calculations for the F9F-2 airplane was for the condition of the tip tanks 3/4 full and as a result it is about twice the value of ${K_{X_0}}^2$ for the flight-test conditions. This difference probably accounts for the calculations underestimating the $\frac{\dot{\phi}}{\delta_a}$ response of the airplane at the higher frequencies (fig. 11).

The effects of Mach number on the frequency-response characteristics of the F-86A at an altitude of 20,000 feet as presented herein (fig. 9) are, in general, similar to those obtained in flight (ref. 11).

CONCLUDING REMARKS

Calculations have been made to provide information on the lateral-frequency-response characteristics of the North American F-86A, Grumman F9F-2, Republic F-84, Douglas D-558-II, and Bell X-1 airplanes through a range of flight conditions. In addition to this information the period and damping of the lateral oscillation and ratio of actual to critical damping have also been determined. The frequency-response data were also put into such a form as to represent the lateral response of these airplanes to sinusoidal lateral disturbances of the air. Aero-elastic and unsteady lift effects have not been accounted for in the calculations and may have an important influence under certain flight conditions.

Langley Aeronautical Laboratory,
National Advisory Committee for Aeronautics,
Langley Field, Va., September 29, 1953.

REFERENCES

1. Polhamus, Edward C.: A Study of the Dynamic Stability of the Bell X-1 Research Airplane. NACA RM L9K04a, 1950.

2. Queijo, M. J., and Goodman, Alex: Calculations of the Dynamic Lateral Stability Characteristics of the Douglas D-558-II Airplane in High-Speed Flight for Various Wing Loadings and Altitudes. NACA RM L50H16a, 1950.

3. Gates, Ordway B., Jr., Schy, Albert A., and Woodling, C. H.: An Analysis of the Lateral Stability of the Douglas D-558-II Airplane Equipped with a Yaw Damper, With Special Reference to the Effect of Yaw-Damper Rate-Gyro Spin-Axis Orientation. NACA RM L52K14a, 1953.

4. Heinle, Donovan R., and McNeill, Walter E.: Correlation of Predicted and Experimental Lateral Oscillation Characteristics for Several Airplanes. NACA RM A52J06, 1952.

5. McNeill, Walter E., and Cooper, George E.: A Comparison of the Measured and Predicted Lateral Oscillatory Characteristics of a 35° Swept-Wing Fighter Airplane. NACA RM A51C28, 1951.

6. Van Meter, J. T.: Nondimensional Equations of Motion of an Airplane in Both Longitudinal and Lateral Modes in Response to Sinusoidal Oscillation of Control Surfaces. Rep. TB-405-F-6, Cornell Aero. Lab., Inc., 1947.

7. Triplett, William C., and Smith, G. Allan.: Longitudinal Frequency-Response Characteristics of a 35° Swept-Wing Airplane As Determined From Flight Measurements, Including a Method for the Evaluation of Transfer Functions. NACA RM A51G27, 1951.

8. Eckhardt, Homer D.: Theoretical Lateral Frequency Response of Douglas A-26 Airplane to (a) Sinusoidally Varying Rudder Angle with Fixed Aileron (b) Sinusoidally Varying Aileron Angle with Fixed Rudder. Rep. 6445-E-7, Instrumentation Lab., M.I.T., 1947.

9. Clemen, Arthur T., Marx, H. F., and Zant, W. L.: Frequency Response Characteristics of the B-36D Airplane. Part II - Lateral Response at 20,000 Ft. Rep. No. FZA-36-256A, Consolidated Vultee Aircraft Corp., Mar. 18, 1952.

10. Mathews, Charles W.: Some Factors Affecting Automatic Control of Airplanes. NACA RM L52A30, 1952.

11. Triplett, William C., and Brown, Stuart C.: Lateral and Directional Dynamic-Response Characteristics of a 35° Swept-Wing Airplane as Determined From Flight Measurements. NACA RM A52I17, 1952.

12. Jones, Arthur L., and Briggs, Benjamin R.: A Survey of Stability Analysis Techniques for Automatically Controlled Aircraft. NACA TN 2275, 1951.

13. Bird, John D.: Some Calculations of the Lateral Response of Two Airplanes to Atmospheric Turbulence With Relation to the Lateral Snaking Problem. NACA RM L50F26a, 1950.

14. Murray, Harry E., and Grant, Frederick C.: Method of Calculating the Lateral Motions of Aircraft Based on the LaPlace Transform. NACA TN 2129, 1950.

15. Rogin, L., and Gottlieb, S.: Stabilization Performance Requirements and Equations and Methods Used in Analytical Determination of Dynamic Characteristics of an Autopilot Servomechanism Required for Structural Flight Testing of High Speed Aircraft. Rep. No. ASL NAM 2432, Pt II, NAES, Philadelphia Navy Yard, Bur. Aero., Sept. 20, 1949.

16. Bird, John D., Fisher, Lewis R., and Hubbard, Sadie M.: Some Effects of Frequency on the Contribution of a Vertical Tail to the Free Aerodynamic Damping of a Model Oscillating in Yaw. NACA TN 2657, 1952.

17. Campbell, John P., and McKinney, Marion O.: Summary of Methods for Calculating Dynamic Lateral Stability and Response and for Estimating Lateral Stability Derivatives. NACA Rep. 1098, 1952. (Supersedes NACA TN 2409.)

18. Michael, William H., Jr.: Analysis of the Effects of Wing Interference on the Tail Contributions to the Rolling Derivatives. NACA Rep. 1086, 1952. (Supersedes NACA TN 2332.)

19. Letko, William: Effect of Vertical-Tail Area and Length on the Yawing Stability Characteristics of a Model Having a 45° Sweptback Wing. NACA TN 2358, 1951.

20. Fisher, Lewis R.: Approximate Corrections for the Effects of Compressibility on the Subsonic Stability Derivatives of Swept Wings. NACA TN 1854, 1949.

21. Osborne, Robert S.: High-Speed Wind-Tunnel Investigation of the Longitudinal Stability and Control Characteristics of a 1/16-Scale Model of the D-558-2 Research Airplane at High Subsonic Mach Numbers and at a Mach Number of 1.2. NACA RM L9C04, 1949.

22. Morril, Charles P., Jr., and Boddy, Lee E.: High-Speed Stability and Control Characteristics of a Fighter Airplane Model With a Swept-Back Wing and Tail. NACA RM A7K28, 1948.

23. DeYoung, John: Theoretical Additional Span Loading Characteristics of Wings With Arbitrary Sweep, Aspect Ratio, and Taper Ratio. NACA TN 1491, 1947.

24. Nicholson, R. A., Iverson, L. F., Katkov, R. B., and Leef, C. R.: Wind-Tunnel Tests of a 0.2-Scale Model of the F-95A (F-86D) Airplane To Determine General Stability and Control Characteristics; Effect of Rocket Pod, Speed Brakes, and Ground Plane; and To Obtain a Static Pressure Distribution Over the Fuselage. Rep. No. NA-50-742 NAAL 164, North American Aviation, Inc., July 6, 1950.

25. Tamburello, V., and Beek, Charles R.: Wind-Tunnel Tests of a 1/5-Scale Powered Model of the XF9F-2 Airplane. Part IV - Aileron Tests. Rep. C-196 Aero 758, David W. Taylor Model Basin, Navy Dept., Feb. 1949.

26. Tamburello, V., and Beek, Charles R.: Wind-Tunnel Tests of a 1/5-Scale Powered Model of the XF9F-2 Airplane. Part VII - Lateral Stability and Control - TED No. TMB DE 301. Rep. C-215 Aero 758, David W. Taylor Model Basin, Navy Dept., April, 1949.

27. Kerker, R., and Miller, C. E.: Summary Report of Model D-558-2 Tests at Cooperative Wind Tunnel. Rep. No. E.S. 20648, Douglas Aircraft Co., Inc., Oct. 1, 1946.

28. Pass, H. R.: Analysis of Wind-Tunnel Data on Directional Stability and Control. NACA TN 775, 1940.

29. Anon.: Specification for Flying Qualities of Piloted Airplanes. NAVAER SR-119B, Bur. Aero. June 1, 1948.

30. Stilwell, W. H., and Wilmerding, J. V.: Flight Measurements With the Douglas D-558-II (Bur Aero No. 37974) Research Airplane. Dynamic Lateral Stability. NACA RM L51C23, 1951.

[redacted]

TABLE I.- PERTINENT AIRPLANE DATA

[All airfoil sections are NACA unless specified. Area of vertical tail of Grumman F9F-2 does not extend to reference line (see fig. 2).]

Data	Airplane				
	North American F-86A	Grumman F9F-2	Republic F-84	Douglas D-558-II	Bell X-1
Wing:					
Span, ft	37.10	35.25	36.42	25.00	28.00
Area, sq ft	287.90	250.00	260.00	175.00	130.00
Tip chord, ft	5.29	4.50	5.24	5.10	3.09
Airfoil section, root	0012-64	64_1-A012	Republic R-4	63-010	65-110a-1
Airfoil section, tip	0011-64	64_1-A012	45-1512-.9	63-012	65-110a-1
Incidence, deg	0	0	0	3.0	2.5, 1.5
Dihedral, deg	3	4	5	-3	0
Sweep of reference line, deg	0.25c, 35.25	0.27c, 0	0.5c, 0	0.333c, 35	0.4c, 0
Twist, deg	-2	0	-2	0	-1
Aspect ratio	4.79	4.97	5.10	3.57	6.00
Taper ratio	0.51	0.46	0.57	0.57	0.50
Mean aerodynamic chord, in	97.03	89.50	88.74	87.30	57.70
Leading edge of mean aerodynamic chord from leading edge of root chord, in	73.00	7.50	10.83	54.13	6.60
Height of root chord line above or below reference line, z_v/b_v	-0.073	-0.080	-0.018	0	0
Vertical tail:					
Span from reference line, ft	8.91	8.65	8.10	8.16	8.26
Area to reference line, sq ft	42.80	35.00	39.40	38.80	41.10
Aspect ratio	1.85	0.94	1.85	1.14	1.66
Effective aspect ratio	2.78	1.48	2.10	1.40	2.10
Longitudinal distance from center of gravity to vertical tail center of pressure, l_v/b_w	0.454	0.416	0.480	0.600	0.350
Vertical distance from center of gravity to vertical tail center of pressure, z_v/b_w	0.154	0.183	0.180	0.100	0.110
Airfoil section, root	0012-64	64_1-A012	R-4,40-010	63-010	----
Airfoil section, tip	0012-64	64_1-A010	R-4,40-010	63-010	----
Tip chord, ft	1.91	1.78	----	2.22	2.22
Taper ratio	0.31	0.14	0.36	0.18	0.34
Sweep of quarter chord, deg	35	41	16.5	53	16
Horizontal tail:					
Span, ft	12.80	17.18	17.00	11.95	11.40
Area, sq ft	35.00	58.30	57.10	39.90	26.00
Aspect ratio	4.65	5.06	5.07	3.59	5.00
Sweep of reference line, deg	0.25c, 35.27	0.25c, 14.47	0.5c, 0	0.333c, 40	0c, 12
Airfoil section, root	0012-64	64_1-A012	R-4,40-010	63-010	
Airfoil section, tip	0012-64	64_1-A010	R-4,40-010	63-010	
Height above reference line, z_H/b_v	0.032	0.132	0.093	0.170	0.256
Tip chord, ft	1.70	2.16	2.33	2.25	1.52
Taper ratio	0.451	0.417	0.56	0.50	0.50
Dihedral, deg	10	0	5	0	0
Fuselage:					
Length, excluding booms, ft	34.40	33.50	36.90	42.00	31.00
General:					
Wing loading, lb/sq ft	46.3	60.0	59.6	76.0	65.0
Center of gravity, percent mean aerodynamic chord	22.5	24.7	26.5	25.0	25.0

[redacted]

TABLE II.- CONDITIONS INVESTIGATED

Airplane	H, ft	M	W/S_W	C_L	α, deg	$K_{X_0}^2$	$K_{Z_0}^2$	ϵ, deg
North American F-86A	1,000	0.4	46.5	0.201	3.13	0.0126	0.0404	2.56
North American F-86A	1,000	.6	46.5	.090	1.45	0.0126	0.0404	2.56
North American F-86A	1,000	.9	46.5	.040	.70	0.0126	0.0404	2.56
North American F-86A	20,000	.4	46.5	.426	6.30	0.0126	0.0404	2.56
North American F-86A	20,000	.6	46.5	.188	2.70	0.0126	0.0404	2.56
North American F-86A	20,000	.9	46.5	.084	1.13	0.0126	0.0404	2.56
Grumman F9F-2	1,000	.4	60.0	.260	4.00	.0327	.0644	2.80
Grumman F9F-2	1,000	.6	60.0	.115	2.38	.0327	.0644	2.80
Grumman F9F-2	1,000	.8	60.0	.066	1.75	.0327	.0644	2.80
Grumman F9F-2	20,000	.4	60.0	.550	7.16	.0327	.0644	2.80
Grumman F9F-2	20,000	.6	60.0	.243	3.65	.0327	.0644	2.80
Grumman F9F-2	20,000	.8	60.0	.138	2.40	.0327	.0644	2.80
Republic F-84	1,000	.4	59.6	.258	2.35	.0628	.0857	2.00
Republic F-84	1,000	.6	59.6	.115	.45	.0628	.0857	2.00
Republic F-84	1,000	.9	59.6	.051	-.50	.0628	.0857	2.00
Republic F-84	20,000	.4	59.6	.547	6.20	.0628	.0857	2.00
Republic F-84	20,000	.6	59.6	.242	1.90	.0628	.0857	2.00
Republic F-84	20,000	.9	59.6	.108	-.10	.0628	.0857	2.00
Douglas D-558-II	1,000	.4	76.0	.329	3.35	.0125	.1310	1.70
Douglas D-558-II	1,000	.6	76.0	.146	.65	.0125	.1310	1.70
Douglas D-558-II	1,000	.9	76.0	.065	-.60	.0125	.1310	1.70
Douglas D-558-II	20,000	.4	76.0	.696	8.75	.0125	.1310	1.70
Douglas D-558-II	20,000	.6	76.0	.307	2.85	.0125	.1310	1.70
Douglas D-558-II	20,000	.9	76.0	.138	.20	.0125	.1310	1.70
Douglas D-558-II	20,000	.4	57.1	.524	6.1	.0163	.1372	4.20
Douglas D-558-II	20,000	.5	57.1	.335	3.4	.0163	.1372	4.20
Douglas D-558-II	20,000	.6	57.1	.231	1.8	.0164	.1371	4.20
Douglas D-558-II	20,000	.7	57.1	.171	.8	.0166	.1369	4.20
Douglas D-558-II	20,000	.75	57.1	.149	.5	.0167	.1368	4.20
Douglas D-558-II	20,000	.8	57.1	.131	.2	.0168	.1367	4.20
Douglas D-558-II	20,000	.9	57.1	.103	-.2	.0169	.1366	4.20
Douglas D-558-II	20,000	.4	57.1	.524	6.1	.0272	.1916	3.70
Douglas D-558-II	20,000	.6	57.1	.231	1.8	.0271	.1896	3.70
Douglas D-558-II	20,000	.9	57.1	.103	-.2	.0277	.1909	3.70
Douglas D-558-II	50,000	.8	57.1	.713	7.10	.0125	.1310	1.70
Douglas D-558-II	50,000	.9	57.1	.550	4.50	.0125	.1310	1.70
Bell X-1	1,000	0.4	65.0	.281	1.60	.0067	.0419	2.00
Bell X-1	1,000	.6	65.0	.125	-.15	.0067	.0419	2.00
Bell X-1	1,000	.9	65.0	.056	-1.00	.0067	.0419	2.00
Bell X-1	20,000	.4	65.0	.596	4.90	.0067	.0419	2.00
Bell X-1	20,000	.6	65.0	.263	1.15	.0067	.0419	2.00
Bell X-1	20,000	.9	65.0	.118	-.65	.0067	.0419	2.00
Bell X-1	50,000	.7	65.0	.775	5.60	.0067	.0419	2.00
Bell X-1	50,000	.8	65.0	.610	3.40	.0067	.0419	2.00
Bell X-1	50,000	.9	65.0	.471	1.40	.0067	.0419	2.00

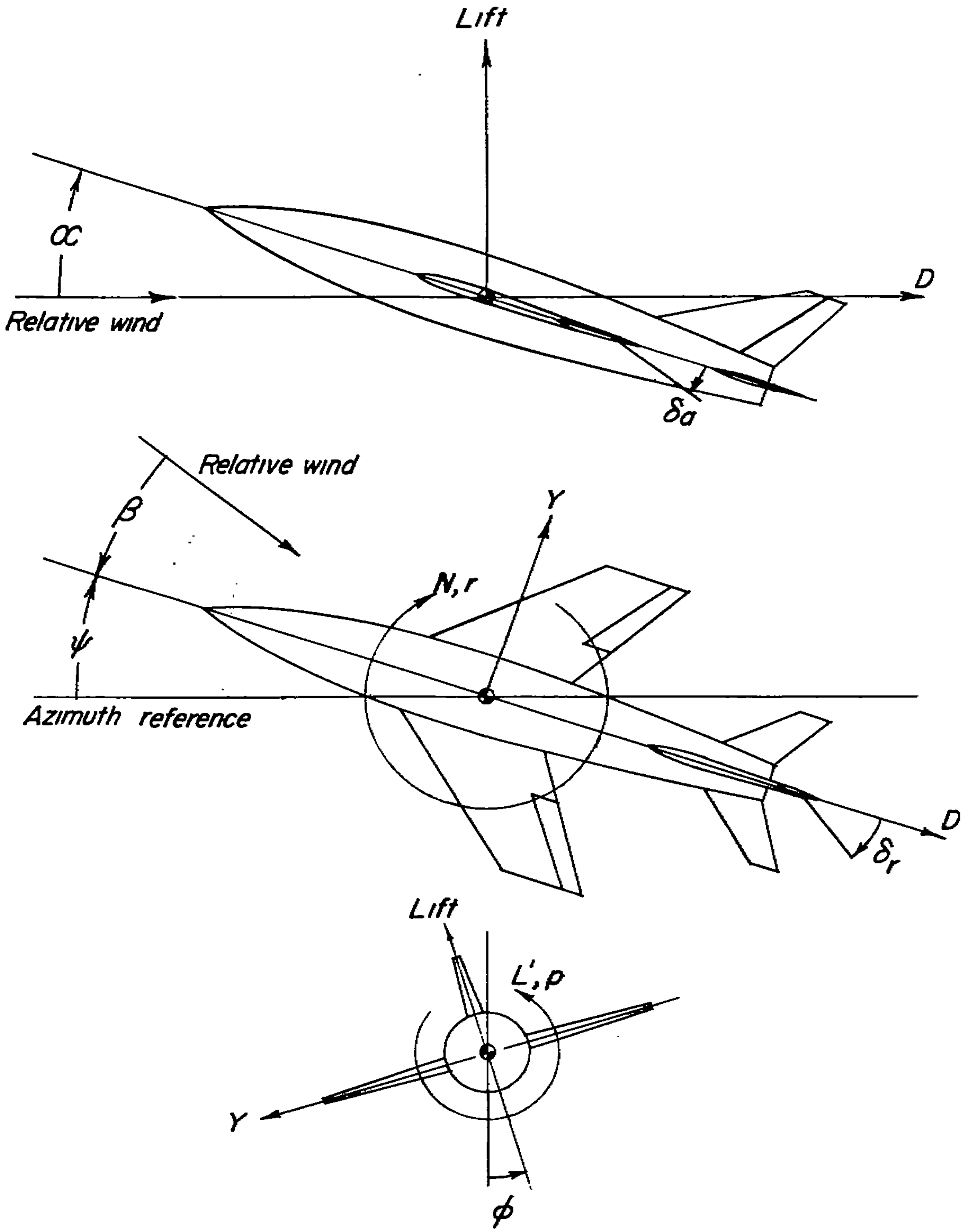

(a) Stability system of axes. Arrows indicate positive direction of forces, moments, and angular velocities.

Figure 1.- System of axes.

[redacted]

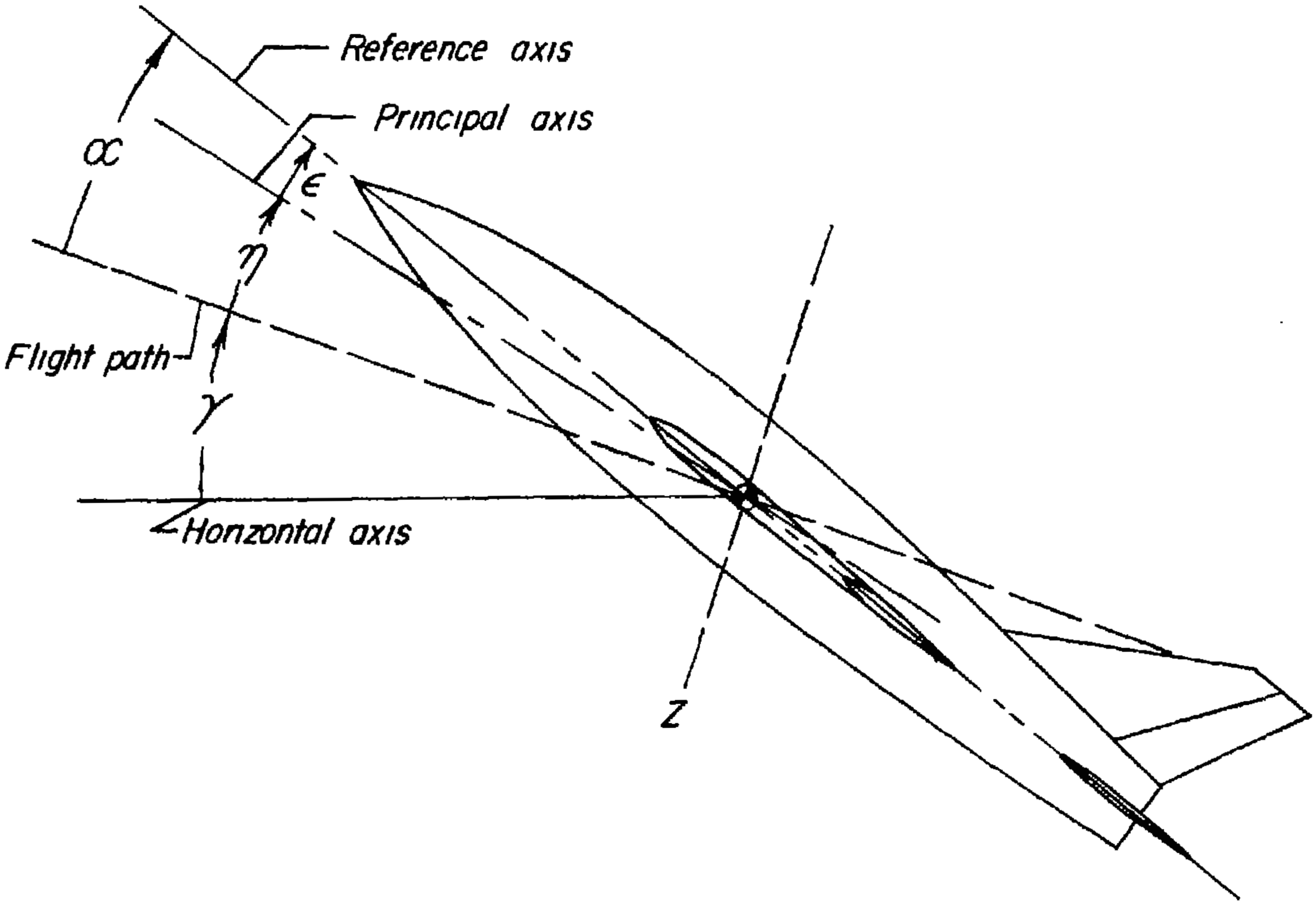

(b) System of axes and angular relationship in flight. Arrows indicate positive direction of angles.

Figure 1.- Concluded.

[redacted]

[redacted]

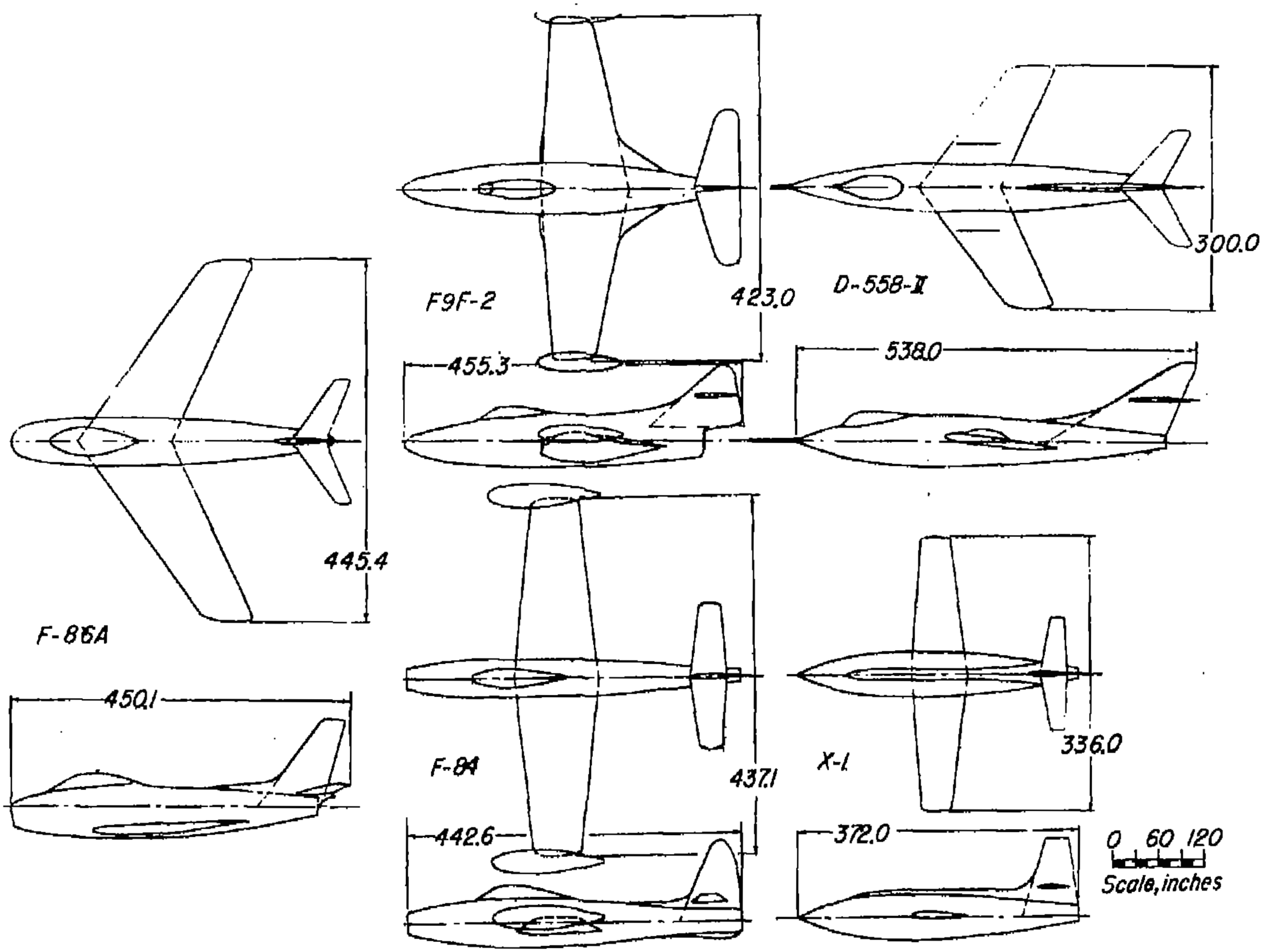

Figure 2.- General arrangement of airplanes. Dimensions in inches.

[redacted]

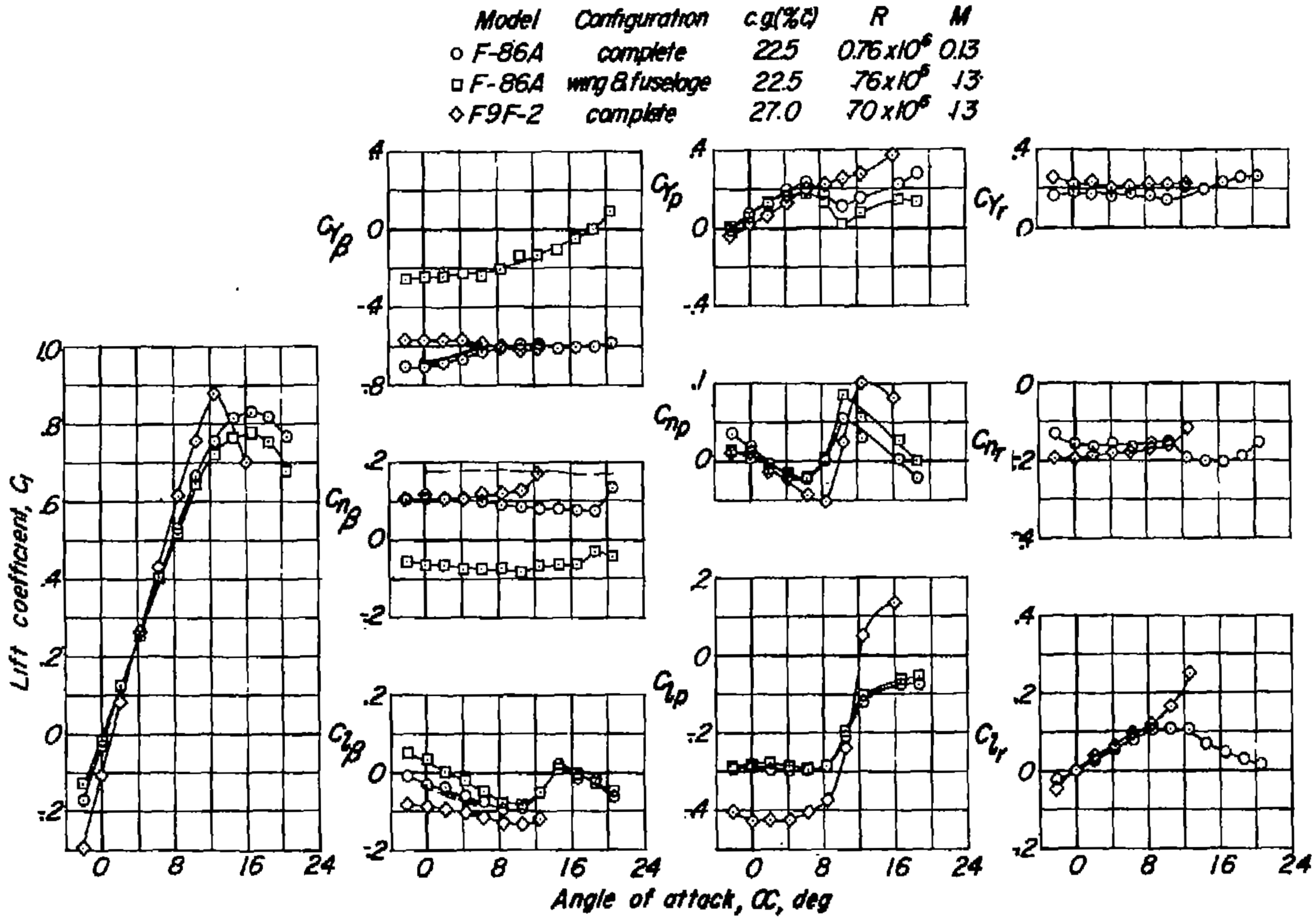

Figure 3.- Experimental variations of C_L, C_{Y_β}, C_{n_β}, C_{l_β}, C_{Y_p}, C_{n_p}, C_{l_p}, C_{Y_r}, C_{n_r}, and C_{l_r} with angle of attack for $\frac{1}{10}$- scale models of the North American F-86A and Grumman F9F-2 airplanes. Tip tanks on for all F9F-2 data.

[redacted]

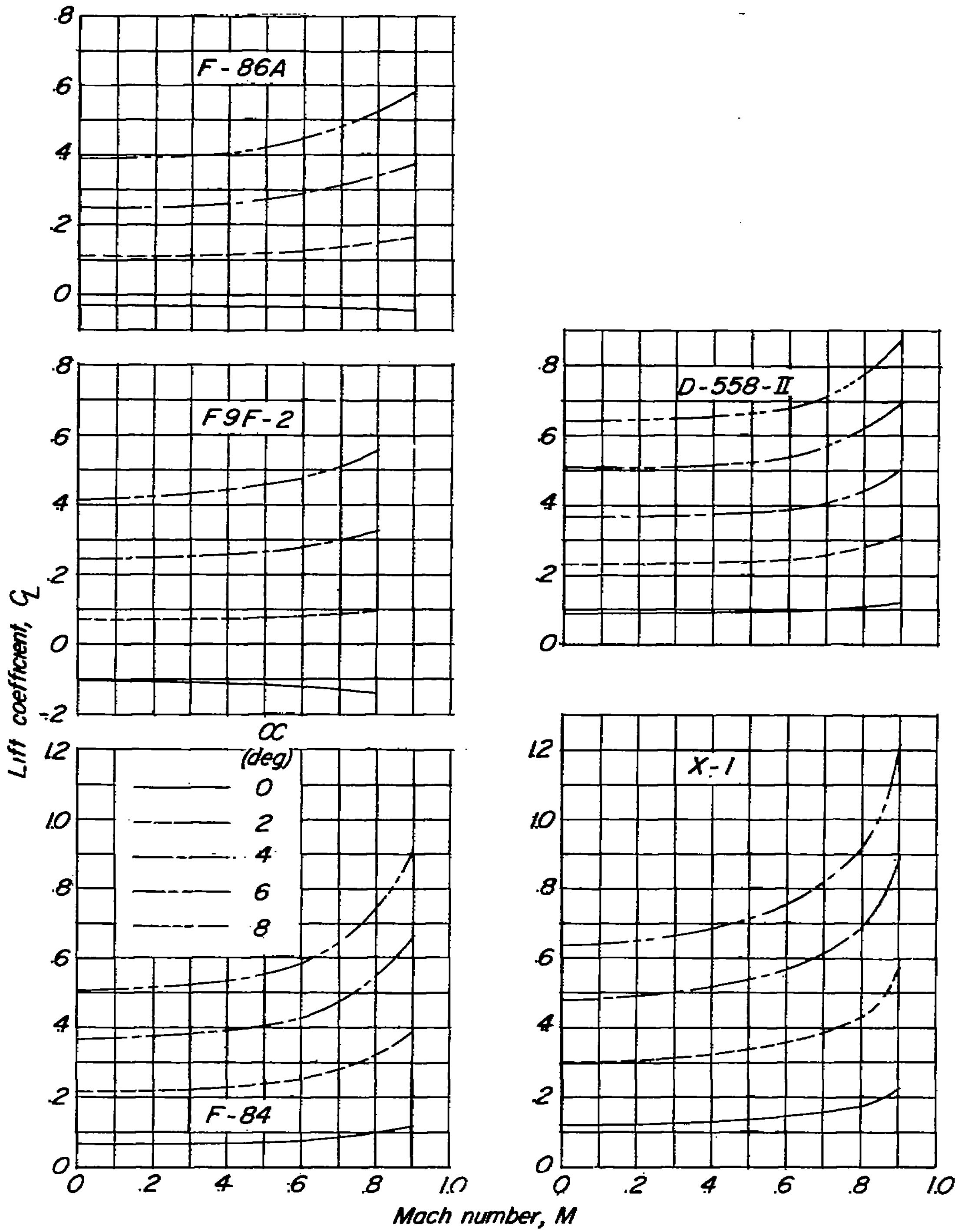

Figure 4.- Variation of C_L with Mach number for several angles of attack for the airplanes investigated.

[redacted]

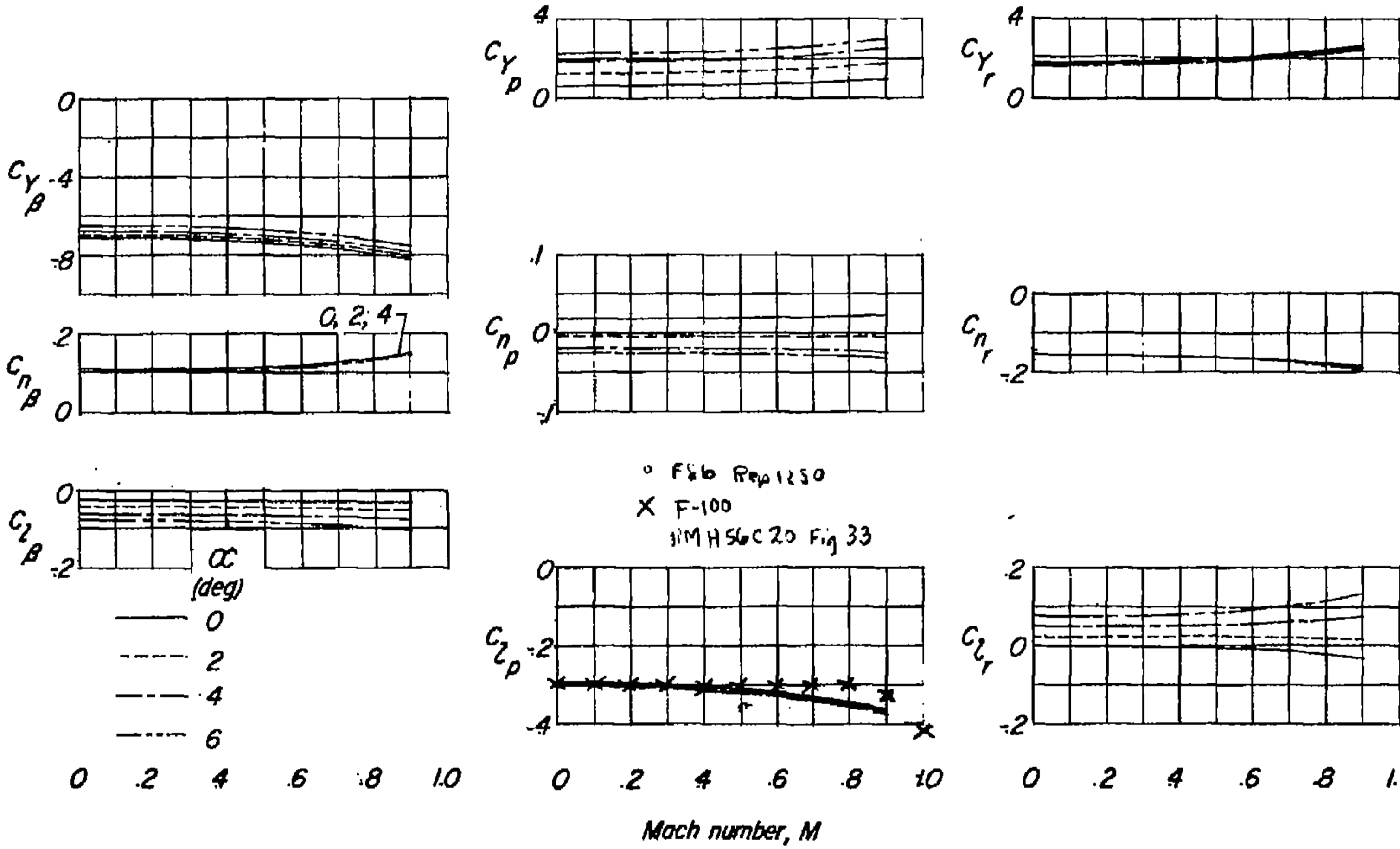

(a) North American F-86A.

Figure 5.- Variation of static and rotary stability derivatives with Mach number for several angles of attack for the airplanes investigated.

[redacted]

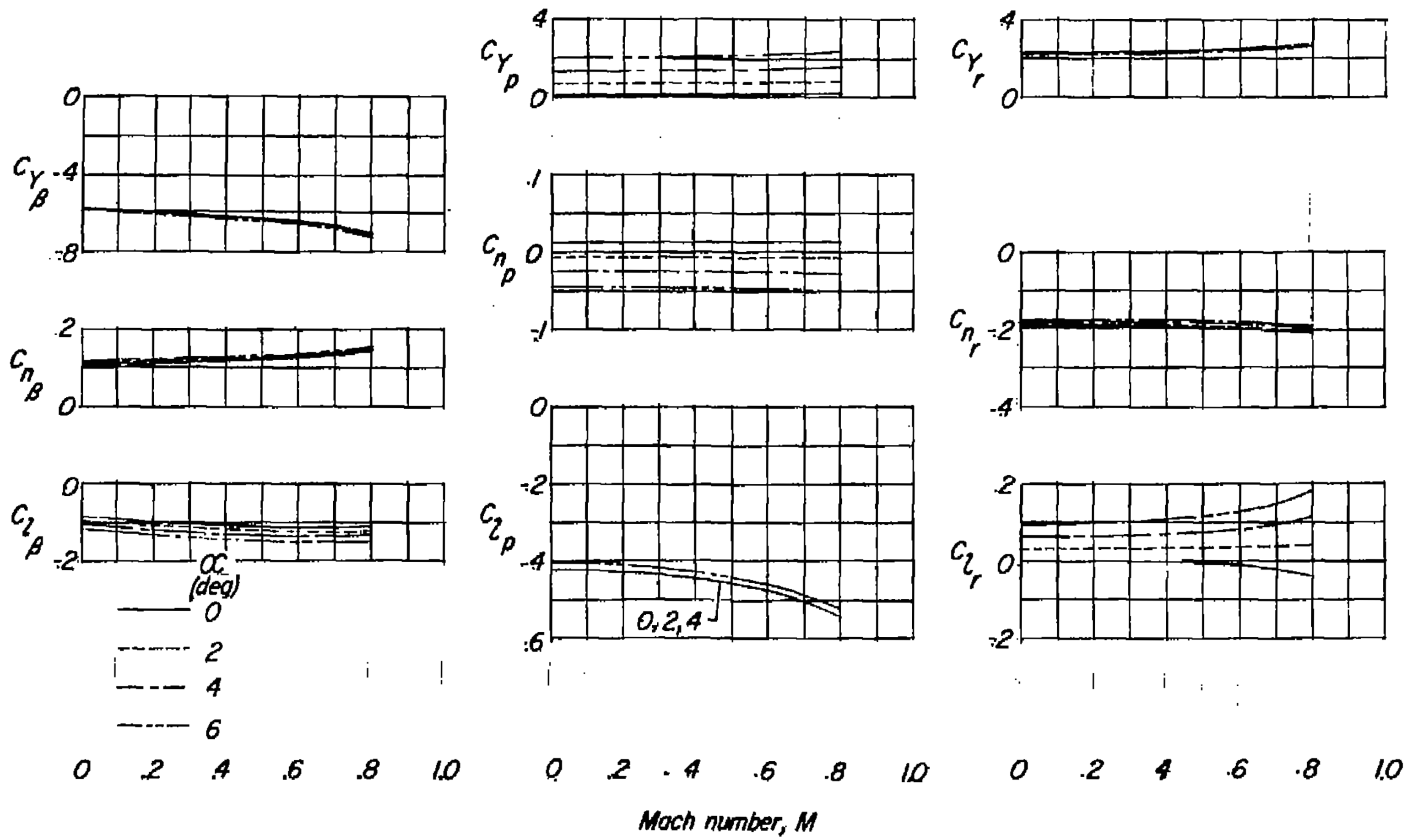

(b) Grumman F9F-2.

Figure 5.- Continued.

[redacted]

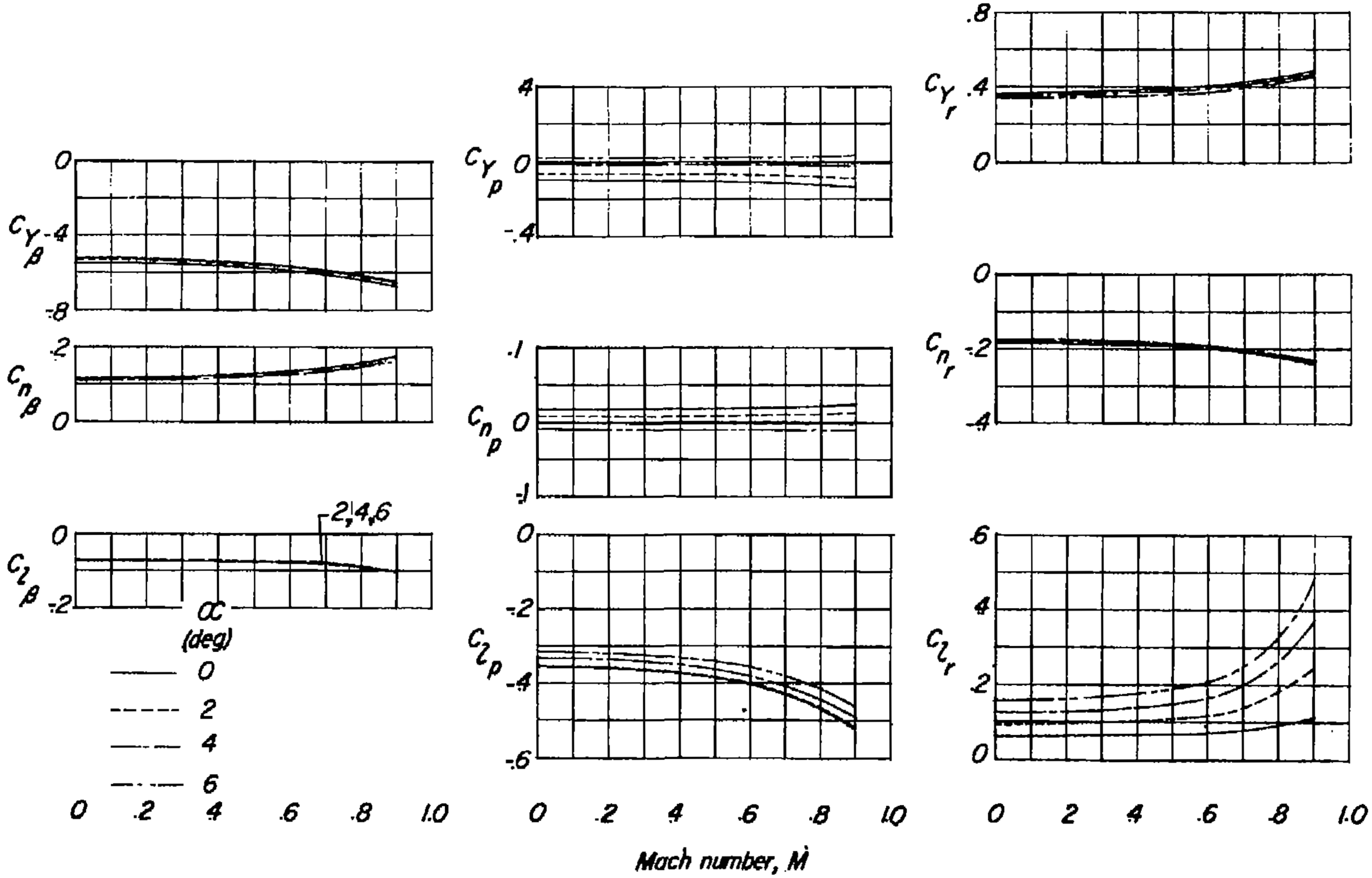

(c) Republic F-84.

Figure 5.- Continued.

[redacted]

[redacted]

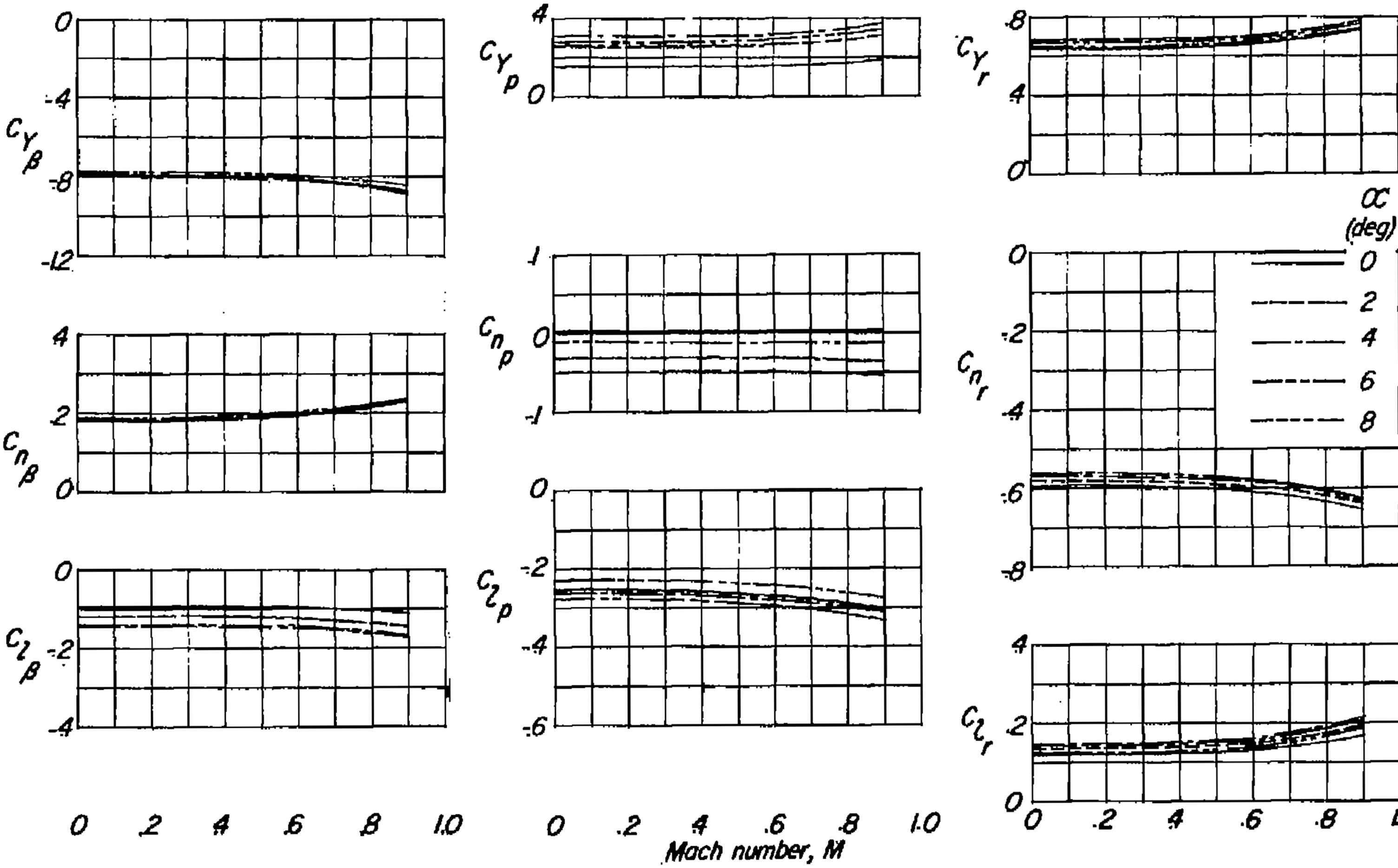

(d) Douglas D-558-II.

Figure 5.- Continued.

[redacted]

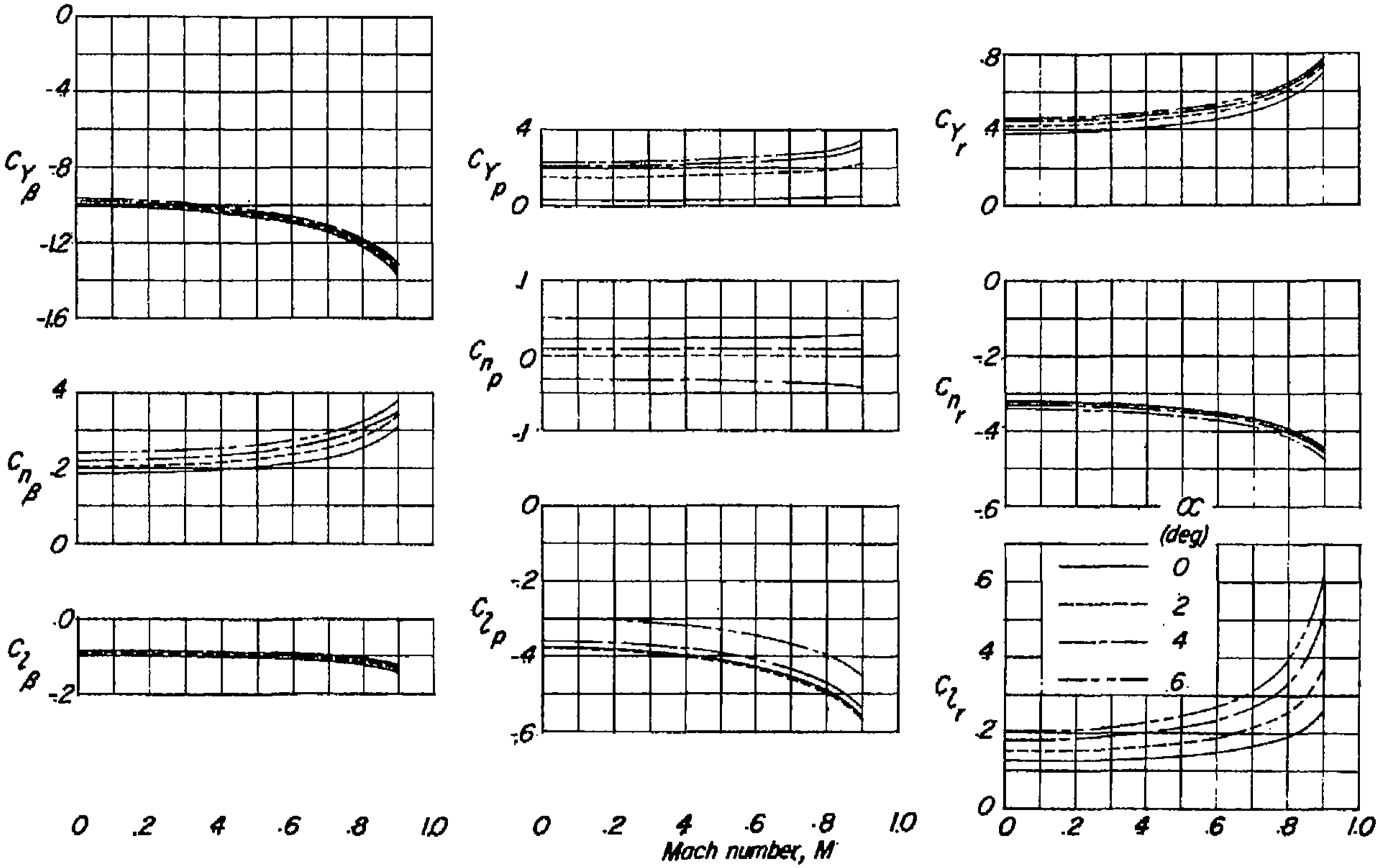

(e) Bell X-1.

Figure 5.- Concluded.

[redacted]

[redacted]

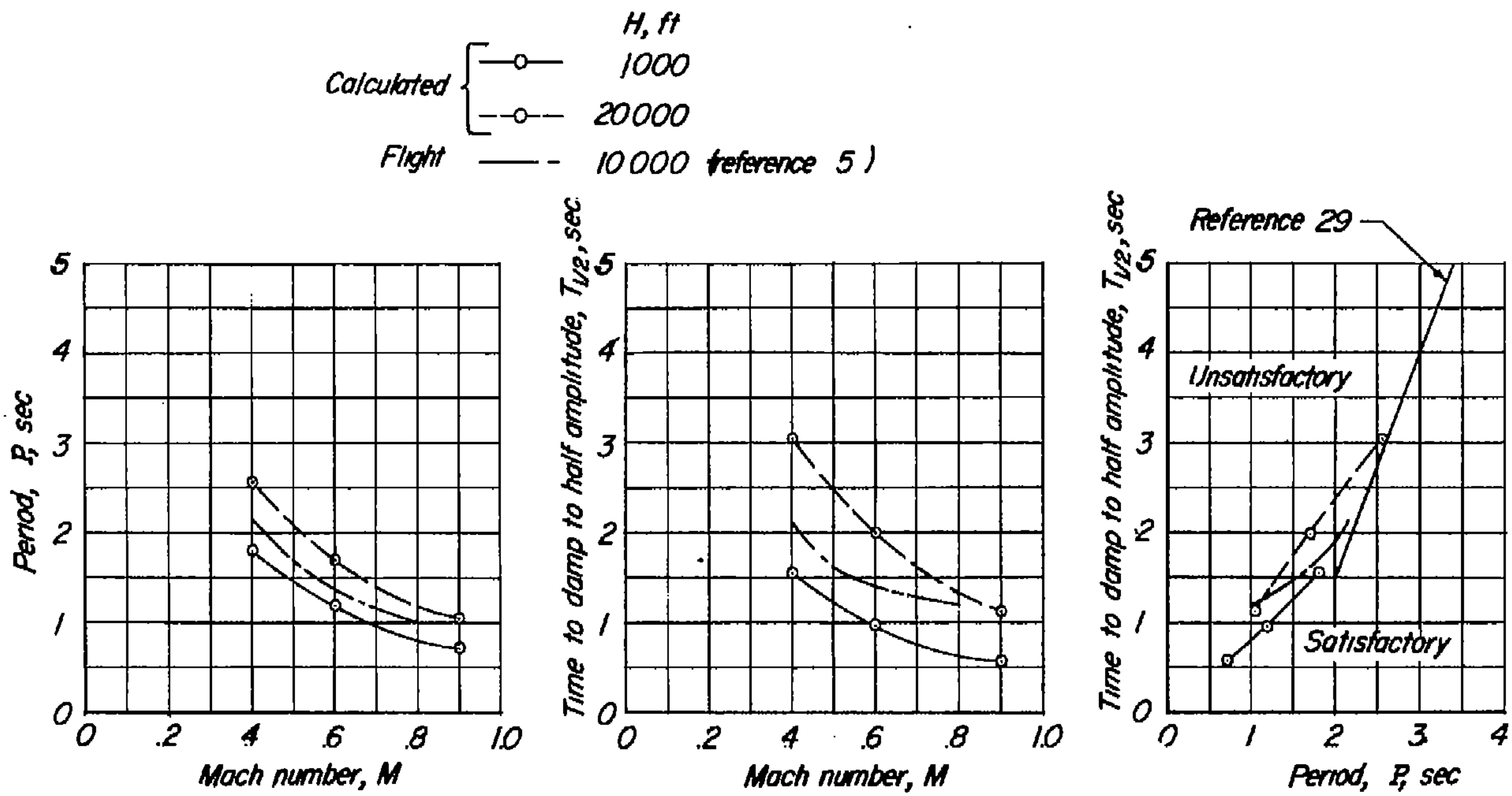

(a) North American F-86A.

Figure 6.- Lateral period and damping characteristics of the airplanes investigated.

[redacted]

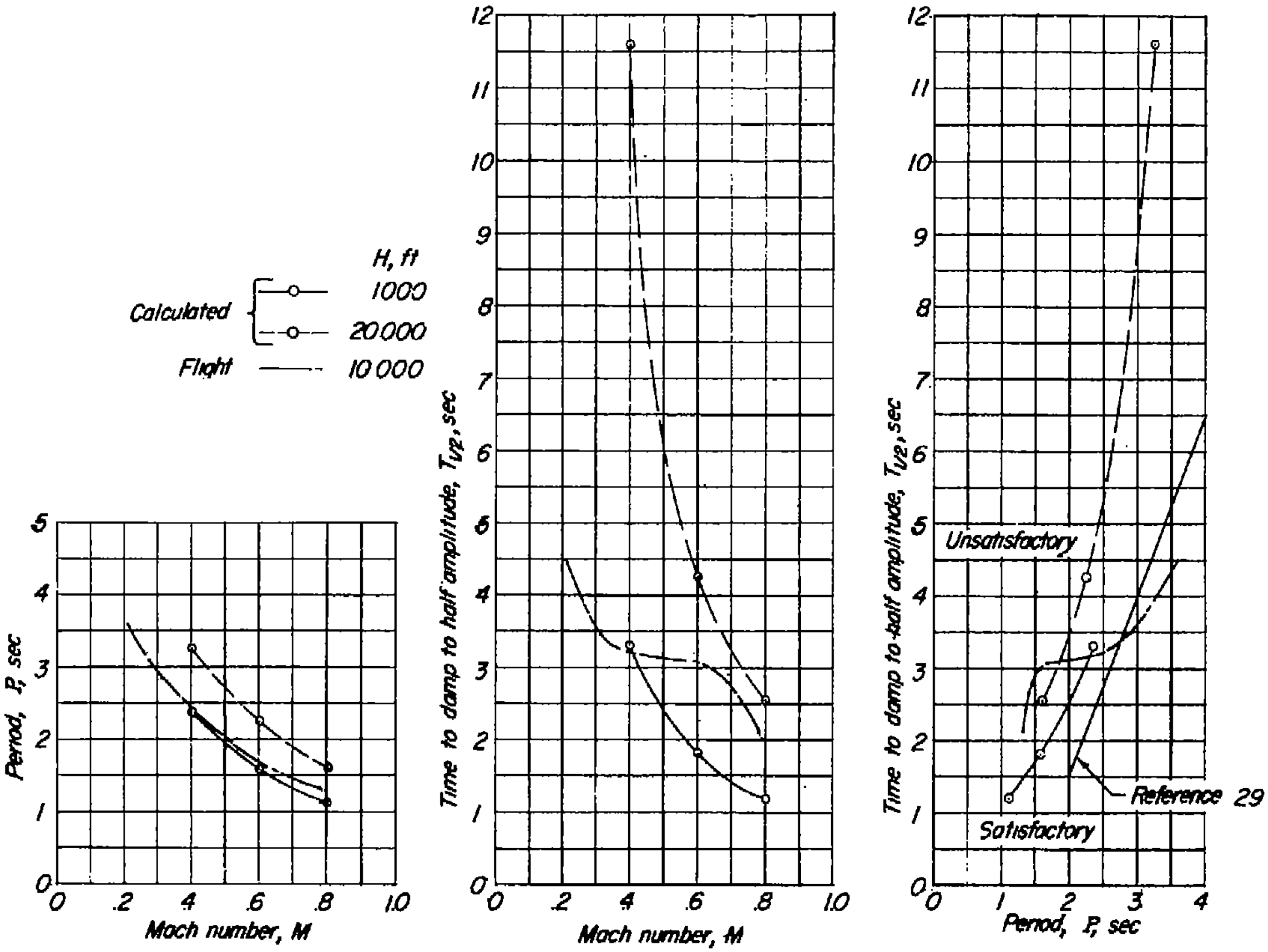

(b) Grumman F9F-2.

Figure 6.- Continued.

[redacted]

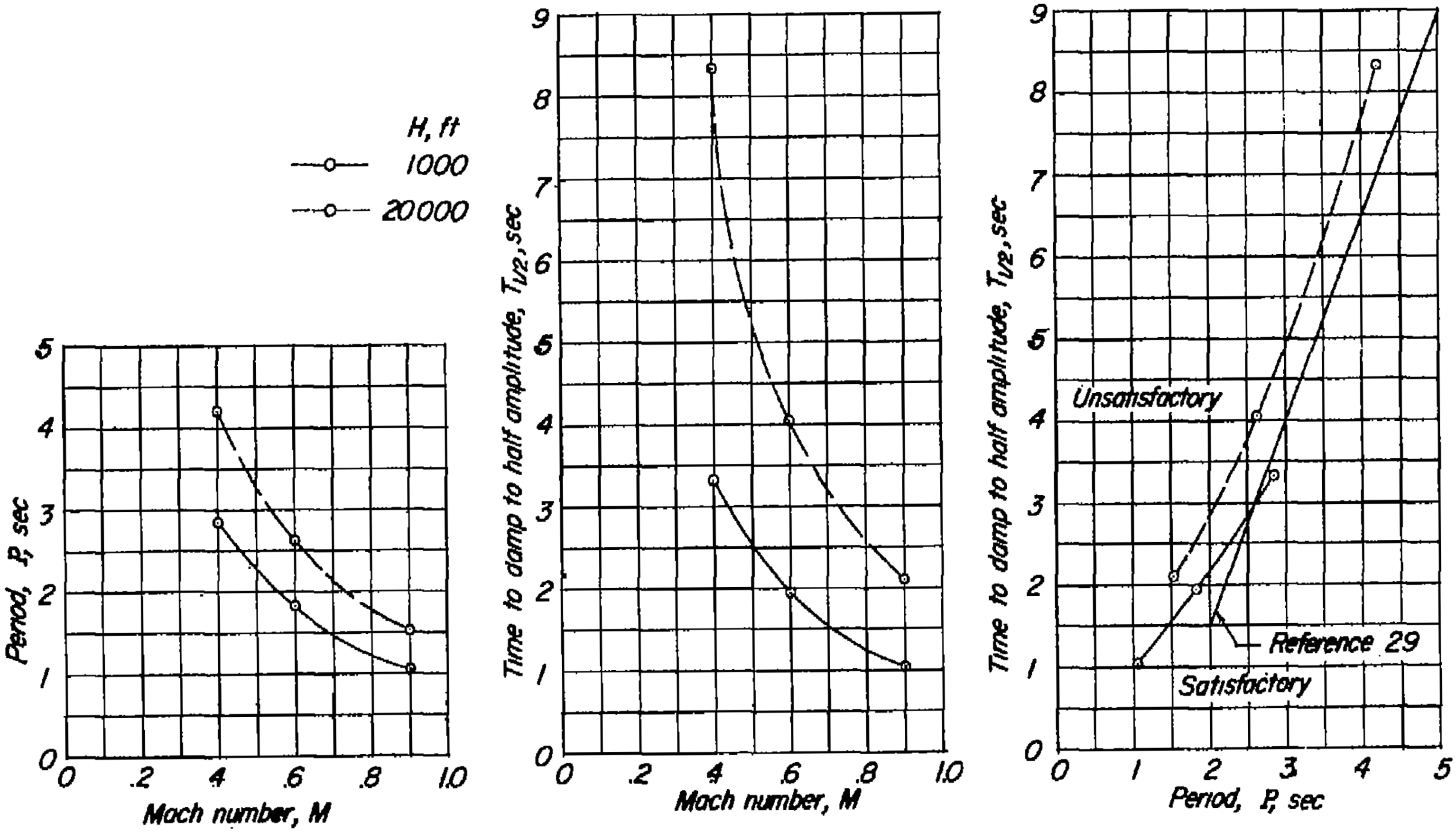

(c) Republic F-84.

Figure 6.- Continued.

[redacted]

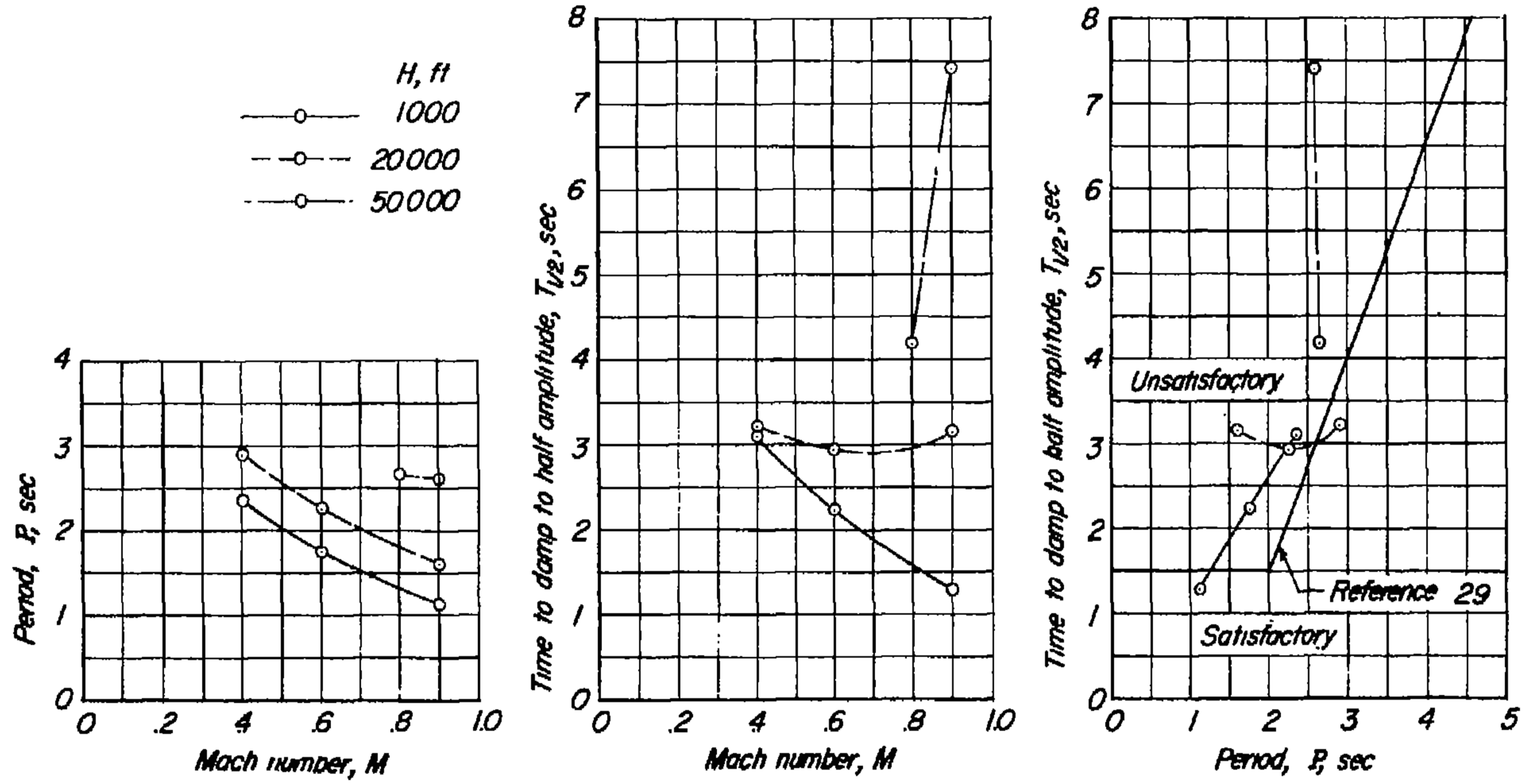

(d) Douglas D-558-II.

Figure 6.- Continued.

[redacted]

[redacted]

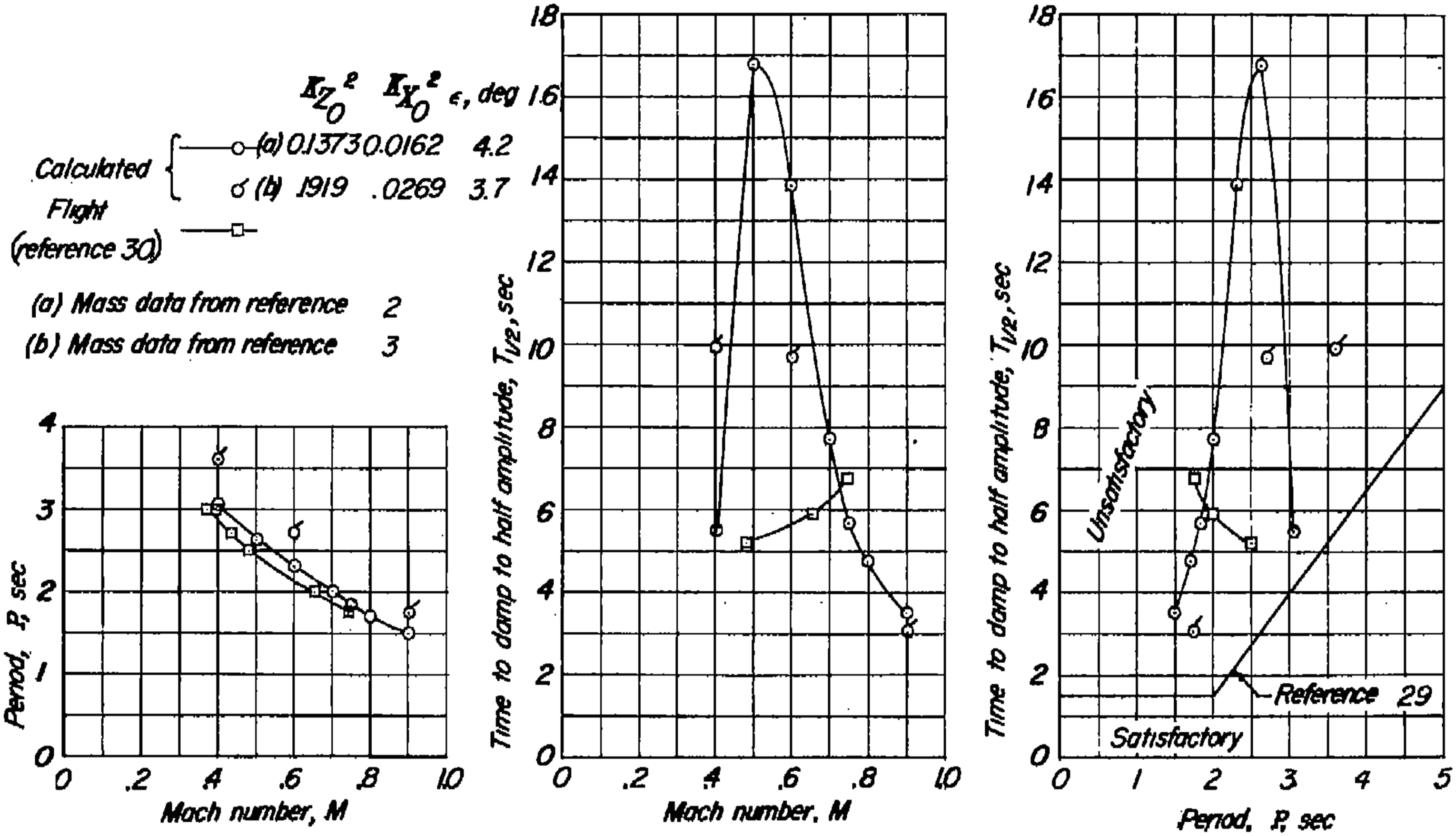

(e) Comparison of calculated and flight values of P and $T_{1/2}$ for the Douglas D-558-II airplane. H = 20,000 feet; W/S_w = 57.1 lb/sq ft.

Figure 6.- Continued.

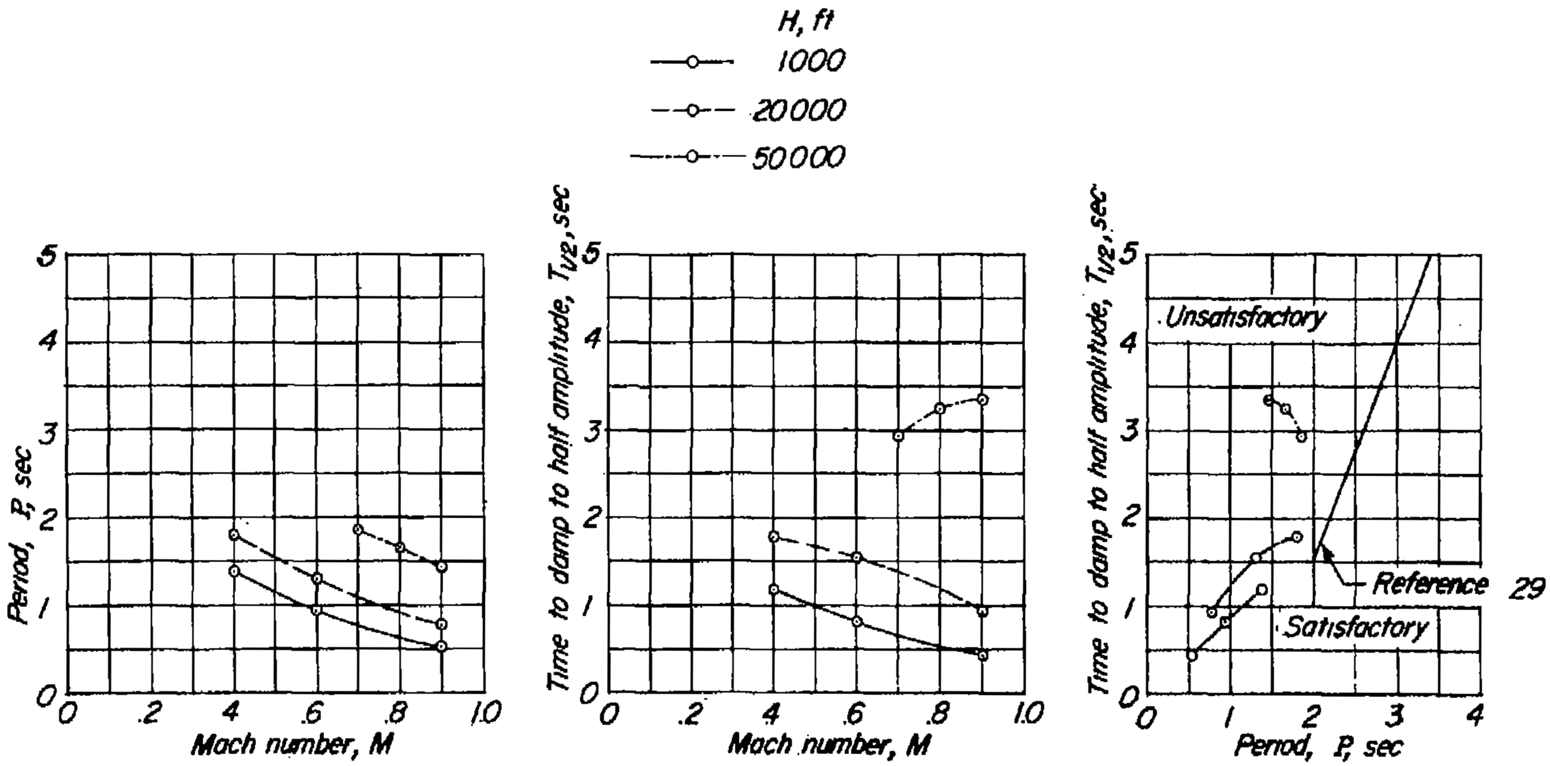

(f) Bell X-1.

Figure 6.- Concluded.

[redacted]

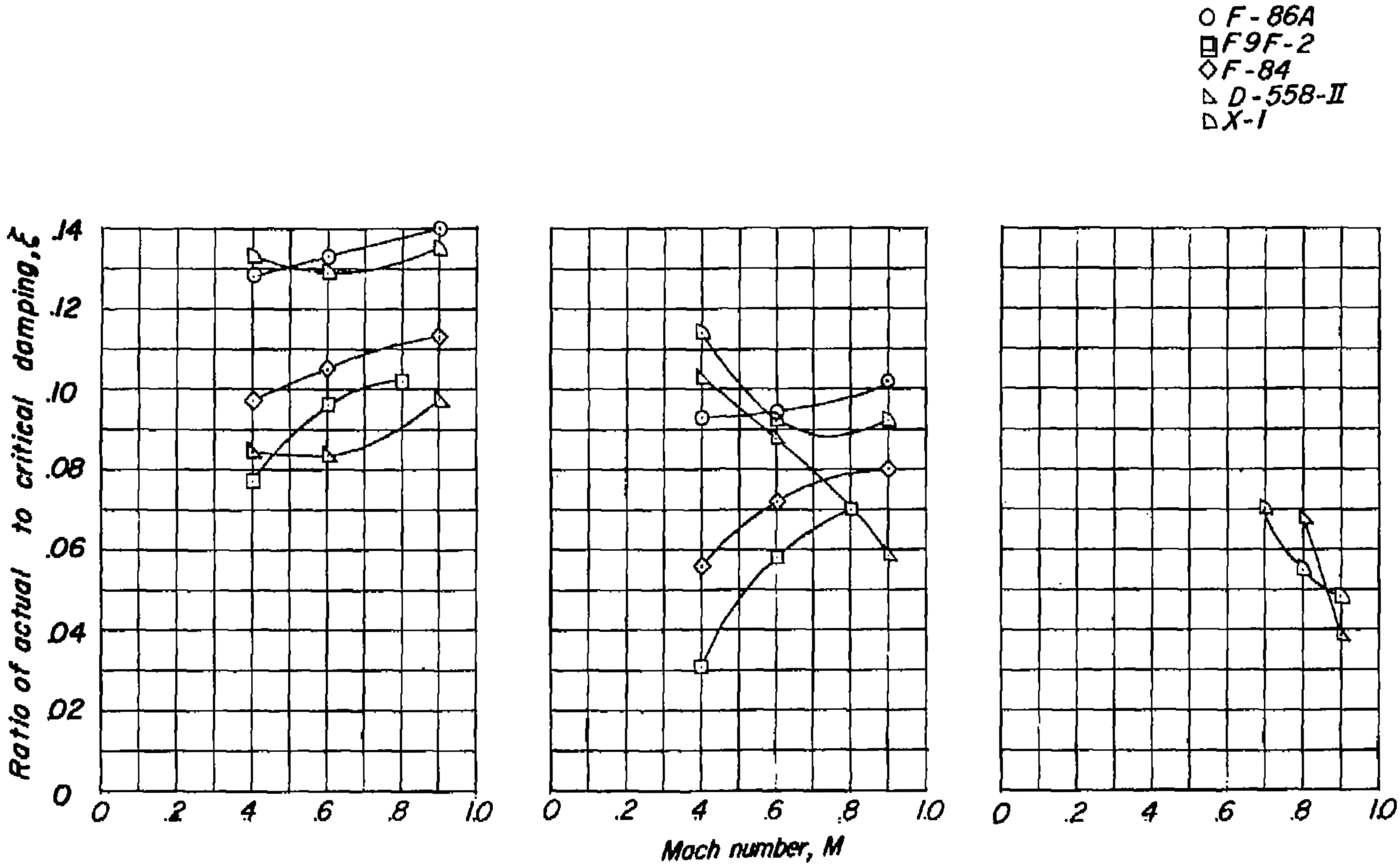

(a) Altitude, 1,000 feet.

(b) Altitude, 20,000 feet.

(c) Altitude, 50,000 feet.

Figure 7.- Effect of Mach number altitude on the ratio of actual to critical damping for the airplanes investigated.

[redacted]

[redacted]

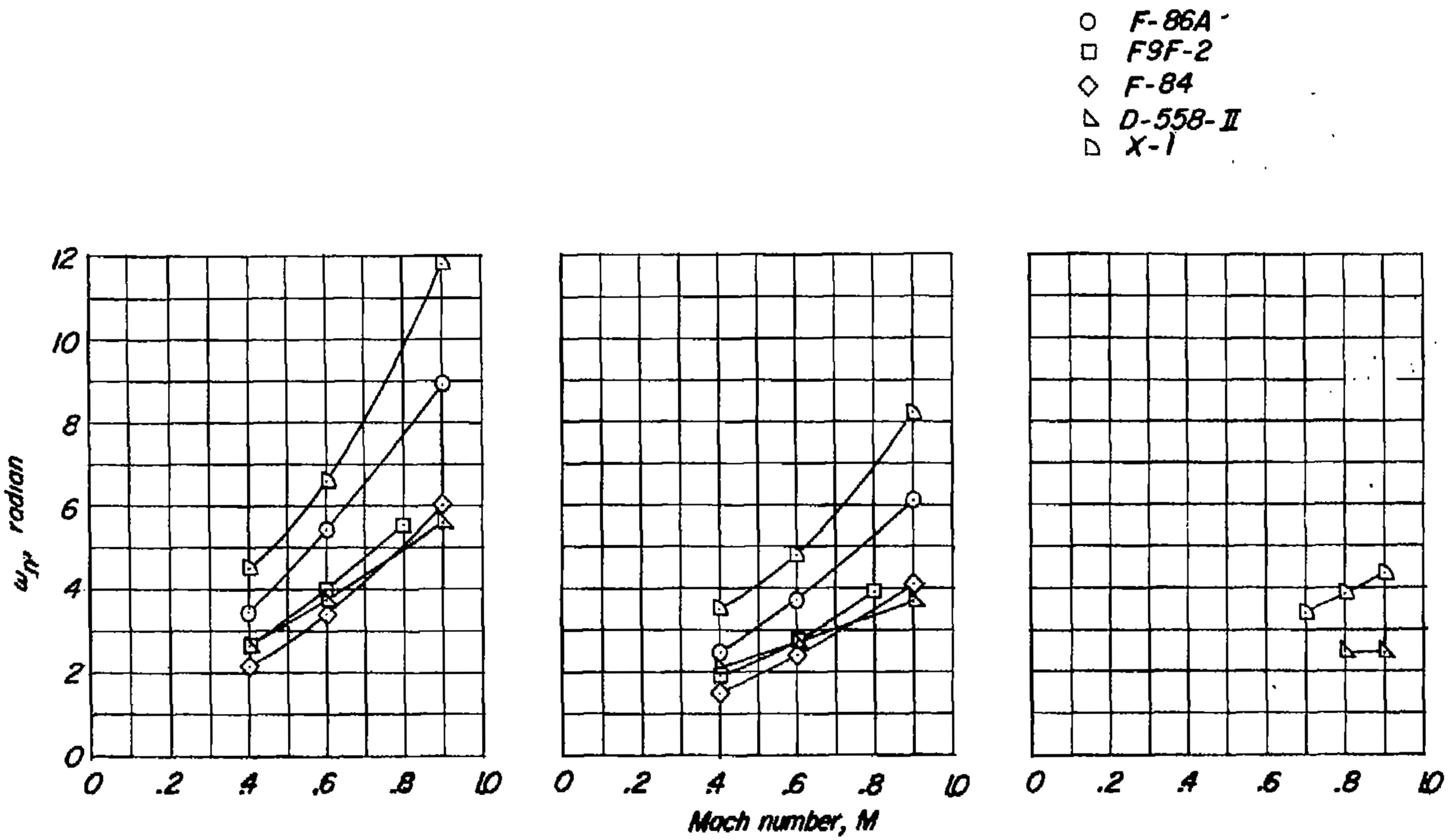

(a) Altitude, 1,000 feet.

(b) Altitude, 20,000 feet.

(c) Altitude, 50,000 feet.

Figure 8.- Variation of the natural frequency with Mach number for the airplanes investigated.

[redacted]

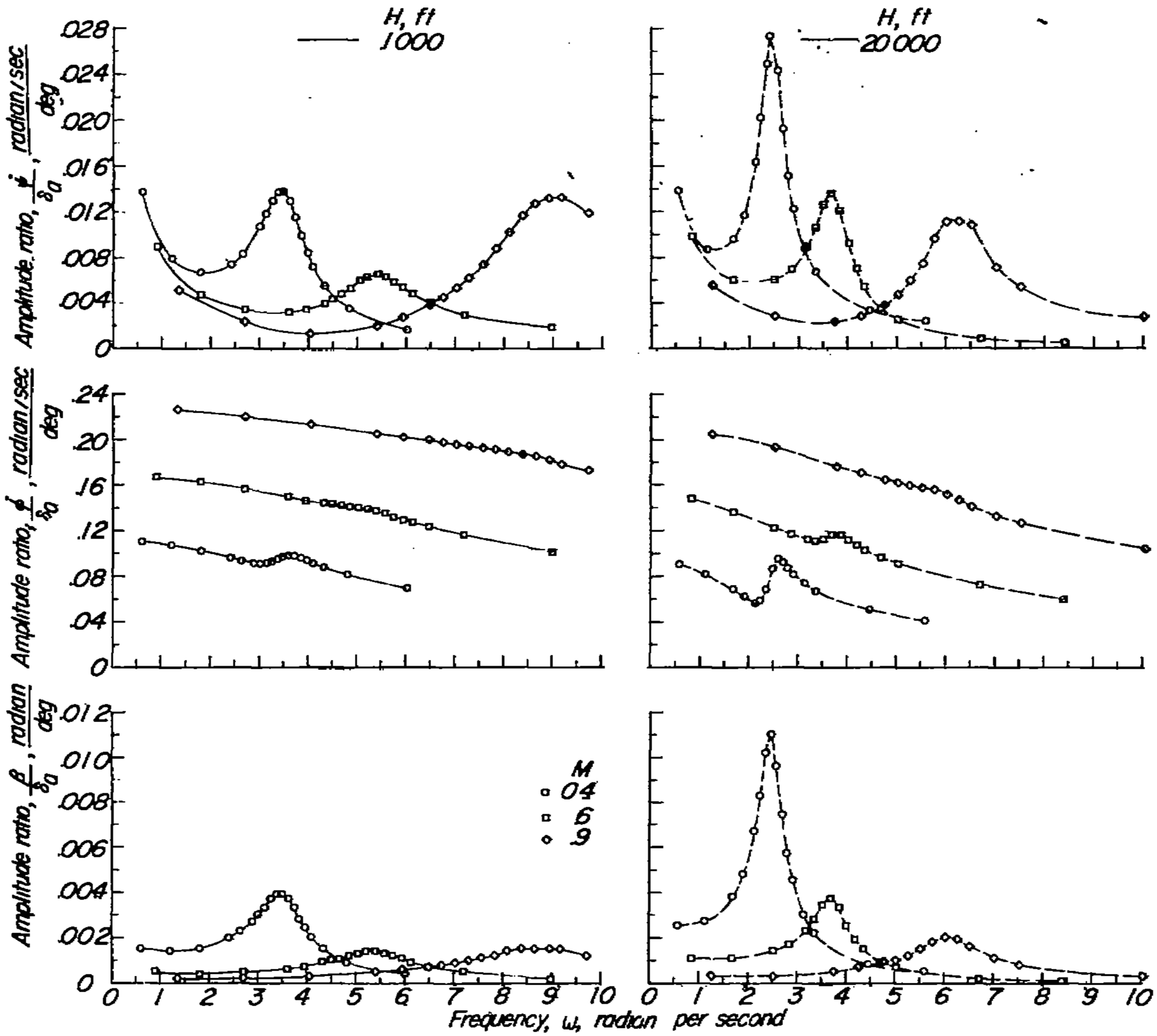

(a) Variation of $\frac{\dot{\psi}}{\delta_a}$, $\frac{\dot{\phi}}{\delta_a}$, and $\frac{\beta}{\delta_a}$ with ω.

Figure 9.- Effect of Mach number and altitude on the lateral frequency response characteristics of the North American F-86A airplane.

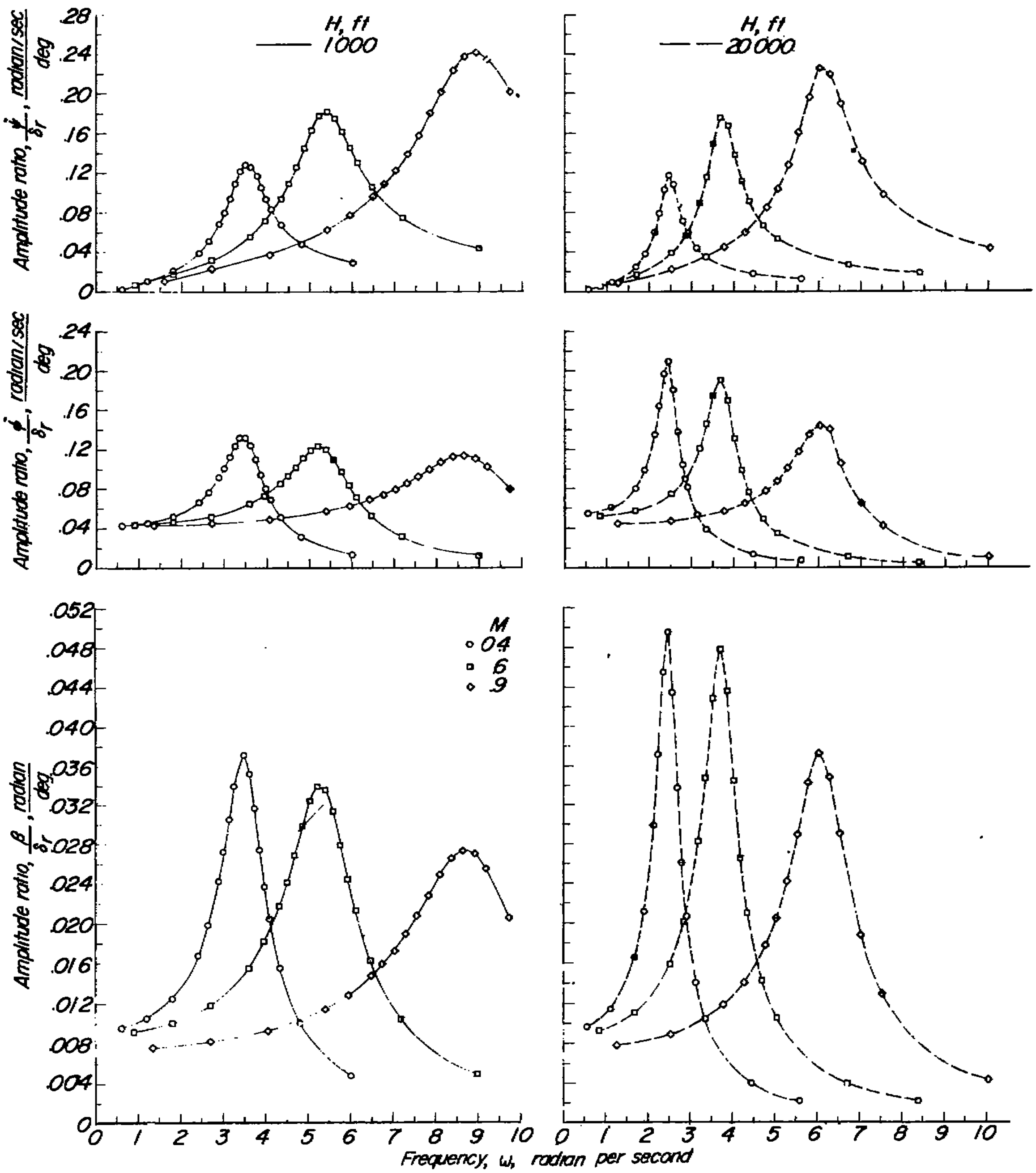

(b) Variation of $\frac{\dot{\psi}}{\delta_r}$, $\frac{\ddot{\phi}}{\delta_r}$, and $\frac{\beta}{\delta_r}$ with ω.

North American F-86A airplane.

Figure 9.- Continued.

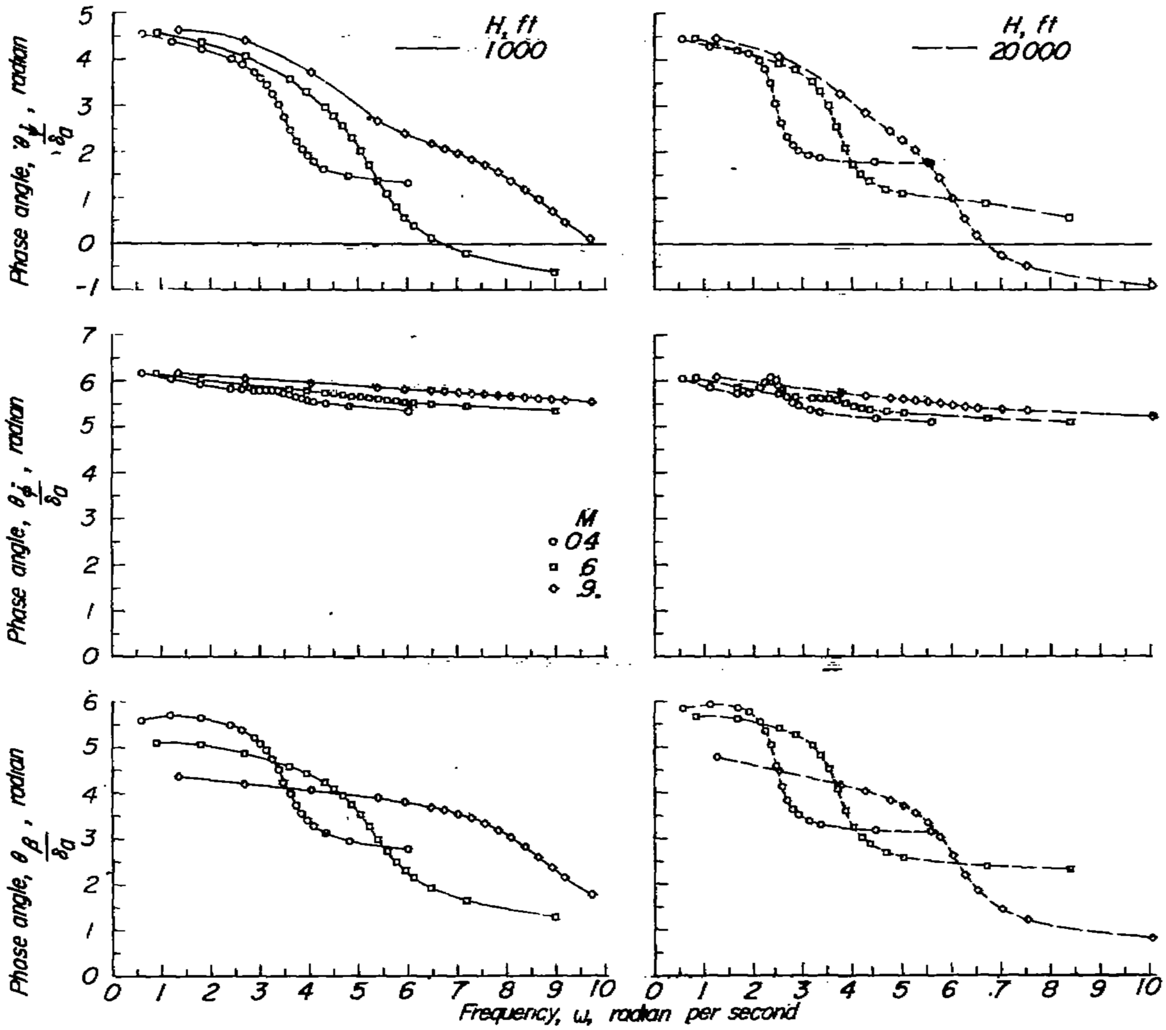

(c) Variation of $\frac{\theta_{\dot{\psi}}}{\delta_a}$, $\frac{\theta_{\dot{\phi}}}{\delta_a}$, and $\frac{\theta_{\beta}}{\delta_a}$ with ω.

North American F-86A airplane.

Figure 9.- Continued.

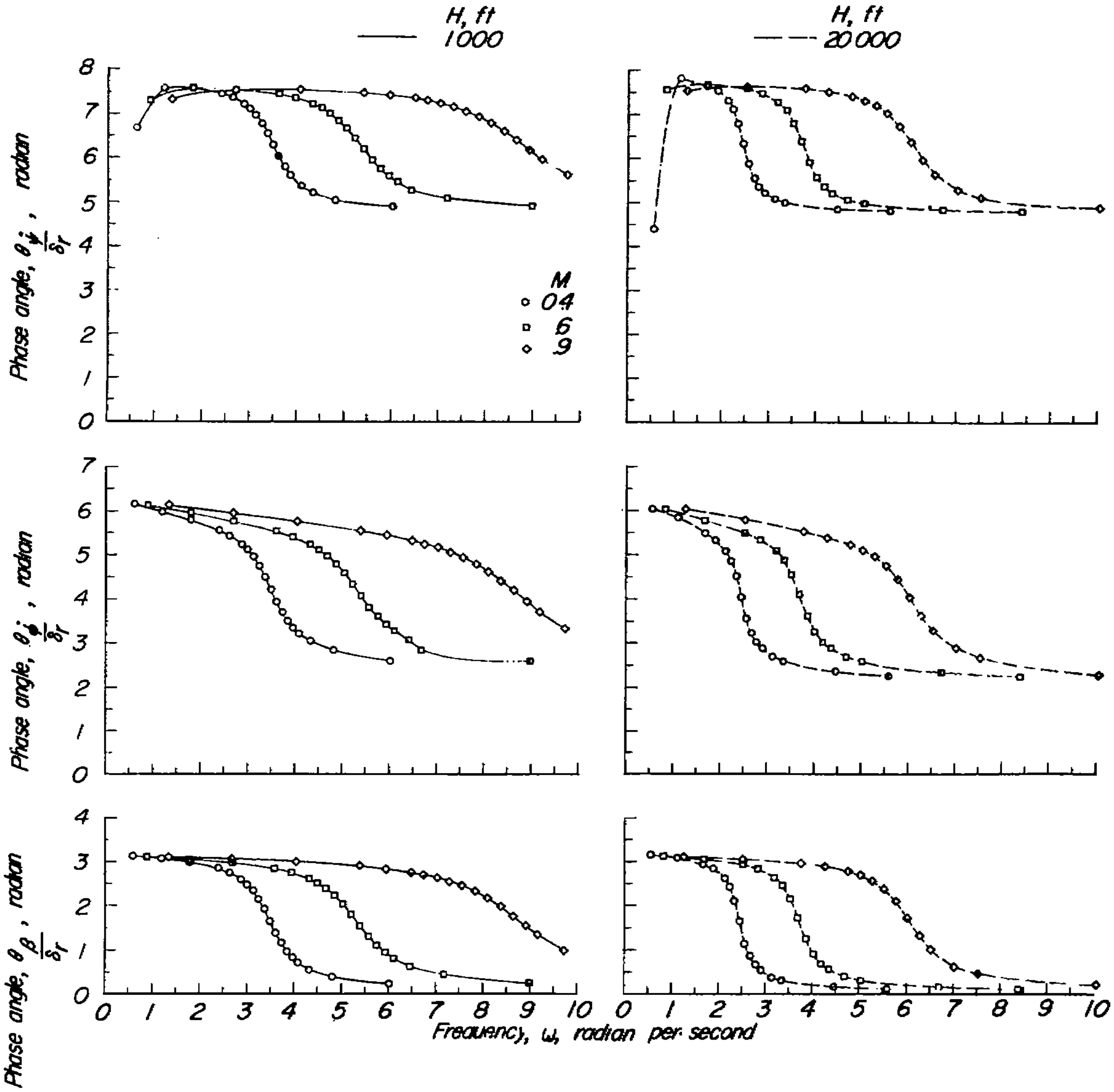

(d) Variation of $\frac{\theta_{\dot{\psi}}}{\delta_r}$, $\frac{\theta_{\dot{\phi}}}{\delta_r}$, and $\frac{\theta_{\beta}}{\delta_r}$ with ω.

North American F-86A airplane.

Figure 9.- Concluded.

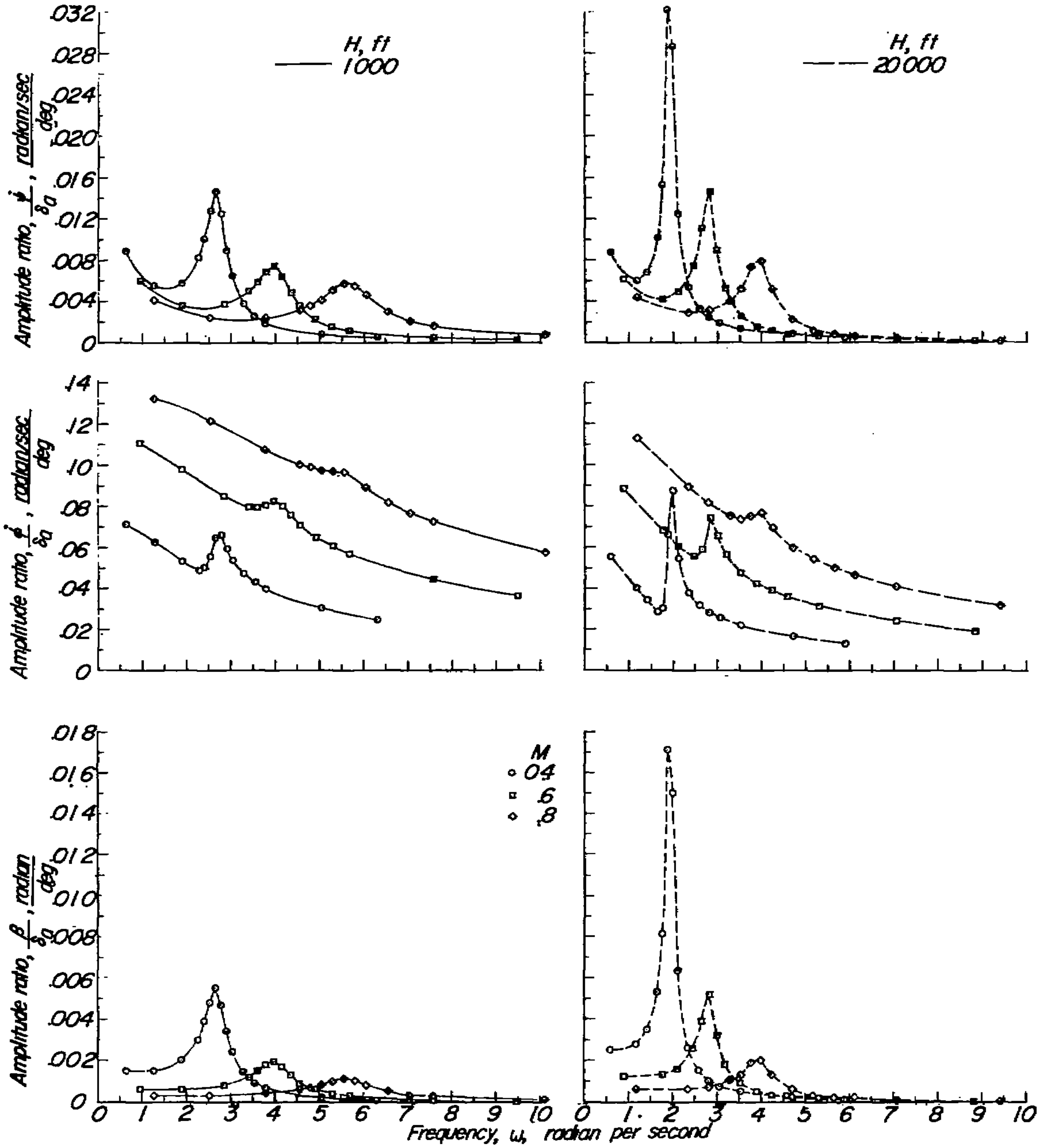

(a) Variation of $\frac{\dot{\psi}}{\delta_a}$, $\frac{\dot{\phi}}{\delta_a}$, and $\frac{\beta}{\delta_a}$ with ω.

Figure 10.- Effect of Mach number and altitude on the lateral frequency response characteristics of the Grumman F9F-2 airplane.

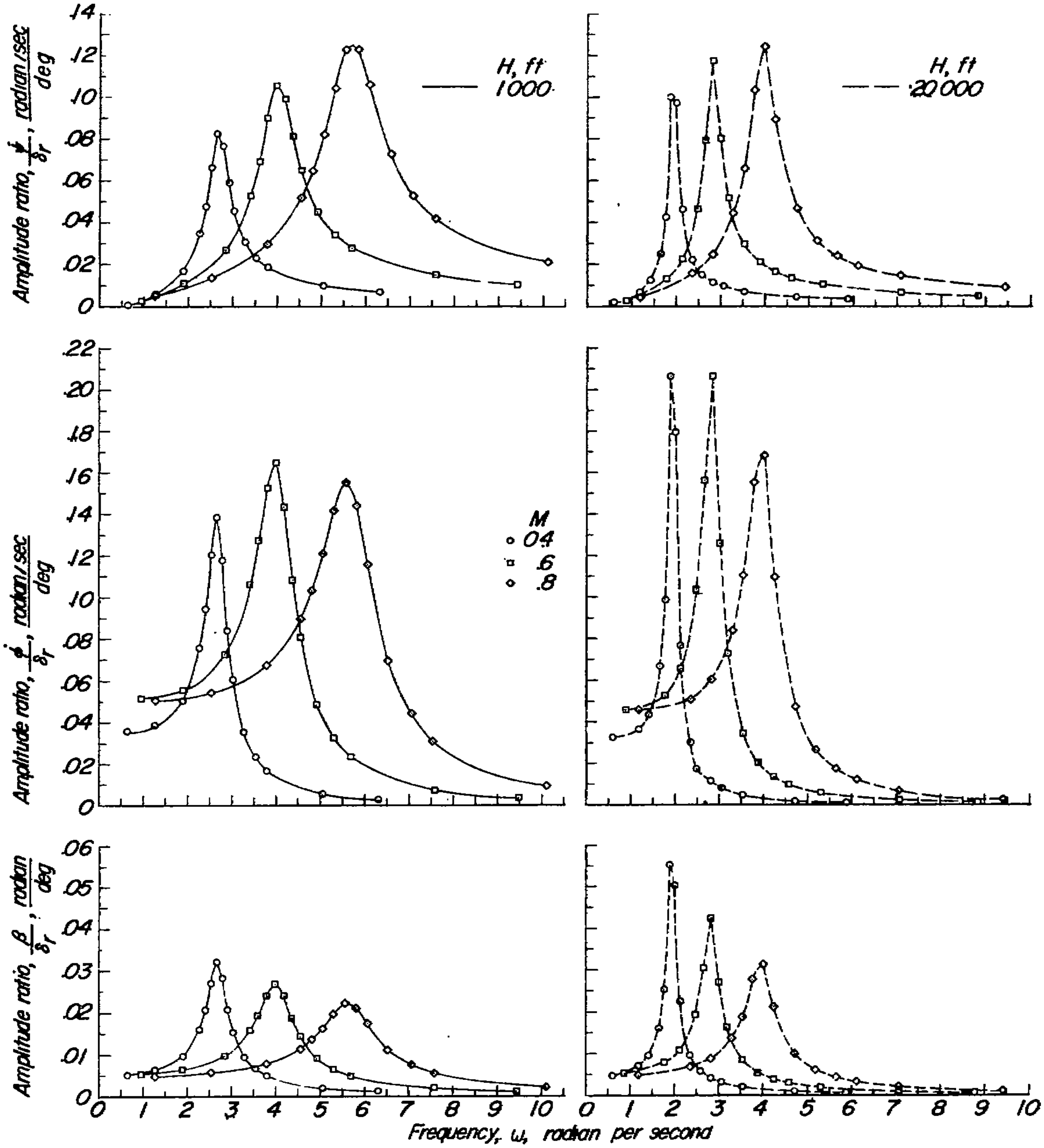

(b) Variation of $\frac{\dot{\psi}}{\delta_r}$, $\frac{\dot{\phi}}{\delta_r}$, and $\frac{\beta}{\delta_r}$ with ω.
Grumman F9F-2 airplane.

Figure 10.- Continued.

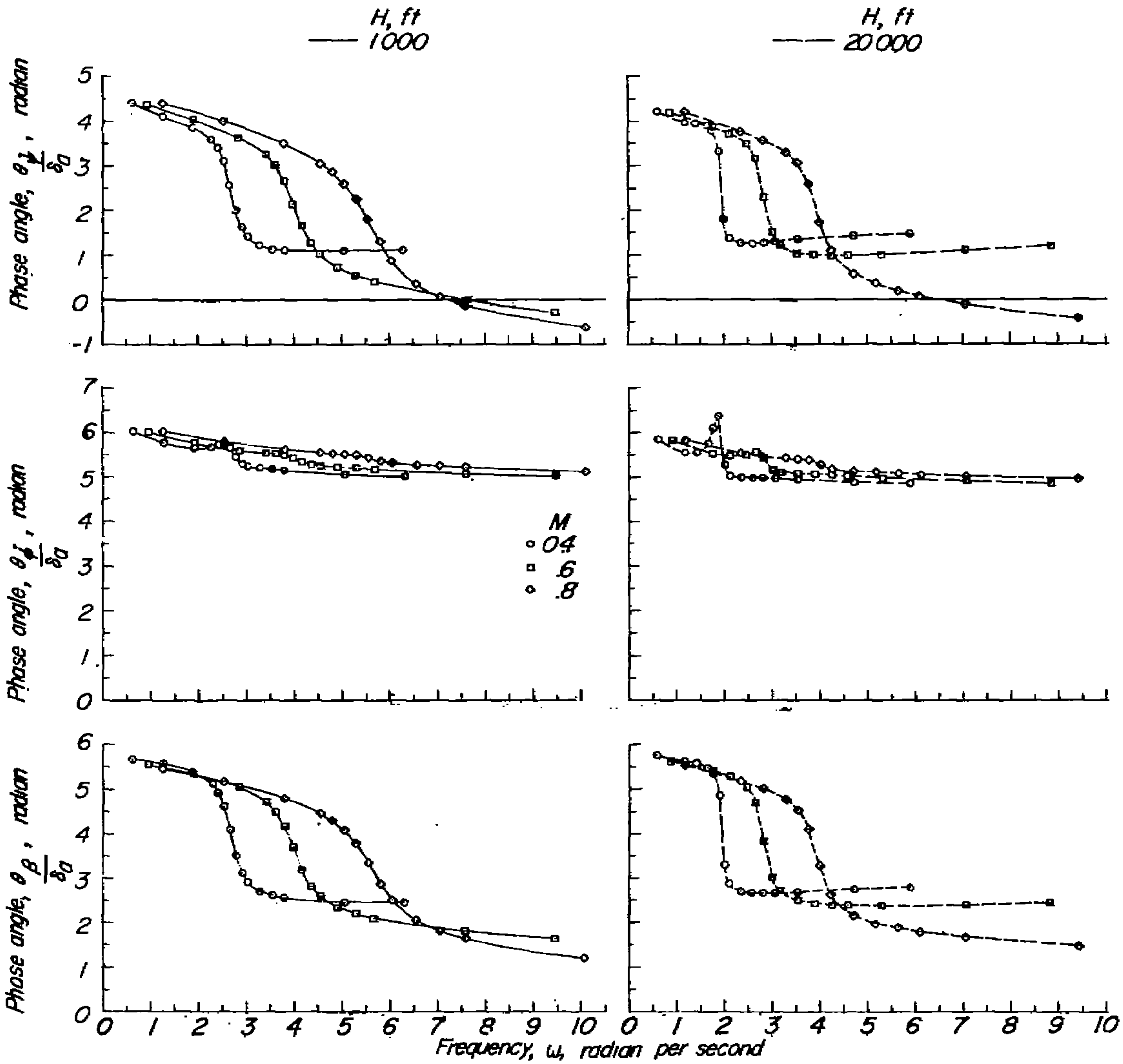

(c) Variation of $\frac{\theta_{\dot{\psi}}}{\delta_a}$, $\frac{\theta_{\dot{\phi}}}{\delta_a}$, and $\frac{\theta_\beta}{\delta_a}$ with ω.

Grumman F9F-2 airplane.

Figure 10.- Continued.

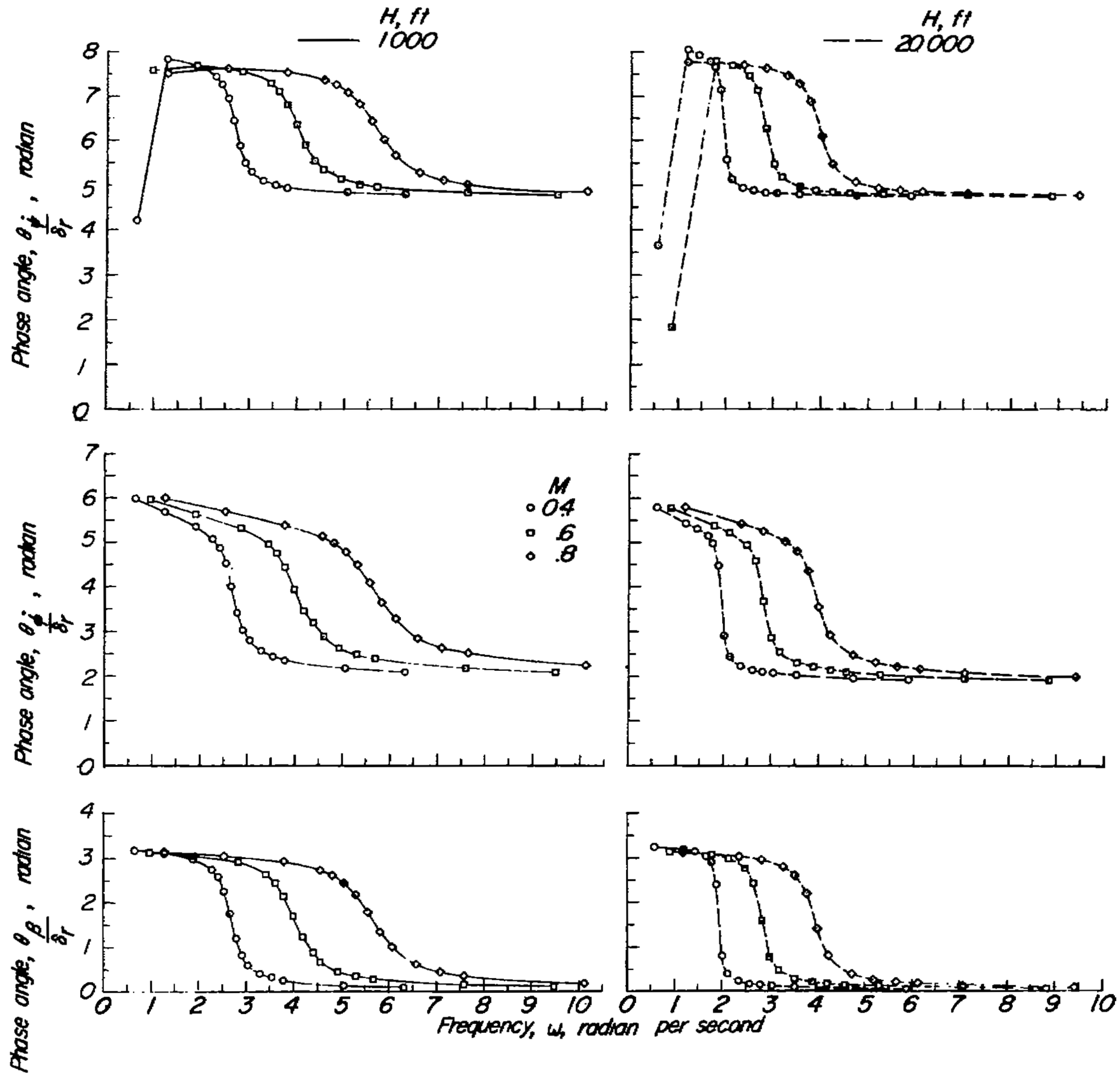

(d) Variation of $\frac{\theta_{\dot\psi}}{\delta_r}$, $\frac{\theta_{\dot\phi}}{\delta_r}$, and $\frac{\theta_\beta}{\delta_r}$ with ω.

Grumman F9F-2 airplane.

Figure 10.- Concluded.

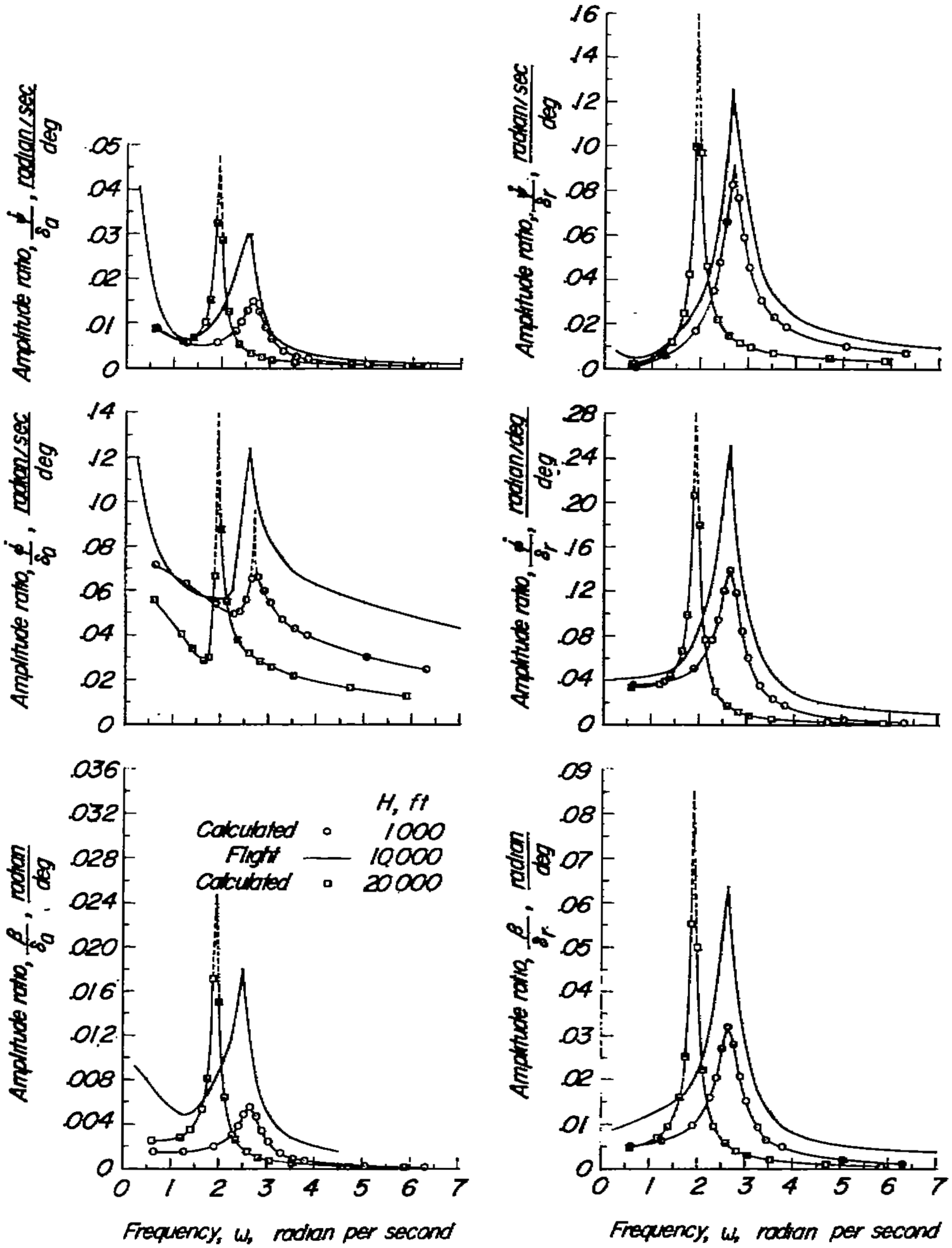

(a) Variation of $\frac{\dot{\psi}}{\delta_a}$, $\frac{\dot{\phi}}{\delta_a}$, and $\frac{\beta}{\delta_a}$ with ω.

(b) Variation of $\frac{\dot{\psi}}{\delta_r}$, $\frac{\dot{\phi}}{\delta_r}$, and $\frac{\beta}{\delta_r}$ with ω.

Figure 11.- Comparison of calculated and flight lateral frequency response characteristics of the Grumman F9F-2 airplane. M = 0.4.

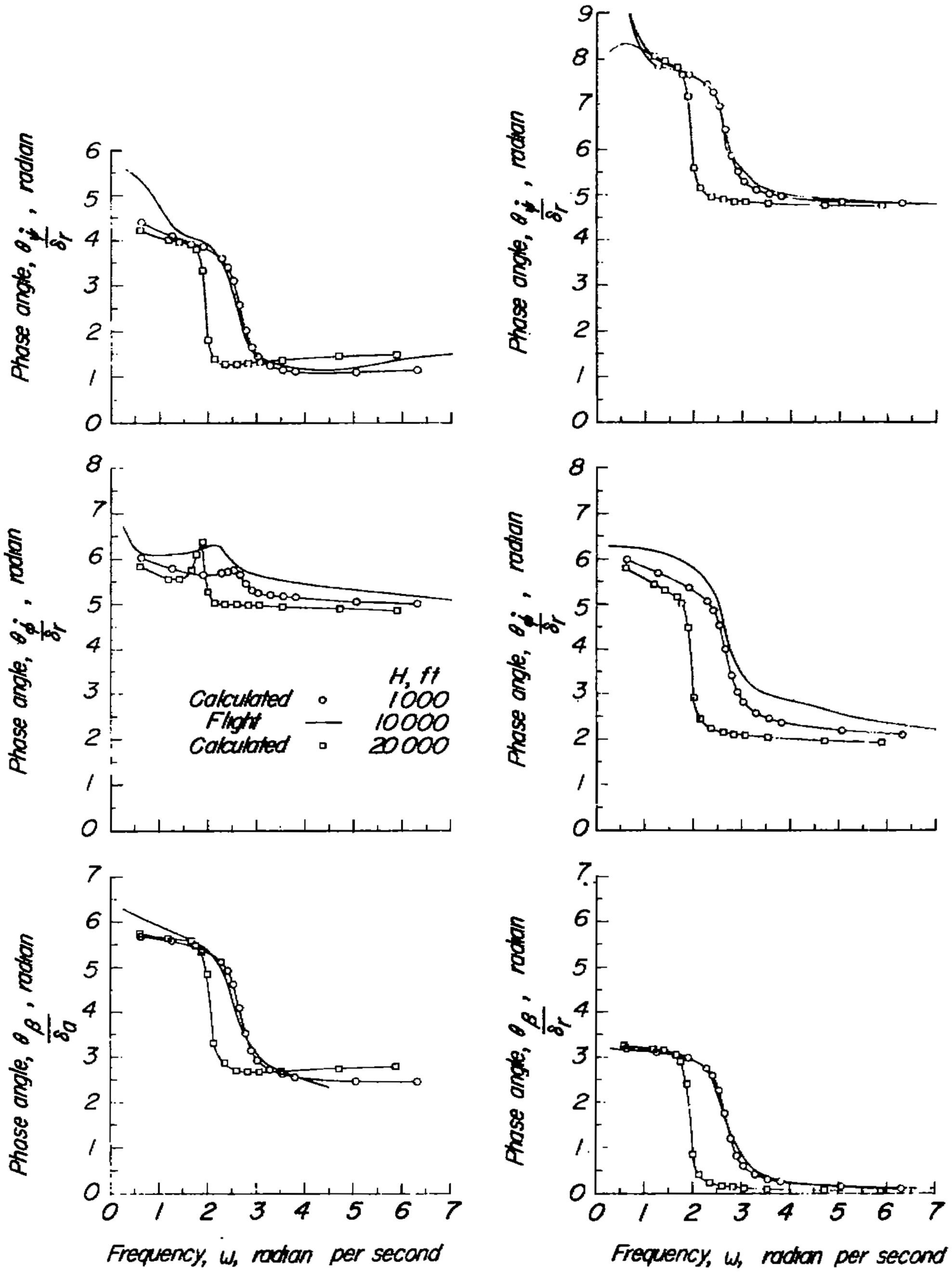

(c) Variation of $\frac{\theta_{\dot{\psi}}}{\delta_a}$, $\frac{\theta_{\dot{\phi}}}{\delta_a}$, and $\frac{\theta_{\beta}}{\delta_a}$ with ω. Grumman F9F-2 airplane.

(d) Variation of $\frac{\theta_{\dot{\psi}}}{\delta_r}$, $\frac{\theta_{\dot{\phi}}}{\delta_r}$, and $\frac{\theta_{\beta}}{\delta_r}$ with ω. Grumman F9F-2 airplane.

Figure 11.- Concluded.

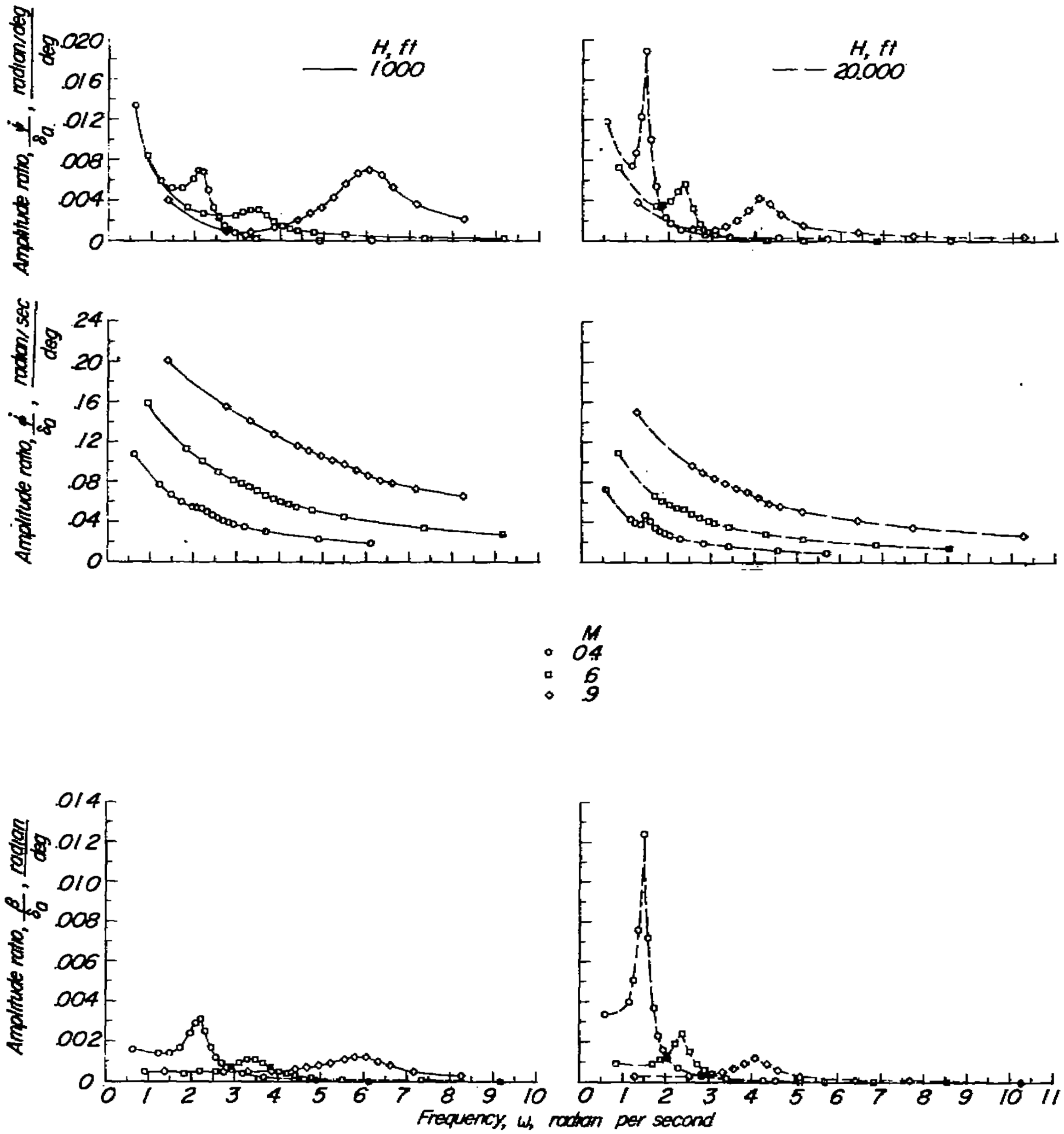

(a) Variation of $\frac{\dot{\psi}}{\delta_a}$, $\frac{\dot{\phi}}{\delta_a}$, and $\frac{\beta}{\delta_a}$ with ω.

Figure 12.- Effect of Mach number and altitude on the lateral frequency response characteristics of the Republic F-84 airplane.

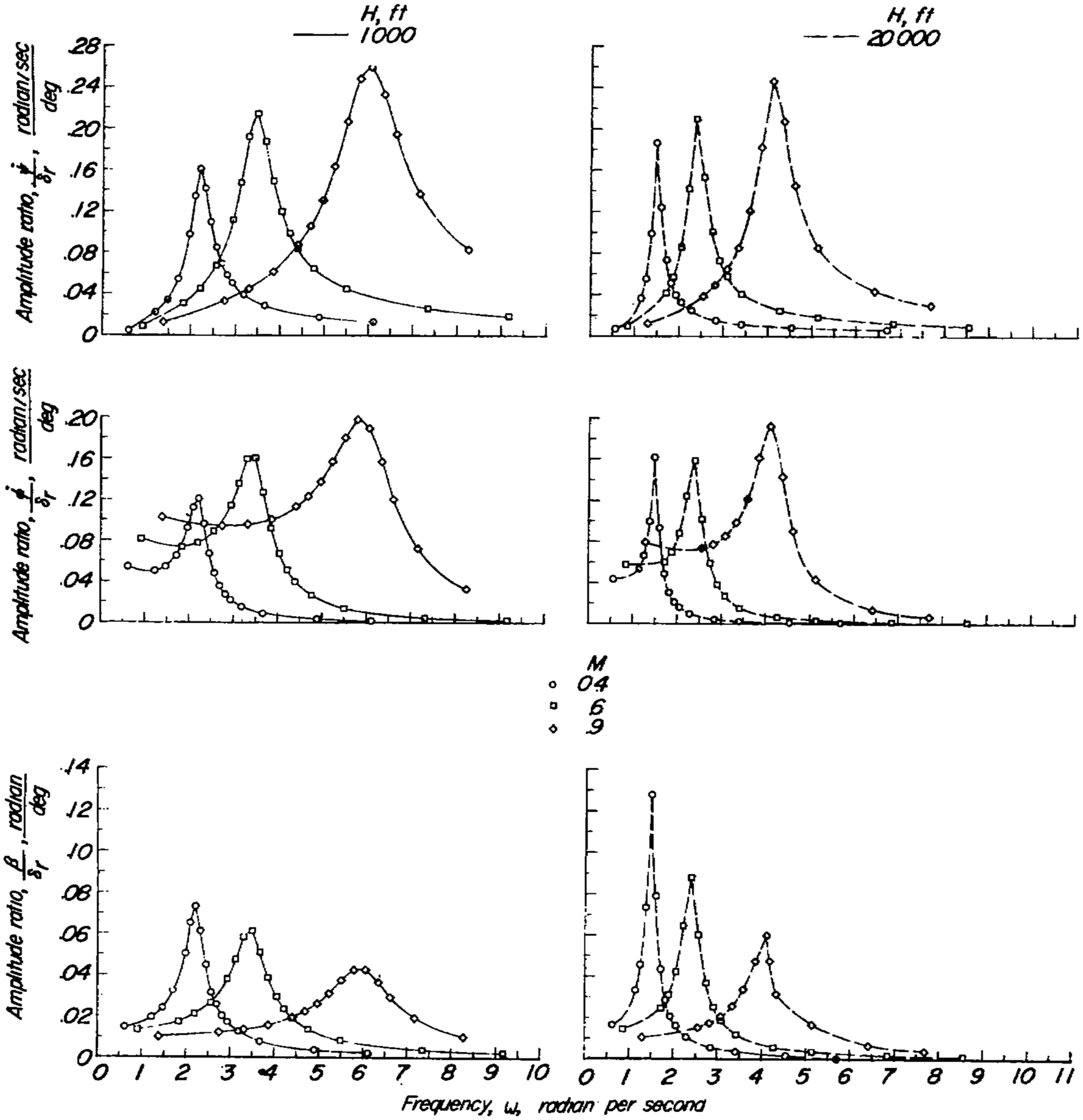

(b) Variation of $\frac{\dot{\psi}}{\delta_r}$, $\frac{\dot{\phi}}{\delta_r}$, and $\frac{\beta}{\delta_r}$ with ω.

Republic F-84 airplane.

Figure 12.- Continued.

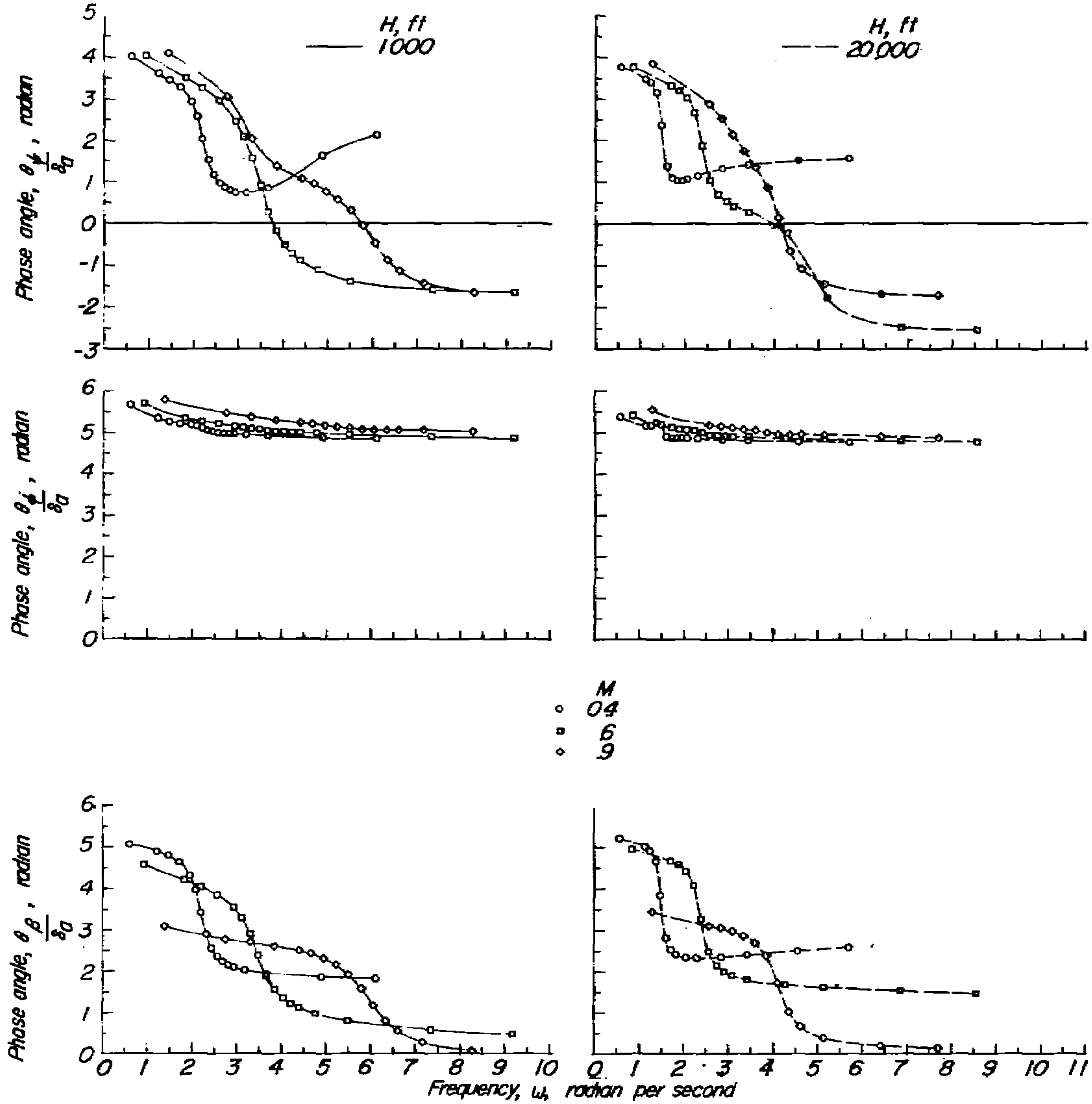

(c) Variation of $\frac{\theta_{\dot{\psi}}}{\delta_a}$, $\frac{\theta_{\dot{\phi}}}{\delta_a}$, and $\frac{\theta_{\beta}}{\delta_a}$ with ω.

Republic F-84 airplane.

Figure 12.- Continued.

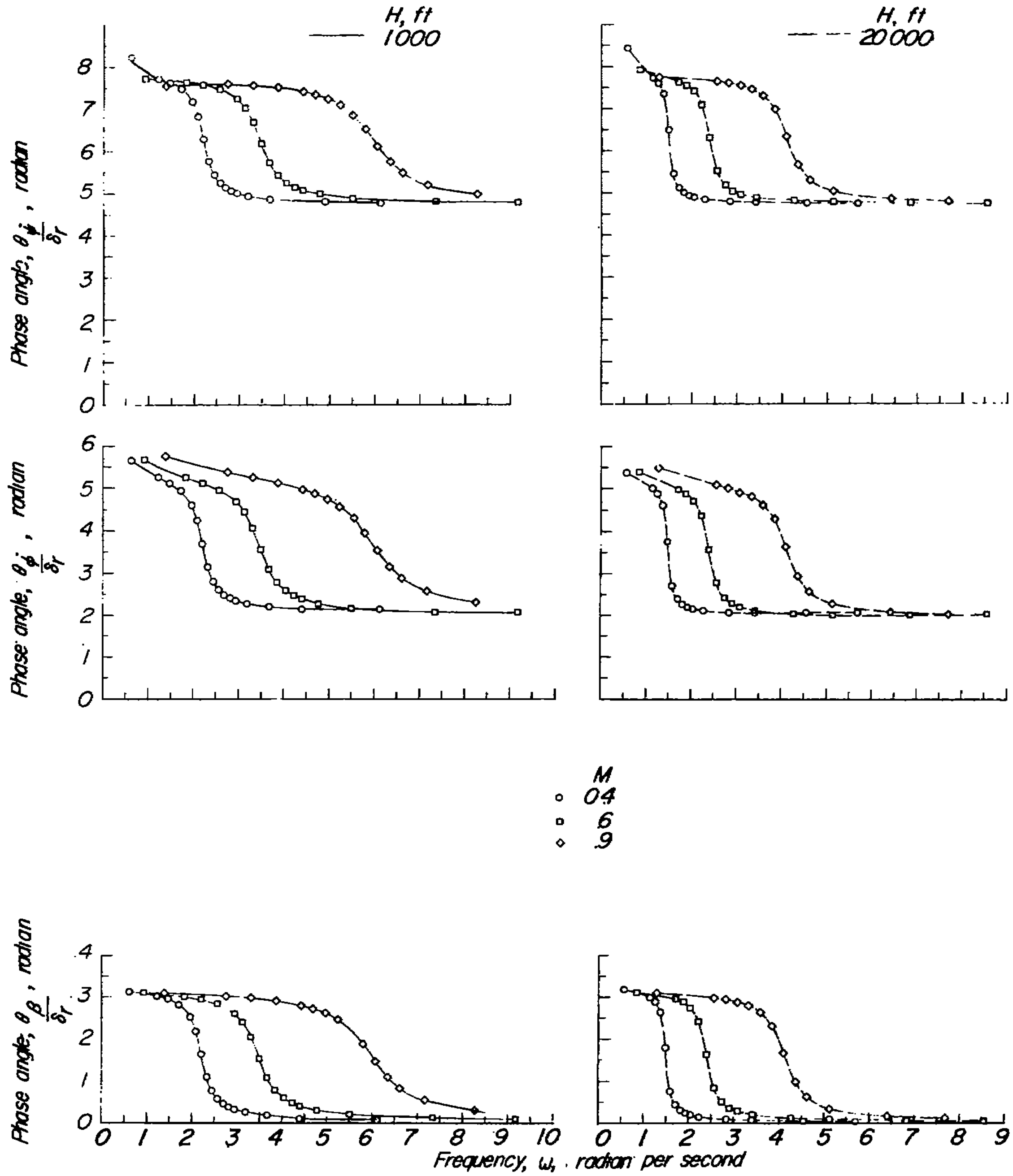

(d) Variation of $\frac{\theta_{\dot{\psi}}}{\delta_r}$, $\frac{\theta_{\dot{\phi}}}{\delta_r}$, and $\frac{\theta_\beta}{\delta_r}$ with ω.

Republic F-84 airplane.

Figure 12.- Concluded.

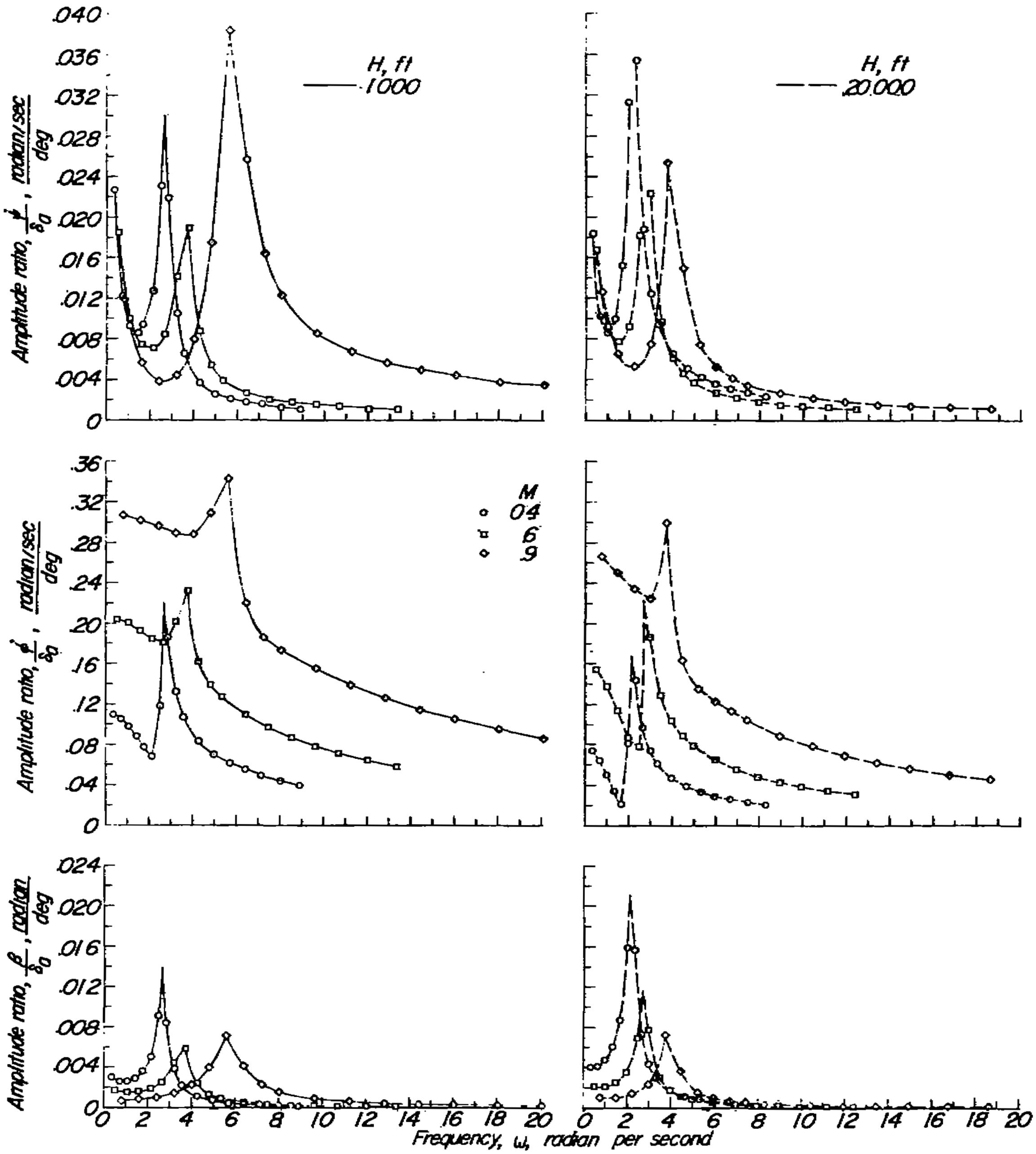

(a) Variation of $\frac{\dot{\psi}}{\delta_a}$, $\frac{\dot{\phi}}{\delta_a}$, and $\frac{\beta}{\delta_a}$ with ω.

Figure 13.- Effect of Mach number and altitude on the lateral frequency response characteristics of the Douglas D-558-II airplane.

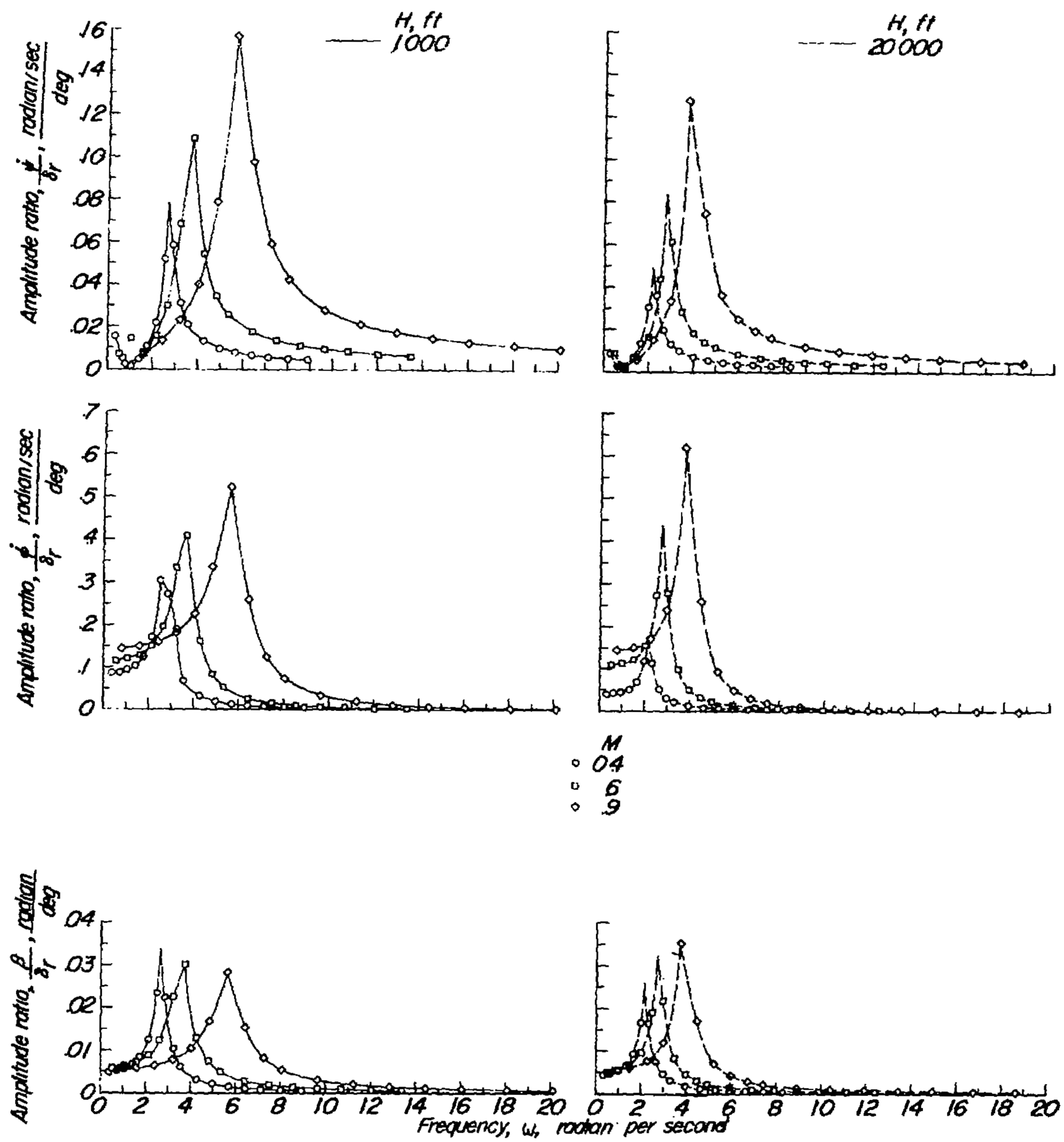

(b) Variation of $\frac{\dot\psi}{\delta_r}$, $\frac{\dot\phi}{\delta_r}$, and $\frac{\beta}{\delta_r}$ with ω.

Douglas D-558-II airplane.

Figure 13.- Continued.

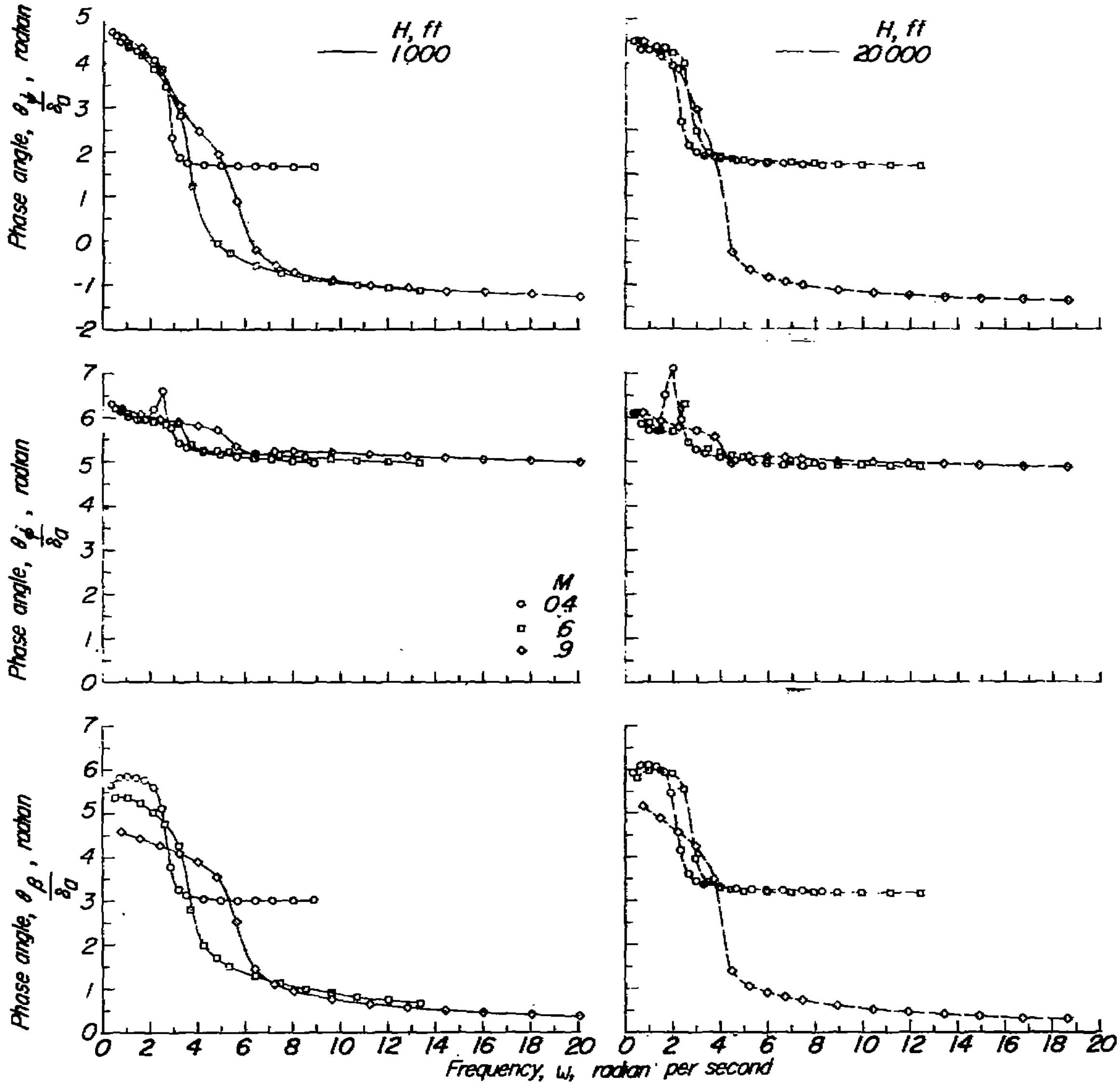

(c) Variation of $\frac{\theta_{\dot\psi}}{\delta_a}$, $\frac{\theta_{\dot\phi}}{\delta_a}$, and $\frac{\theta_\beta}{\delta_a}$ with ω.

Douglas D-558-II airplane.

Figure 13.- Continued.

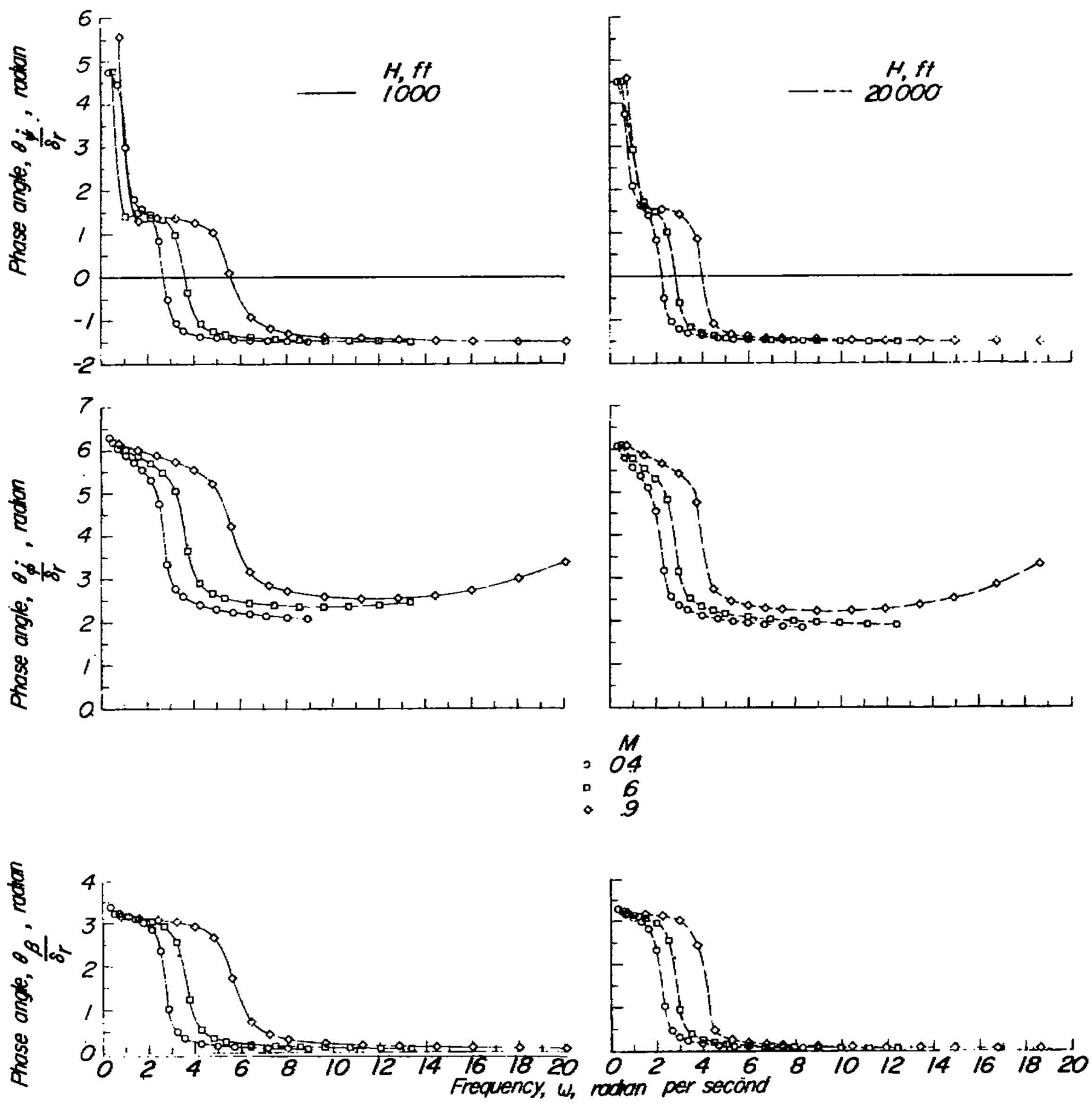

(d) Variation of $\frac{\theta_{\dot{\psi}}}{\delta_r}$, $\frac{\theta_{\ddot{\phi}}}{\delta_r}$, and $\frac{\theta_\beta}{\delta_r}$ with ω.

Douglas D-558-II airplane.

Figure 13.- Concluded.

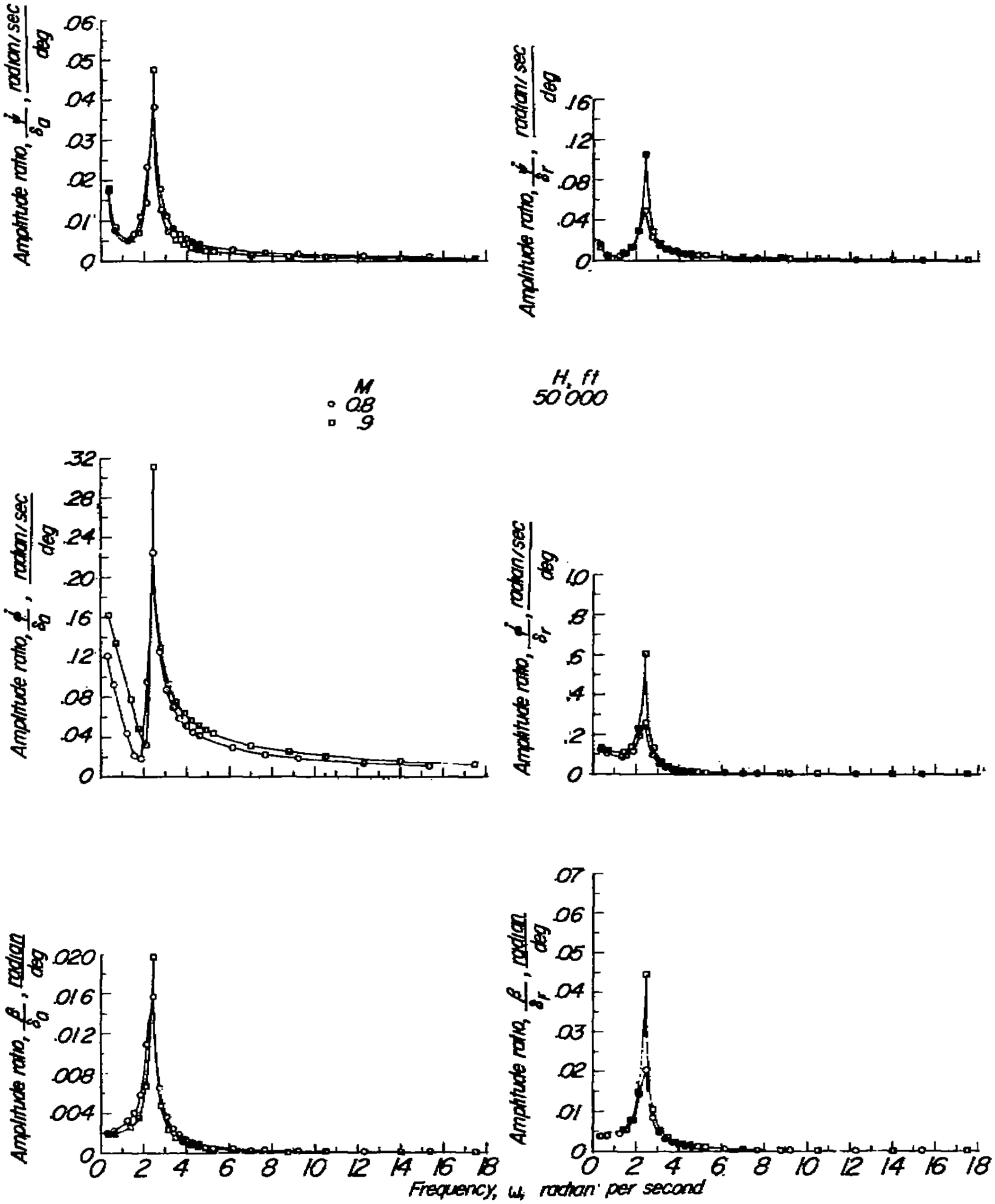

(a) Variation of $\frac{\dot{\psi}}{\delta_a}$, $\frac{\dot{\phi}}{\delta_a}$, and $\frac{\beta}{\delta_a}$ with ω.

(b) Variation of $\frac{\dot{\psi}}{\delta_r}$, $\frac{\dot{\phi}}{\delta_r}$, and $\frac{\beta}{\delta_r}$ with ω.

Figure 14.- Effect of Mach number on the lateral frequency response characteristics of the Douglas D-558-II airplane.

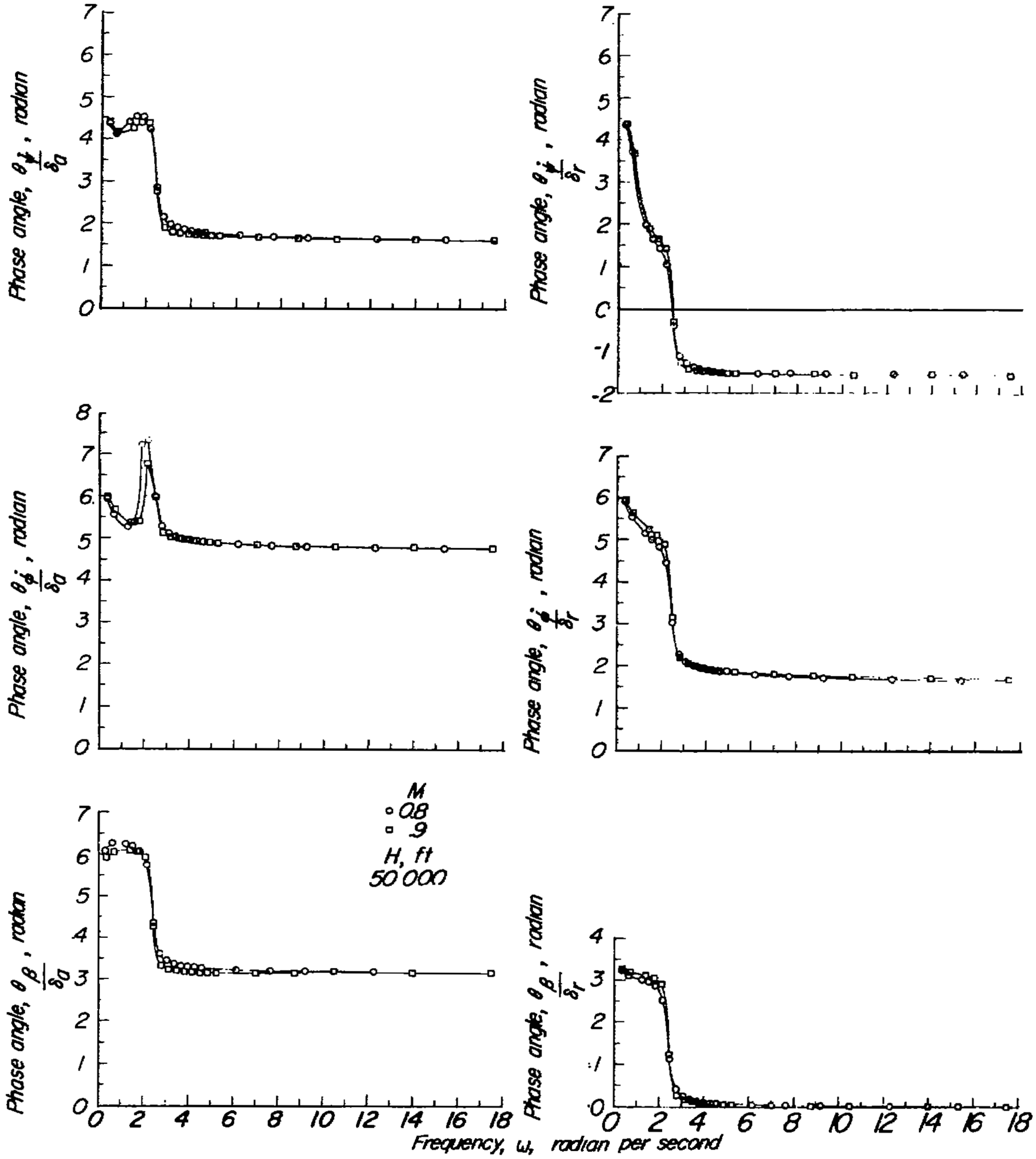

(c) Variation of $\frac{\theta_{\dot{\psi}}}{\delta_a}$, $\frac{\theta_{\dot{\phi}}}{\delta_a}$, and $\frac{\theta_\beta}{\delta_a}$ with ω. Douglas D-558-II airplane.

(d) Variation of $\frac{\theta_{\dot{\psi}}}{\delta_r}$, $\frac{\theta_{\dot{\phi}}}{\delta_r}$, and $\frac{\theta_\beta}{\delta_r}$ with ω. Douglas D-558-II airplane.

Figure 14.- Concluded.

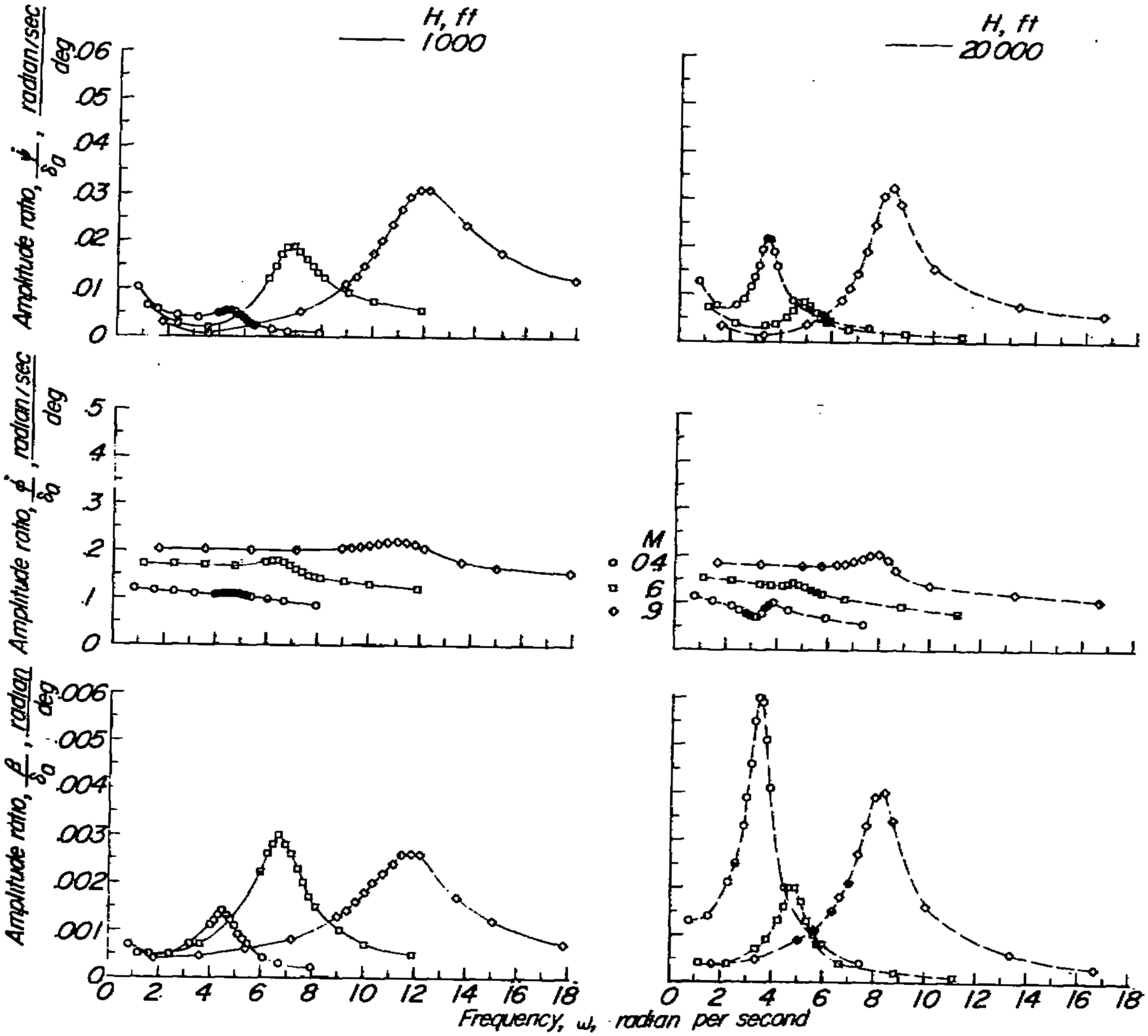

(a) Variation of $\frac{\dot{\psi}}{\delta_a}$, $\frac{\dot{\phi}}{\delta_a}$, and $\frac{\beta}{\delta_a}$ with ω.

Figure 15.- Effect of Mach number and altitude on the lateral frequency response characteristics of the Bell X-1 airplane.

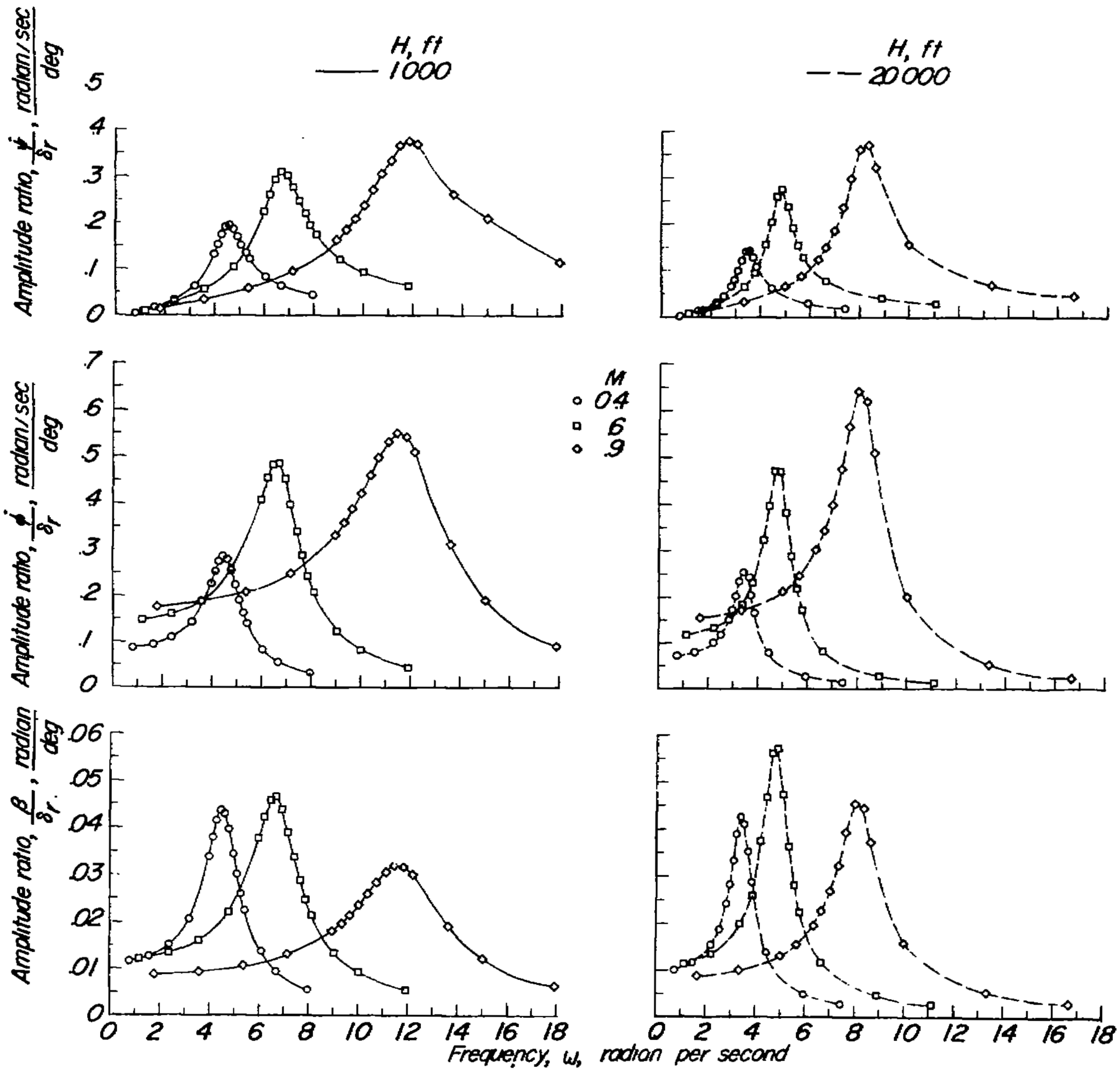

(b) Variation of $\frac{\dot{\psi}}{\delta_r}$, $\frac{\dot{\phi}}{\delta_r}$, and $\frac{\beta}{\delta_r}$ with ω.

Bell X-1 airplane.

Figure 15.- Continued.

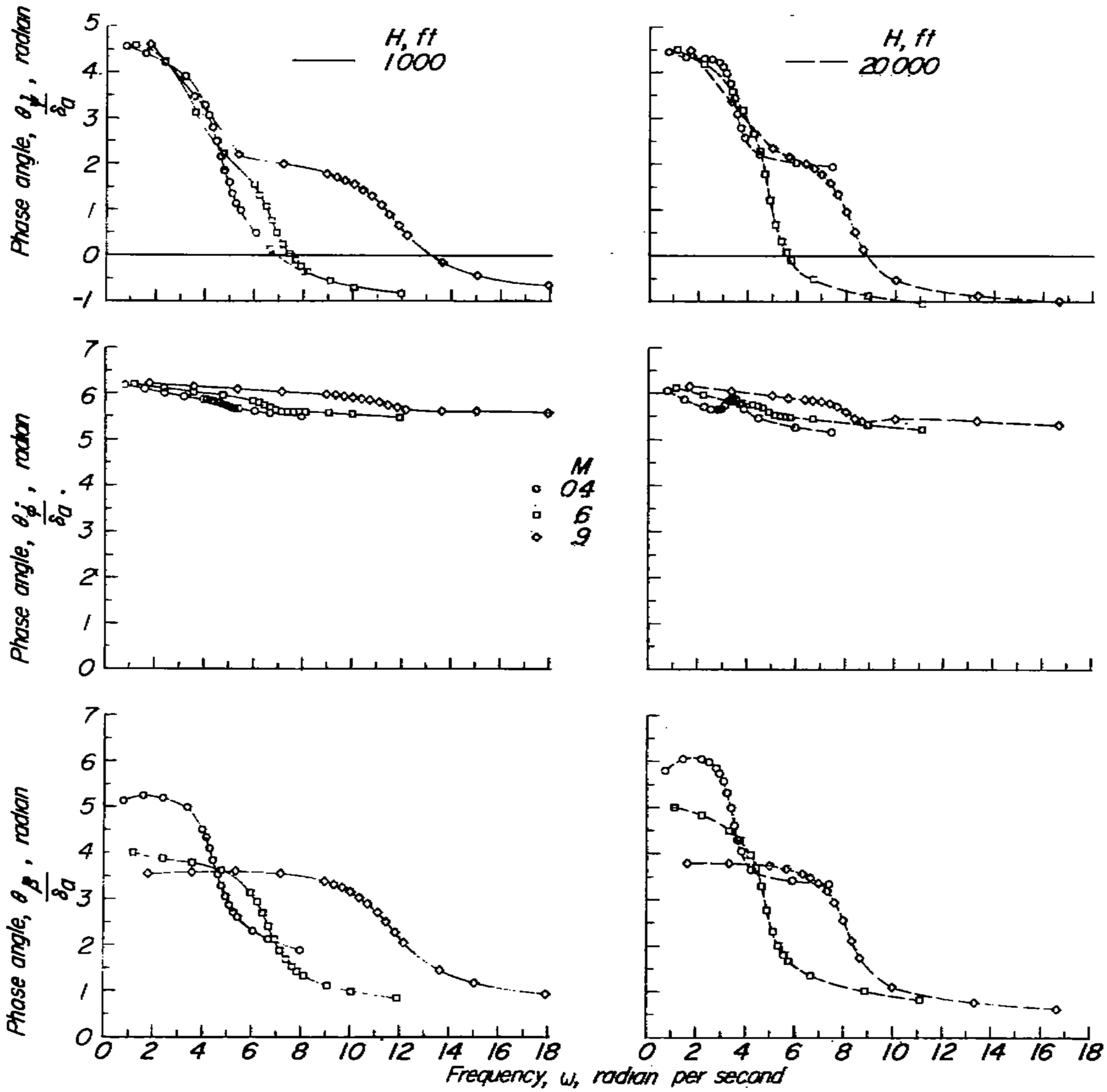

(c) Variation of $\frac{\theta_{\dot{\psi}}}{\delta_a}$, $\frac{\theta_{\dot{\phi}}}{\delta_a}$, and $\frac{\theta_{\beta}}{\delta_a}$ with ω.

Bell X-1 airplane.

Figure 15.- Continued.

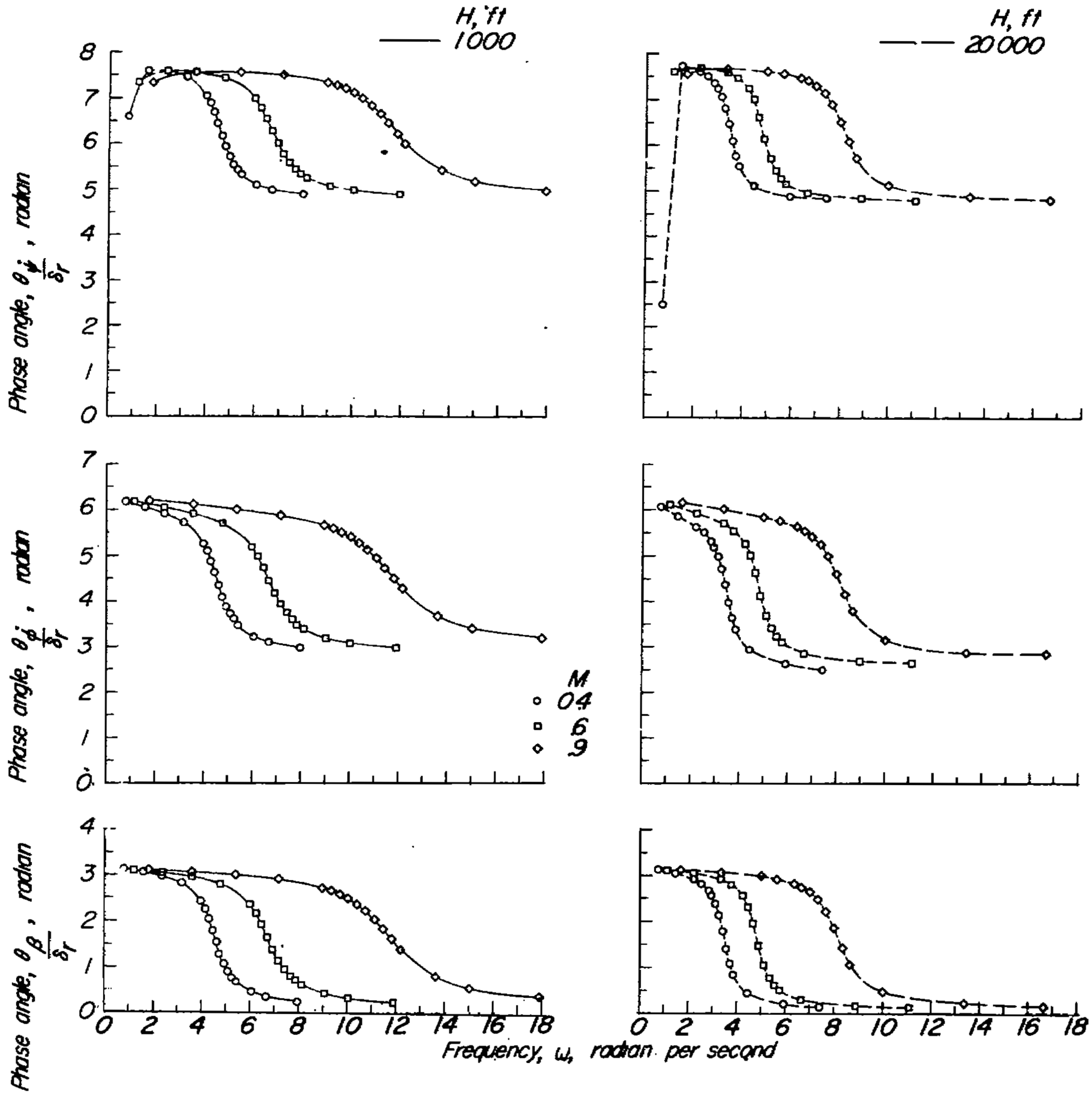

(d) Variation of $\frac{\theta_{\dot\psi}}{\delta_r}$, $\frac{\theta_{\dot\phi}}{\delta_r}$, and $\frac{\theta_\beta}{\delta_r}$ with ω.

Bell X-1 airplane.

Figure 15.- Concluded.

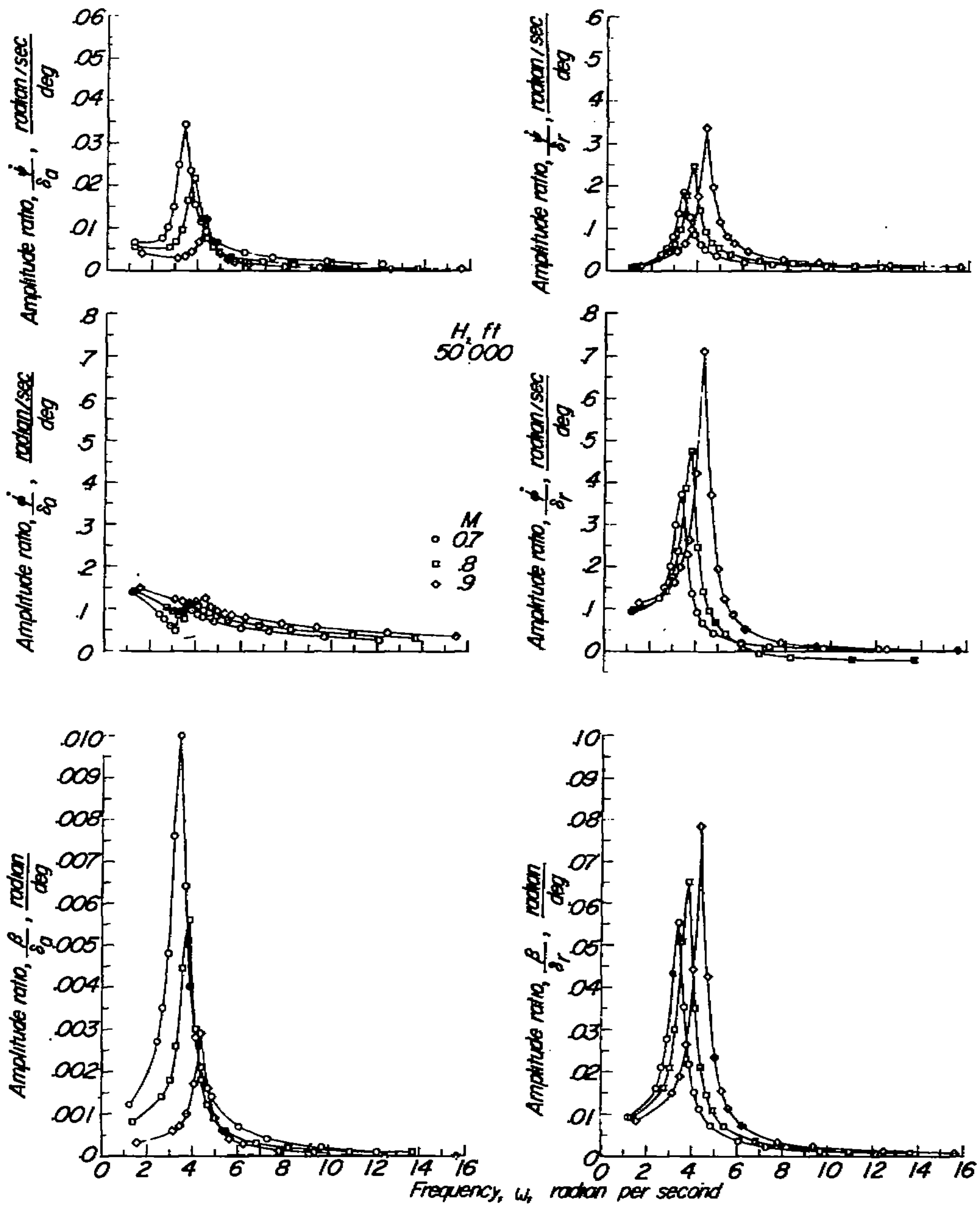

(a) Variation of $\frac{\dot{\psi}}{\delta_a}$, $\frac{\dot{\phi}}{\delta_a}$, and $\frac{\beta}{\delta_a}$ with ω.

(b) Variation of $\frac{\dot{\psi}}{\delta_r}$, $\frac{\dot{\phi}}{\delta_r}$, and $\frac{\beta}{\delta_r}$ with ω.

Figure 16.- Effect of Mach number on the lateral frequency response characteristics of the Bell X-1 airplane.

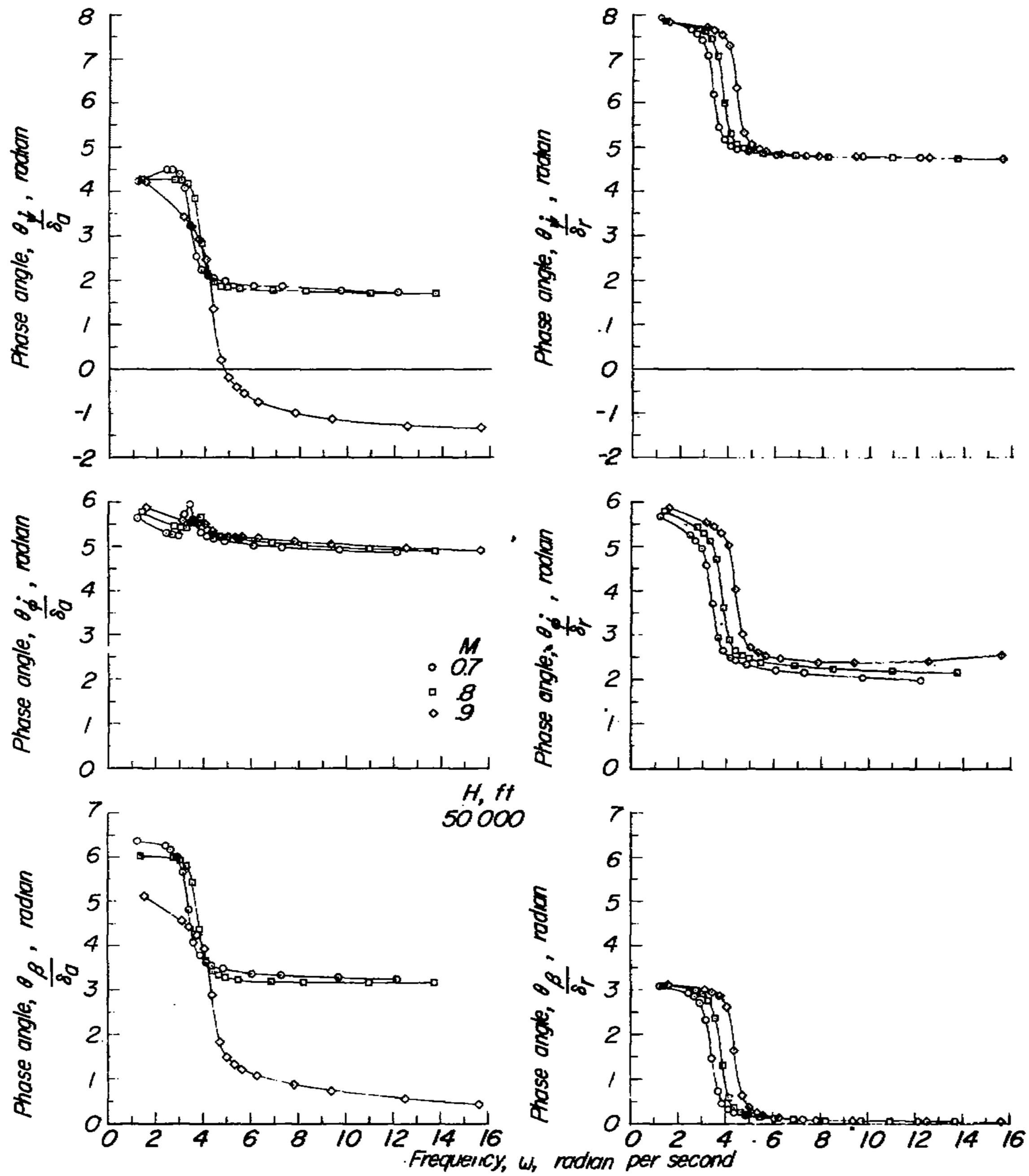

(c) Variation of $\frac{\theta_{\dot{\psi}}}{\delta_a}$, $\frac{\theta_{\dot{\phi}}}{\delta_a}$, and $\frac{\theta_\beta}{\delta_a}$ with ω. Bell X-1 airplane.

(d) Variation of $\frac{\theta_{\dot{\psi}}}{\delta_r}$, $\frac{\theta_{\dot{\phi}}}{\delta_r}$, and $\frac{\theta_\beta}{\delta_r}$ with ω. Bell X-1 airplane.

Figure 16.- Concluded.

[redacted]

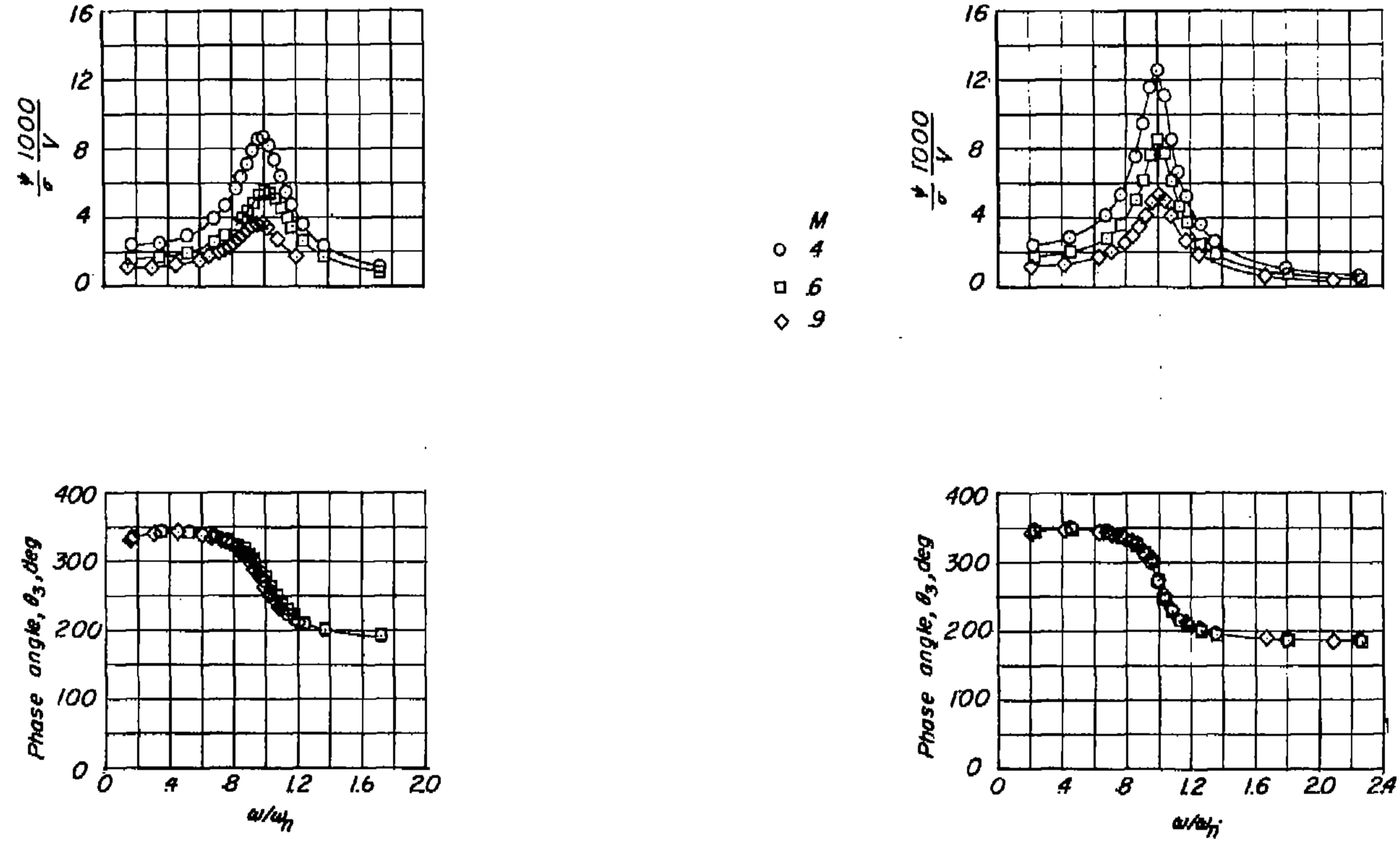

(a) Altitude, 1,000 feet.

(b) Altitude, 20,000 feet.

Figure 17.- Lateral frequency response of North American F-86A airplane to a sinusoidal lateral gust distribution.

[redacted]

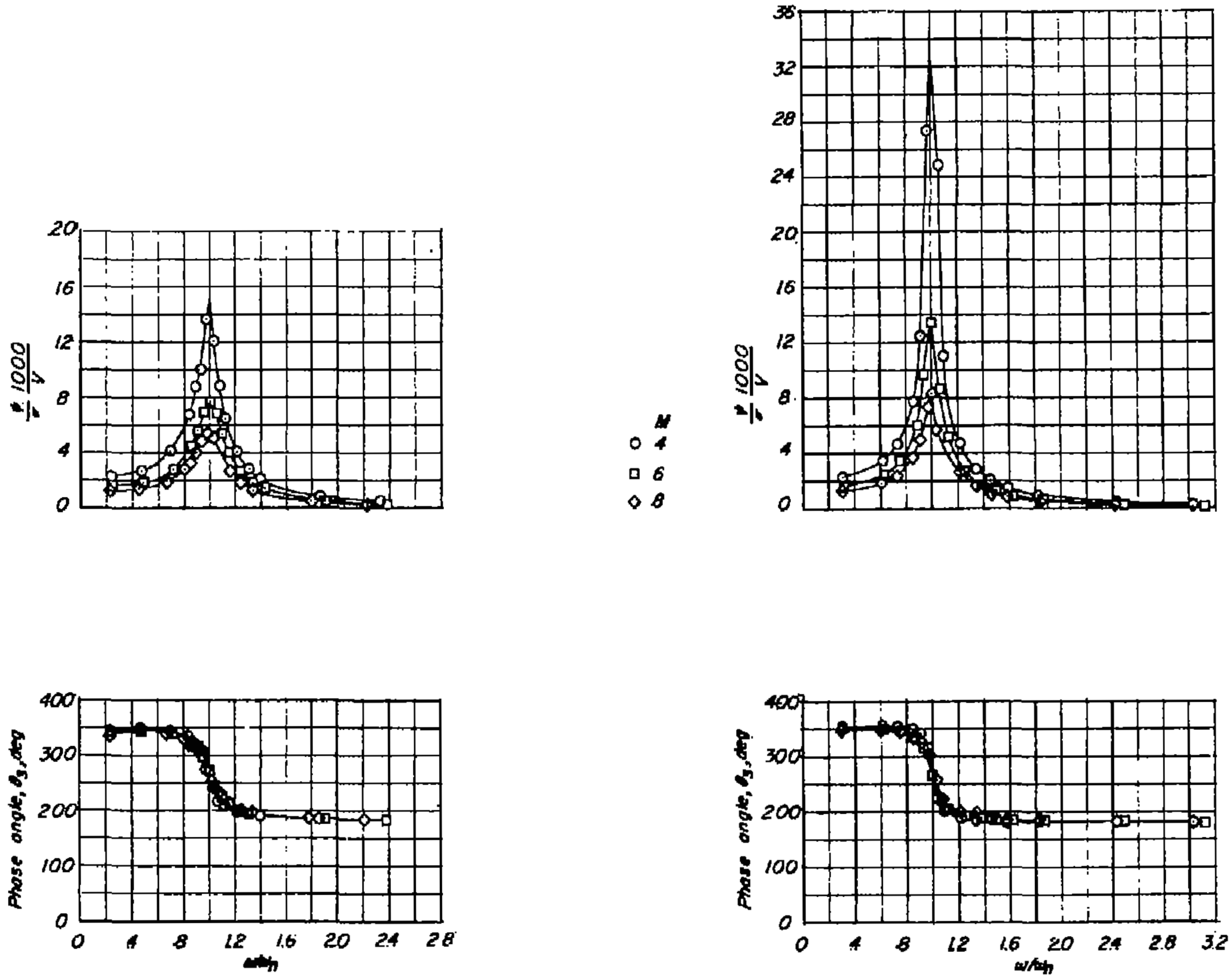

(a) Altitude, 1,000 feet.

(b) Altitude, 20,000 feet.

Figure 18.- Lateral frequency response of Grumman F9F-2 airplane to a sinusoidal lateral gust distribution.

[redacted]

[redacted]

[redacted]

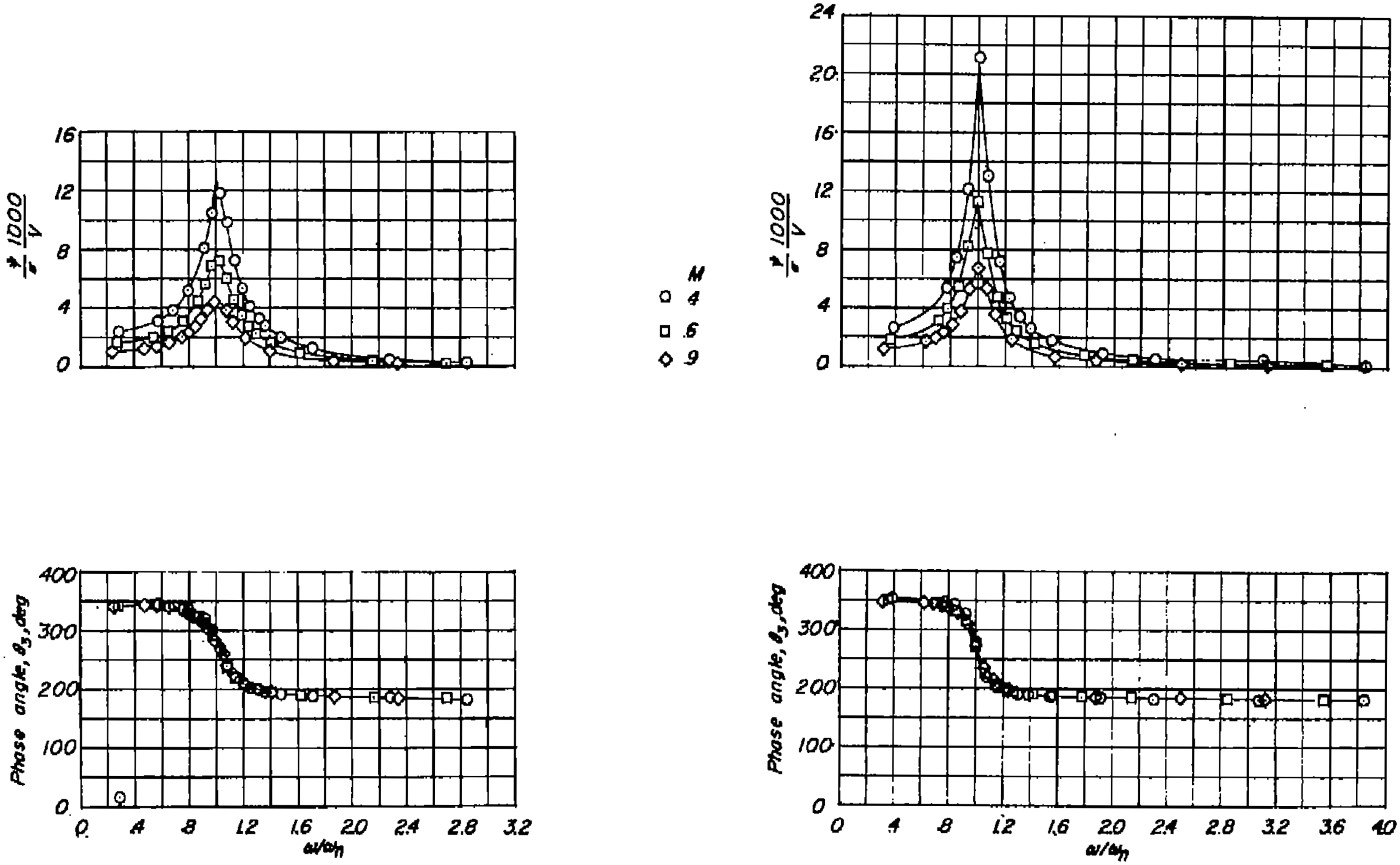

(a) Altitude, 1,000 feet.

(b) Altitude, 20,000 feet.

Figure 19.- Lateral frequency response of Republic F-84 airplane to a sinusoidal lateral gust distribution.

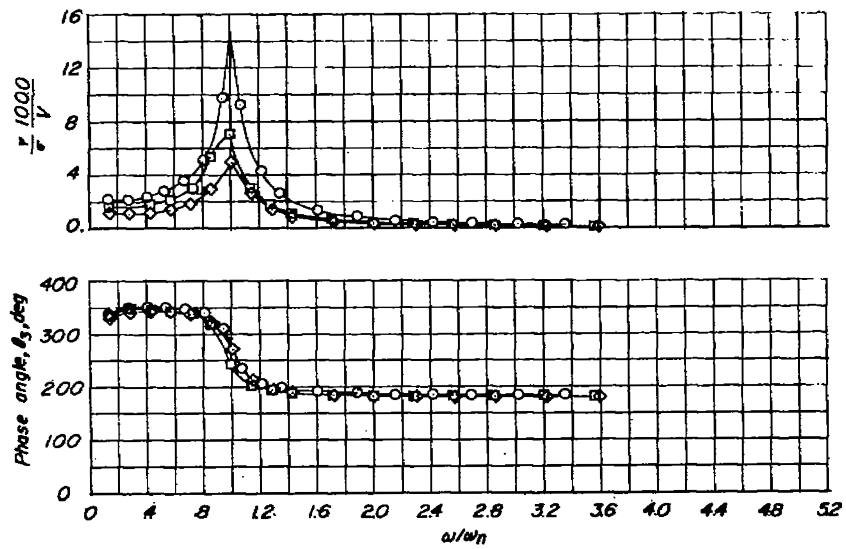

(a) Altitude, 1,000 feet.

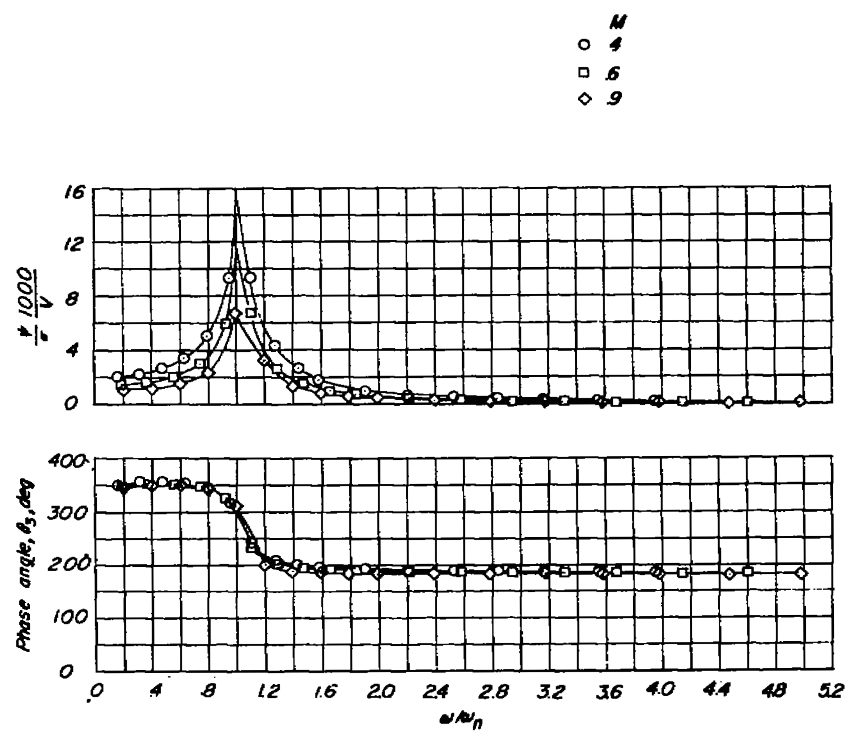

(b) Altitude, 20,000 feet.

Figure 20.- Lateral frequency response of Douglas D-558-II airplane to a sinusoidal lateral gust distribution.

[redacted]

CONF[redacted]

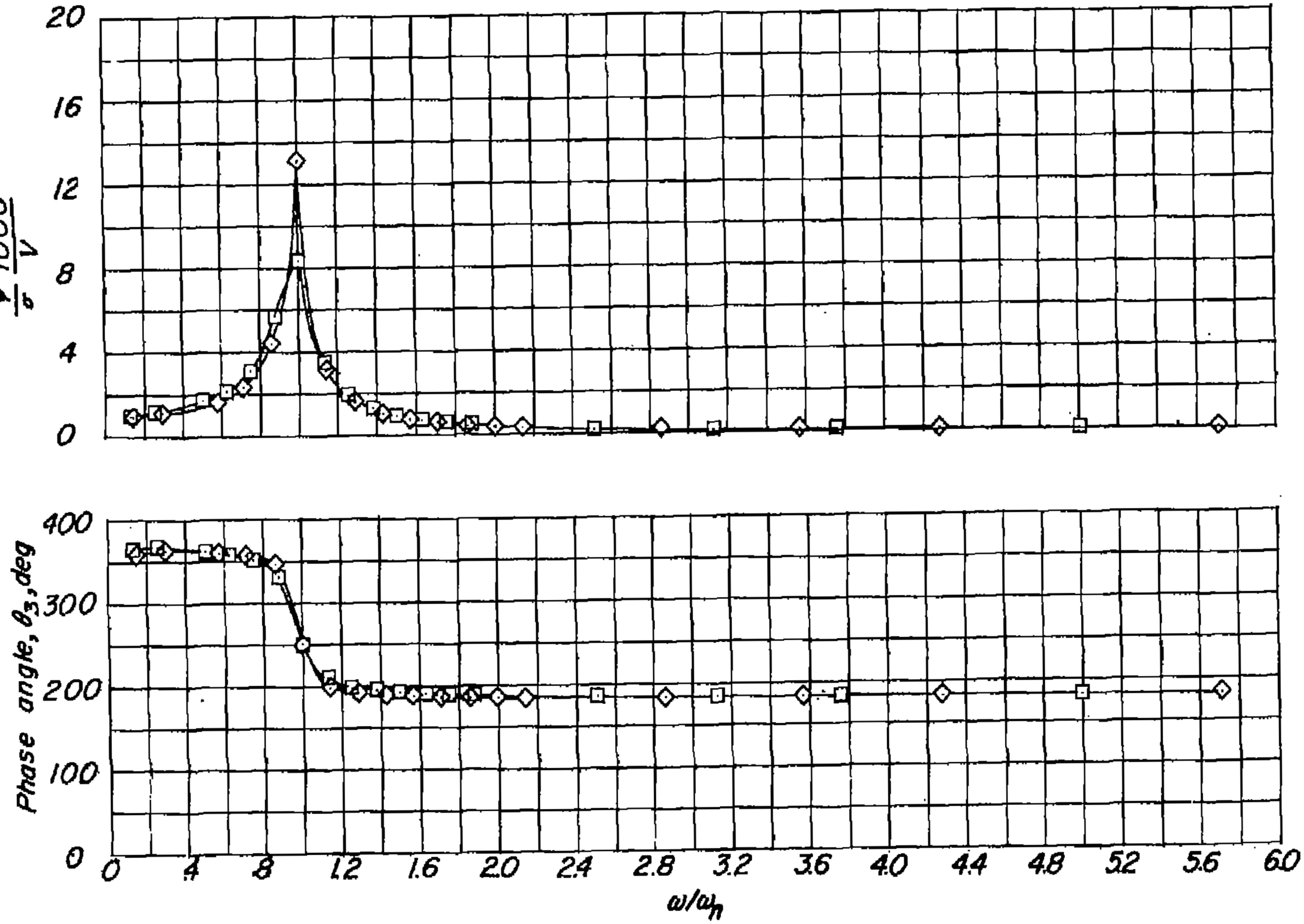

(c) Altitude, 50,000 feet.

Figure 20.- Concluded.

[redacted]

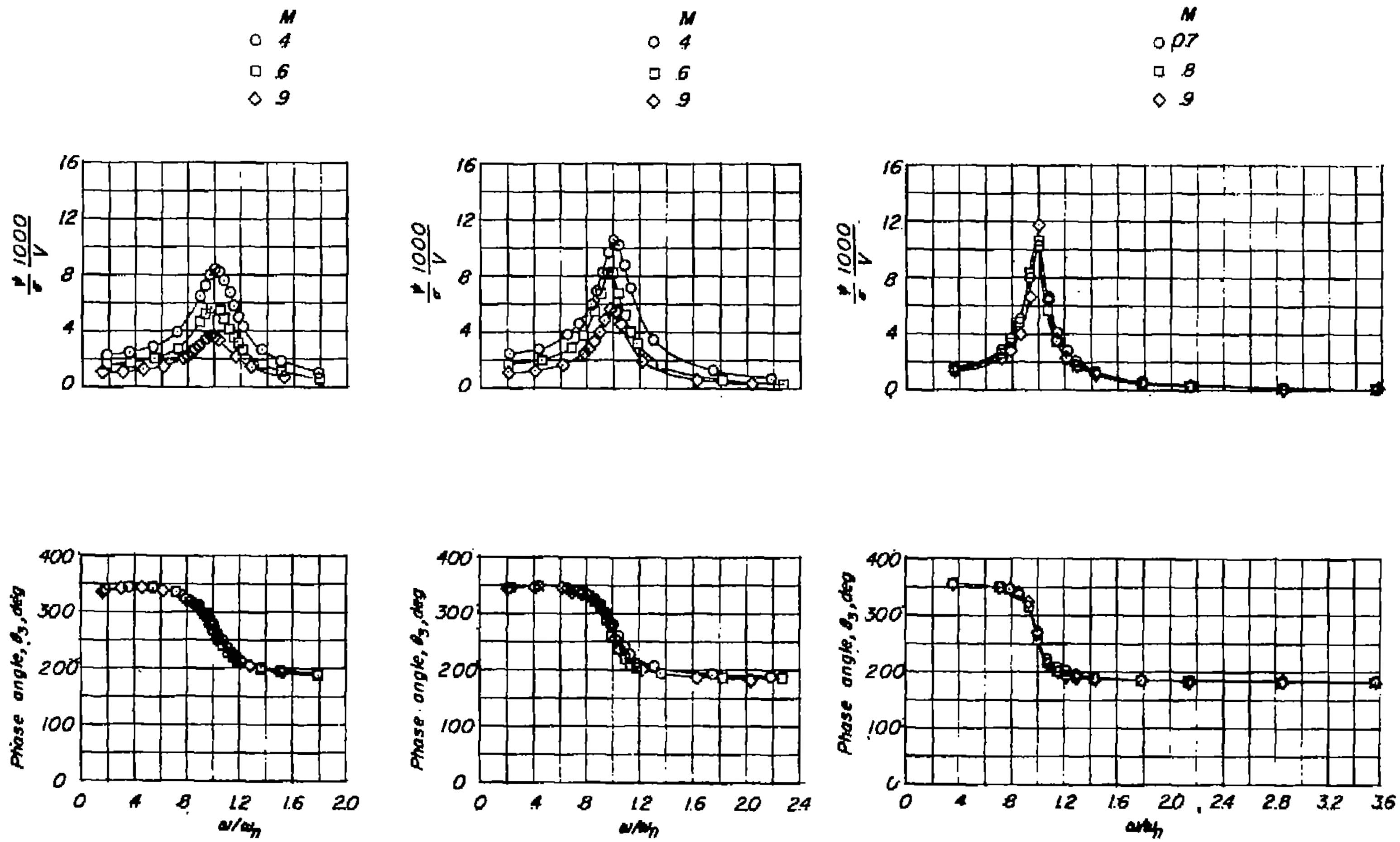

(a) Altitude, 1,000 feet.

(b) Altitude, 20,000 feet.

(c) Altitude, 50,000 feet.

Figure 21.- Lateral frequency response of Bell X-1 airplane to a sinusoidal lateral gust distribution.

[redacted]

NACA-Langley - 12-10-53 - 125